NOTE TO USERS

Page(s) not included in the original manuscript and are unavailable from the author or university. The manuscript was scanned as received.

70

This reproduction is the best copy available.

UMI®

Performance of Micropiles

Juliana Cristina Frassetto

A Thesis

in

The Department

of

Building, Civil and Environmental Engineering

Presented in Partial Fulfillment of the Requirements

For the Degree of Master of Applied Science at

Concordia University

Montreal, Quebec, CANADA

July 2004

Your file Votre référence
ISBN: 0-612-94686-X
Our file Notre référence
ISBN: 0-612-94686-X

ABSTRACT

Performance of Micropiles

Juliana Cristina Frassetto

Micropiles are known to be small in diameter (maximum 300 mm), replacement piles, drilled, composed of placed or injected grout under pressure. These piles may be installed in a uniform or in an increased cross-section. They are designed to withstand axial and lateral loads, and work as components in a composite soil/pile mass or as small-diameter substitutes for conventional piles. Micropiles are extensively used as a vital underpinning technique, as a replacement to the old foundation to support the existing load in part or in full. They are also used as a temporary foundation for retaining walls and structures.

Literature review showed that the load-transfer mechanism of micropiles is commonly assumed to be similar to those governing the performance of ground anchors and/or large diameter bored piles. The design methods of these piles are currently based on empirical formulae, which are not developed to incorporate the effect of the pile installation technique. Accordingly, the need for a pile load test is essential.

This study presents a critical review of the existing design methods and examines the parameters governing the design of these piles. Furthermore, a design procedure is proposed to take into account the geometry of the micropiles, the interaction with the soil and to incorporate the parameters, which seemed to be ignored in the previous methods. The proposed designed procedure was validated against field tests, where good agreement could be found.

Numerical models were developed using the finite element technique to provide solutions for the case stated. The first model was to simulate the installation techniques of the micropiles and to perform a parametric study. The second numerical model was to simulate the cavity expansion caused by grouting pressure and to develop the relationships of pressure versus expansion of the pile diameter, length of expansion and soil properties.

The models were validated against field data and theory with good agreement.

AKNOWLEDGEMENTS

I would like to express my gratefulness to my supervisor, Professor A. M. Hanna for his important guidance and support throughout the execution of this work. This investigation couldn't be done without his assistance.

I would like to declare my sincere gratitude to my parents, who always encouraged and supported me, giving me the opportunity to become all I could and wanted. Their pride and belief in me is my strength.

A deep appreciation I pronounce to my friend Michael for his patience and kindness.

I also want to recognize Danuta and Eduardo Potworowski for being so generous and caring, and Mohab Sabry for valuable discussions.

TABLE OF CONTENTS

LIST OF SYMBOLS

Symbols		Represents
α	=	Lumped constant of proportionality
α_c	=	Diameter correction factor
β	=	Proportionality coefficient
β_c	=	Proportionality coefficient (after CCTG, 1993)
β_m	=	Field average proportionality coefficient
β_p	=	Predicted proportionality coefficient
χ	=	Ratio of stiffness of existing foundation to underpinned foundation
Δ	=	Pile butt displacement
δ	=	Angle of soil/pile friction
ϕ	=	Angle of shear strength of the soil
ϕ'	=	Effective angle of shearing strength of the soil
$\phi_{interface}$	=	Angle of shear strength at the interface soil/pile
γ	=	Unit weight of soil
γ_{sat}	=	Unit weight of the saturated soil
γ_{unsat}	=	Unit weight of the unsaturated soil
λ	=	Proportion of load carried by underpinning piles
ν	=	Poisson's ratio
σ_θ	=	Circumferential normal stress
$\sigma'_{h,o}$	=	Initial horizontal effective stress

σ_p	=	Value of σ_r at R_p
σ_r	=	Radial normal stress
$\sigma'_{v,o}$	=	Initial vertical effective stress
σ'_{vm}	=	Mean vertical effective stress
σ'_{vz}	=	Vertical effective stress
τ	=	Maximum shear stress
τ_{max}	=	Maximum value of shear stress when Mohr's circle touch Coulomb failure
τ_{rel}	=	Relative shear stress
ψ	=	Dilatancy angle
a	=	Curve fitting parameter
A_c	=	Area of pile grout
A_p	=	Area of pile tip
A_y	=	Area of steel reinforcement
c	=	Cohesion of the soil
C	=	Relation load-displacement transversally
c_{inter}	=	Cohesion on interface soil/pile
CPT	=	Cone penetration test
C_t	=	Coefficient of lateral elastic-plastic support
c_u	=	Undrained cohesion
d	=	Expanded pile diameter
D	=	Effective pile diameter
D_i	=	Effective pile diameter on layer i.
D_L	=	Nominal pile diameter

d_{li} = Depth of considered layer

D_o = Diameter of the drilled hole

D_s = Shaft diameter

E = Young's modulus of the soil

E_c = Young's modulus of column

E_l = Deformability modulus of the layers over and under the low resistance one

E_p = Young's modulus of the pile

E_s = Modulus of horizontal subgrade reaction

f'_c = Characteristic unconfined compressive strength of the grout

f_{av} = Average unit shaft resistance

F_{ce} = Critical Euler buckling force

f_s = Ultimate unit shaft resistance

f_{sav} = Average unit shaft resistance

$f_{s(p)}$ = Ultimate unit shaft resistance due to primary grouting

$f_{s(s)}$ = Ultimate unit shaft resistance due to secondary grouting

f_{si} = Ultimate unit shaft resistance for the soil layer i

f_y = Characteristic yield stress of reinforced steel

g = Grout partial factor

h = Thickness of the low resistance layer

I_L = Non-dimensional coefficient of form

I_p = Moment of inertia of the pile

k = Coefficient representing the connection between column and structure

K = Coefficient of earth pressure

K'	=	Combined factor (after Littlejohn, 1980)
K_1	=	Earth pressure coefficient (after Littlejohn, 1970)
K_2	=	Coefficient representing the increase in diameter due to grouting pressure
K_F	=	Footing or pile stiffness
K_{L1}	=	Coefficient that represents the average bond between pile and soil
K_o	=	Coefficient of earth pressure at rest
K_{pr}	=	Piled-raft stiffnes
K_r	=	Raft foundation stiffness
l	=	Length of expanded pile diameter
L	=	Pile length
L_1*	=	Thickness of the layer over the low resistance layer
L_2	=	Interpreted failure load
L_2*	=	Thickness of the layer under the low resistance layer
l_c	=	Length of column
l_{fl}	=	Distance between the connections of the pile
L_L	=	Length of pile (after Lizzi, 1982)
l_o	=	Transfer length
L_s	=	Shaft depth
L_{st}	=	Slope tangent value of load
m	=	Number of soil layers
m_c	=	Curve fitting parameter
n	=	Factor of safety
N	=	Number of blows from SPT test

N_c^* = Bearing capacity factor

n_e = Integer number to yield minimum critical buckling load

$n_{found.}$ = Factor of safety of foundation

n_{pile} = Factor of safety of pile

OCR = Over-consolidation ratio

p = Uniform internal pressure

P = Applied load

p_l = Limit pressure from pressuremeter test

p_l^* = Modified limit pressure

P_{cr} = Critical load

P_F = Footing or pile load

p_g = Grout pressure

P_p = Pile load taken by underpinning piles

P_{tot} = Total applied load on foundation

p_u = Ultimate cavity pressure

Q = Load carrying capacity

q_c = CPT resistance

Q_{fl} = Critical buckling load

Q_i = Load capacity curve

Q_{Ls} = Ultimate axial loading capacity (after Lizzi, 1982)

Q_p = End-bearing resistance

q_s = Limit unit shaft resistance

$q_{s\,max}$ = SPT resistance

Q_s	=	Shaft resistance
$Q_{s(L2)}$	=	Interpreted side resistance using L_2 method
Q_w	=	Design ultimate axial load
r	=	Expanded pile radius
R	=	Pile radius
R_i	=	Initial cavity radius
R_{inter}	=	Strength reduction factor at the interface pile/soil
R_p	=	Radius of plastic cavity zone
R_u	=	Ultimate cavity radius
s	=	Steel partial factor
S_F	=	Foundation displacement
SPT	=	Standard penetration test
S_{TF}	=	Total final settlement of existing foundation
S_{TFP}	=	Total final settlement of foundation underpinned by piles
S_{ti}	=	Total settlement of foundation at time t_i
s_u	=	Undrained shear strength
t	=	Time
u	=	Pore-water pressure
u_p	=	Radial displacement of point at distance R_p
x	=	Cartesian coordinate
y	=	Cartesian coordinate
z	=	Depth

LIST OF FIGURES

Description **Page**

LIST OF TABLES

Description **Page**

CHAPTER 1

INTRODUCTION

1.1. PREFACE

Micropiles (also called pinpiles, minipiles, root piles, needle piles and 'pali radice') can be defined generically as small-diameter (maximum 300mm) drilled and grouted piles. They can withstand axial and lateral loads, and can work as a component in a composite soil/pile mass or as a small-diameter substitute for a conventional pile.

The technology of micropiling was first proposed by Dr. F. Lizzi in the early 1950's (FHWA, 1997) and introduced into North America more than two decades later. Although they have been used throughout the world for various purposes, and it is a technique that is growing rapidly, micropiles still lack reliable design guidelines.

The purpose of this study is to improve the current state of practice for design of micropiles whose philosophy of behavior can be defined as directly loaded piles for axial conditions.

Special focus is given in their work as underpinning elements, where they have being used widely because they can be drilled through virtually every ground condition (natural and artificial) and through existing structures, with minimal vibration, disturbance and noise; at any angle below horizontal. The equipment can be adapted to operate in locations with low headroom and severely restricted access, in close proximity to existing piles, without interrupting facility operations, and without threatening the stability of the structure. They are also environmentally responsive, due to small diameter drilling and easily controllable flush effluent.

There has been little demand and very few applications for micropiles in North America. There are many research challenges to be met that can promote micropiles growth, such as more user-friendly design procedures as proposed in this work.

1.2. RESEARCH OBJECTIVES

The objectives of this work are:

1. To conduct a literature research on the subject of micropiles for underpinning.
2. To critically review the design methods available for micropiles for underpinning.
3. To examine the parameters governing the design of micropiles.
4. To propose a design procedure.
5. To recommend future research on the subject.

CHAPTER 2

LITERATURE REVIEW

2.1. GENERAL

The design for micropiles today is mostly based on the experience and research performed on large-diameter drilled shaft piles and ground anchors, as are the codes and specifications available in North America. Load tests confirmed that the result is conservative design and extraneous costs (FHWA, 1997).

Underpinning by piles is widely used but approaches to the design of piles specific for this kind of work are also poorly developed. It is important to consider in the design the load sharing between the piles and the old foundation (raft or strip).

The design of conventional piles is normally governed by the external (or ground related) carrying capacity, while micropiles design can be controlled by the internal design, or selection of pile components (FHWA, 1997). Therefore micropiles can have small cross- sections due to the high grout/ground bond capacities that are usually mobilized as a consequence of micropile installation methods, and the high capacity steel elements occupying up to 50% of the whole volume. The ratio of circumference to the cross-sectional area is extremely high; thus, the perimetric area governs the load transfer mechanism (unit shaft resistance), as opposed to end bearing.

The design methods available are empirical, commonly requiring site-specific loading tests, and there is a lack of convenient and reliable design specifications for micropiles subjected to axial load.

2.2. REVIEW OF PREVIOUS WORK

2.2.1. DEFINITIONS AND CLASSIFICATIONS

FHWA (1997) provided a comprehensive state-of-practice review to assist the Federal Highway Administration in USA in establishing reliable design guidelines, construction specifications, and quality control procedures, based on a critical assessment of data published worldwide on micropiles.

Their intention was to be a cooperative partner to the French project "FOREVER" ('fondations renforcées verticalement'), whose objective is to promote the use of micropiles in all fields: deep foundations of new buildings and structures, stabilization of slopes and embankments, consolidation of existing foundations, retaining walls, reduction of embankment settlement, and shallow foundations.

According to the Fleming et al. (1985) classification of bearing pile types, micropiles can be defined as a small-diameter subset of cast-in-place replacement piles. In the report they were defined as: a small diameter (less than 300 mm), replacement, drilled piles composed of placed or injected grout, and having some form of steel reinforcement to resist a high proportion of the design load.

A new and rigorous classification was adopted by FHWA (1997) based on two criteria: philosophy of behavior and method of grouting.

Based on philosophy of behavior micropiles can be classified as:

1. Case 1: directly loaded piles (individual or group of piles), whether for axial or lateral loading conditions (Figure 2.1).

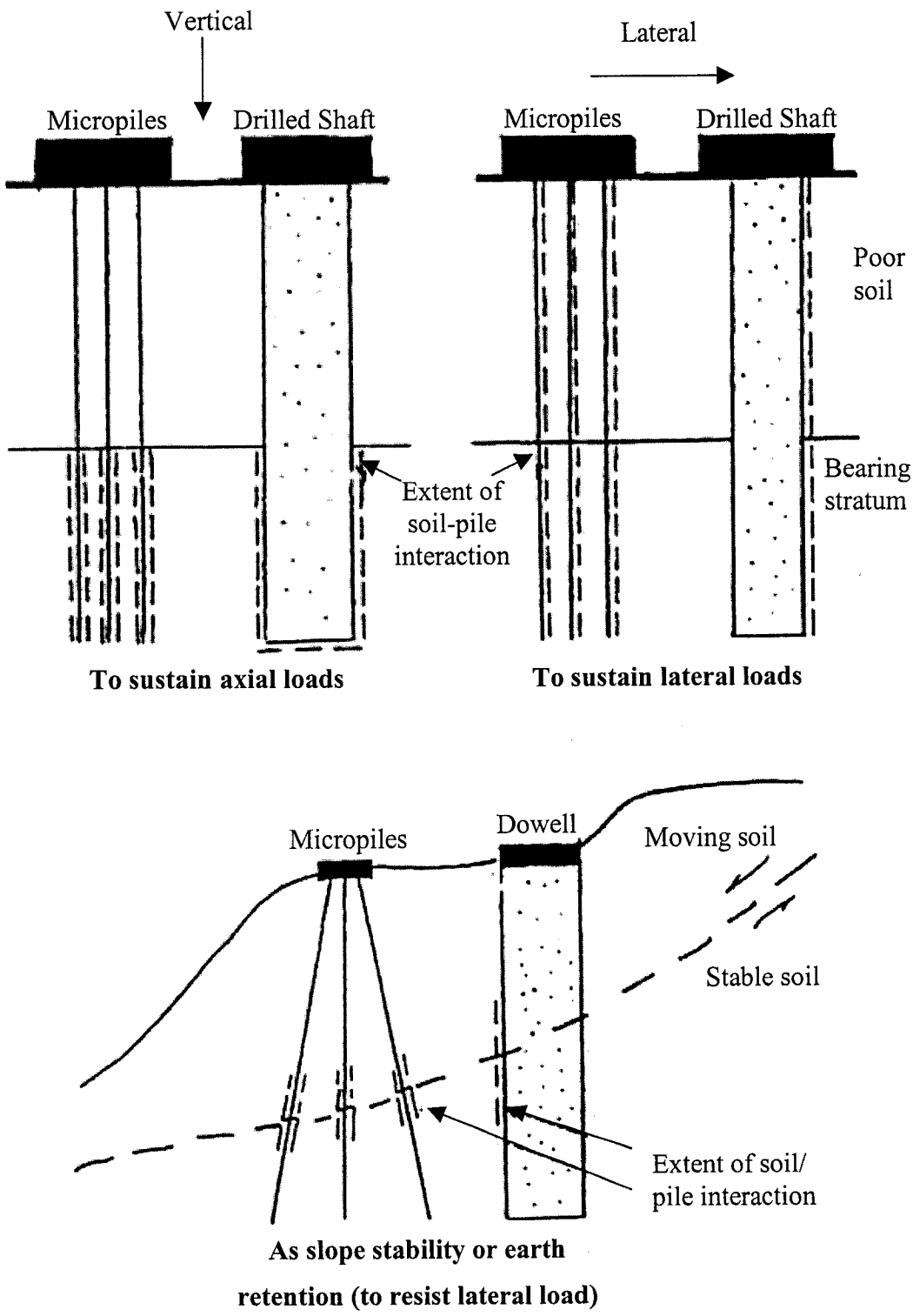

Figure 2.1. Classification based on interaction with soil - Case 1 (FHWA, 1997).

2. Case 2: 'root piles', with support and stabilization by locking onto a three-dimensional network of reticulated piles forming a soil/pile composite structure (Figure 2.2).

According with FHWA (1997) based on the method of grouting micropiles can be classified as (Figure 2.3):

a) Type A: grout is placed in the pile under gravity head only.
b) Type B: neat cement grout is injected into the drilled hole as the temporary steel drill casing is withdrawn. Pressures are typically in the range of 0.3 to 1 MPa.
c) Type C: neat cement grout is placed in the hole, as done for type A. After 15 to 25 minutes, before hardening of this primary grout, similar grout is injected once via a preplaced sleeved grout pipe at a pressure of at least 1MPa. This type of pile is common practice only in France.
d) Type D: neat cement grout is placed in the hole, as done for Type A. Some hours later, when this primary grout has hardened, similar grout is injected via a preplaced sleeved grout pipe. In this case, however, a packer is used inside the sleeved pipe so, that specific horizons can be treated several times if necessary, at pressures of 2 to 8 Mpa.

This proposed classification is very efficient and easily employed, it can be readily found in works of different authors such as Jeon and Kulhawy (2001). The results were based on a comprehensive research on national and international publications.

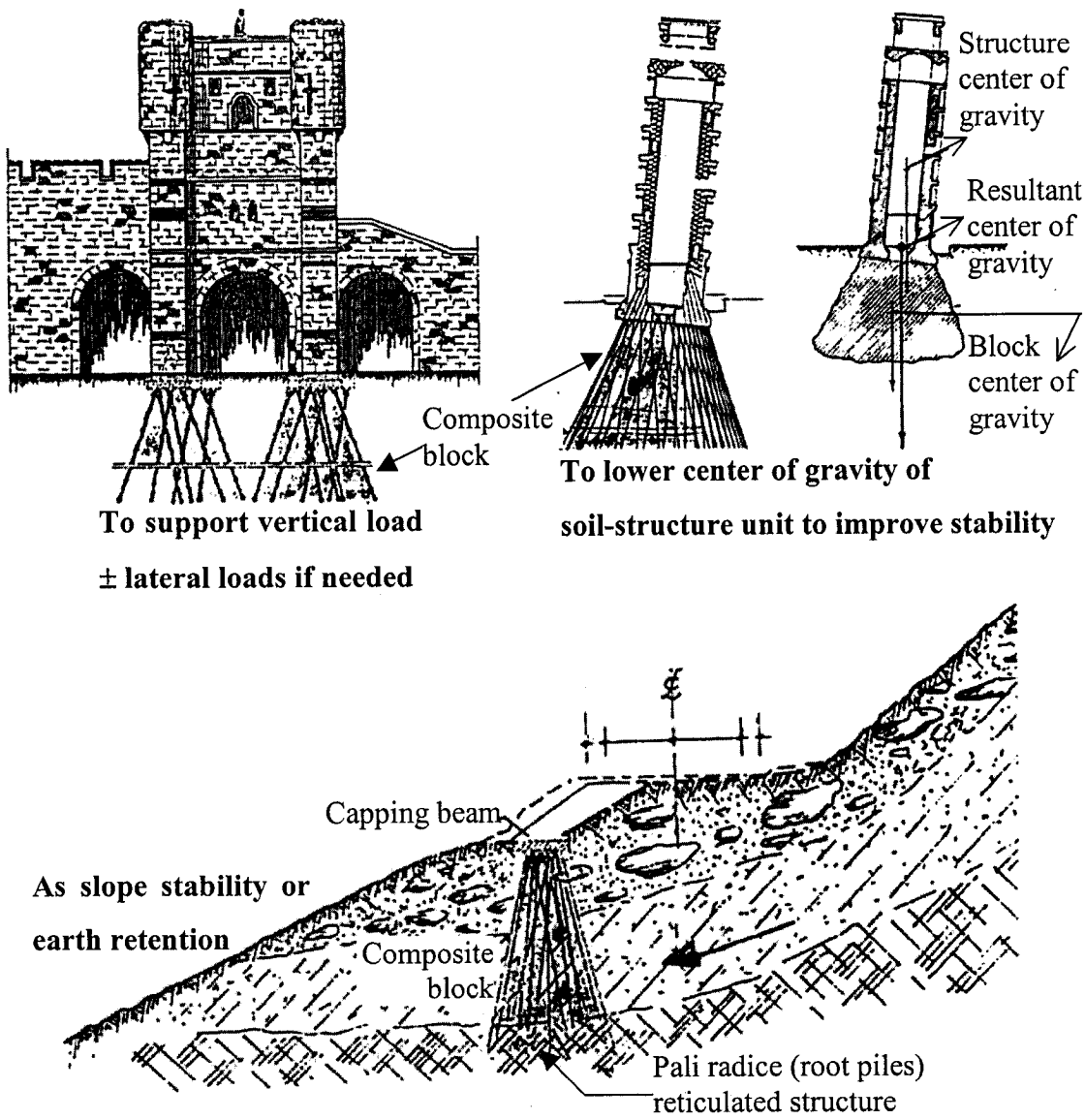

Figure 2.2. Classification based on micropiles interaction with soil – Case 2 (FHWA, 1997).

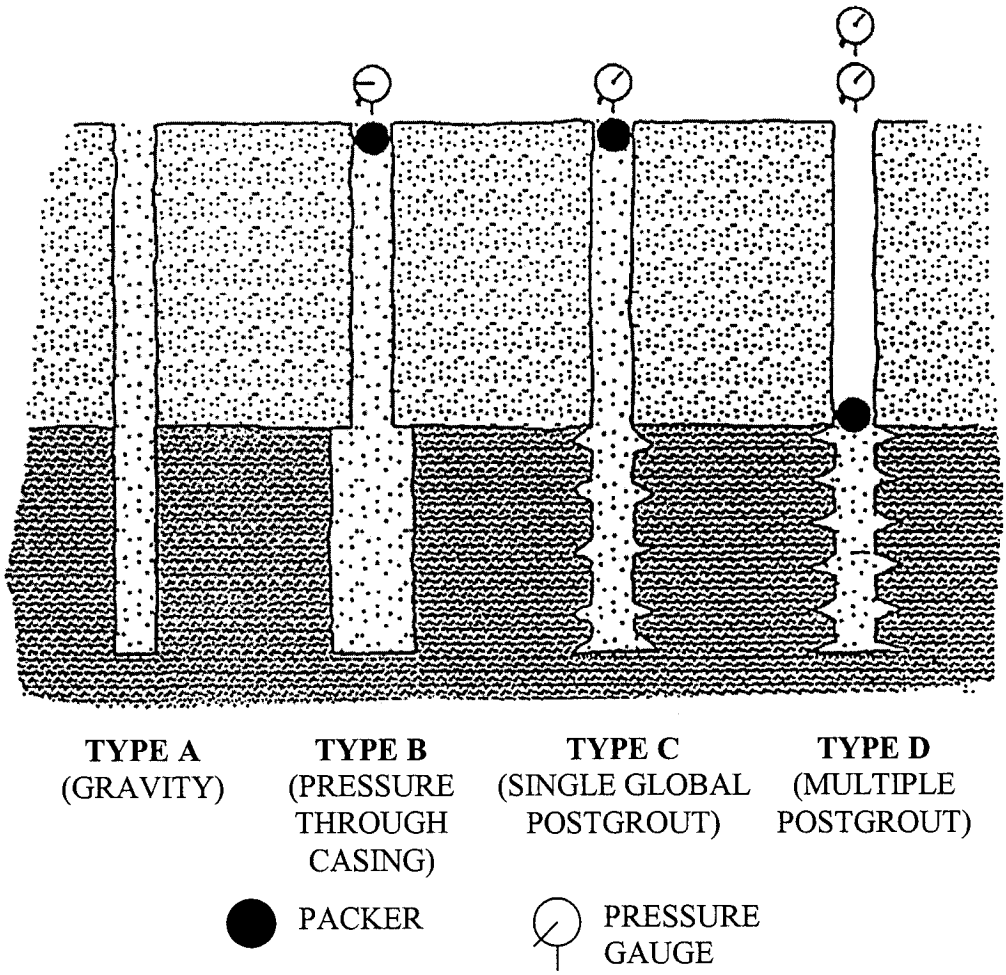

Figure 2.3. Classification of micropile based on type of grouting (FHWA, 1997).

2.2.2. MICROPILES FOR UNDERPINNING

According to Bullivant and Bradbury (1996) the problem of settlement has been with us since the earliest times. During these times, little science was involved in the design of foundations. The knowledge that existed about soils and structures had been collected from local experience and the skills handed down by artisans.

The application of a scientific approach to foundation work began in the seventeenth century and almost exclusively, the work involved techniques that can be grouped under the heading 'traditional underpinning'.

There are basically four general categories of underpinning: remedial, conversion, protective and mining.

The demand for underpinning has increased steadily as renewals and refurbishment work have gained popularity and, as more buildings have been constructed on substandard land because the best sites have already been developed or, have become prohibitively expensive.

Experience in mainstream piling has inevitably led to the use of piles in underpinning systems and pilling techniques can be classified as: angle piling, pin piling (floor slab piling), needle piling (pile and beam), jack-down piles and pretest piles.

Although pile solutions are appropriate in many cases, their use is rare in comparison with traditional systems, the reasons are: perceived cost advantages, contractual ability and ground conditions. Piled systems will grow rapidly as the benefits become more widely understood and the techniques become cheaper in line with the increased volume of work.

Bullivant and Bradbury (1996) made a good review of the different conditions that can necessitate underpinning and how to evaluate them, the techniques available for underpinning, and a sequence of operations to minimize disturbance to the structure and the occupiers of the building. Some recommendations are made for mini piling such as for buckling where the length should be restricted to about 70 times their internal diameter, but no design methods are presented.

Lizzi wrote for Thorburn and Hutchison (1985) about his invention 'pali radice'. The most significant feature of the 'pali radice' used in underpinning is the quick response to any movement, however slight, of the structure. This essential feature is due to the technology of its construction in which a 'pali radice' is essentially a friction pile.

'Pali radice' underpinning can be considered practically inactive at the moment of its construction. If the building has a subsequent, albeit minimal, settlement the pilling responds immediately, absorbing part of the load and reducing at the same time the stress on the soil. If, despite this, the building continues to settle, the piles continue to take the load, until finally; the entire building load is supported by them. In even the most extreme case the settlements would be limited to a maximum of a few millimeters.

Lizzi (Thorburn and Hutchison, 1985) stated that any action on a building subject to settlement has to take into account the essential fact that the construction already exists, and during the repair work there is, therefore, the risk to worsening, rather than improving its critical condition. Several conditions must be satisfied:

a) The reinforcement must be reliable and based on confirmed load bearing elements.
b) The strengthening work has to proceed as quickly as possible, giving a progressive relief to the structure.

c) The reinforcement once installed must give an immediate response to any, even the most minimal, further movement on the building.

Lizzi (1982) suggested that micropiles were an ideal underpinning tool for the following reasons:

I. Their execution did not introduce, even temporarily, any undue weakness or overstress in the structure as well as the soil.

II. They responded immediately to additional structural movement.

III. They enabled the assessment of a new factor of safety (n), which will be $n = n_{found} + n_{pile}$.

He also suggests that the modern tendency to increase more and more the diameter of foundation piles, in order for them to support greater loads in the range of thousands of tons, is perhaps a mistake. Such piles, spaced widely, are generally very long, because they have to rely essentially on the deep strata, neglecting (at least in terms of safety) the possible contribution of the upper layers of soil. A denser pattern of smaller-diameter piles, however, of not exaggerated length, is probably more suitable for involving the collaboration of the soil, and therefore returning to its essential role as principal support of any human-made construction.

Lizzi (1982) introduces in this publication a good review of all the essential aspects of his technique together with many important case histories. There is also a suggestion of a simple empirical formula for the ultimate load of 'pali radice' as:

$$Q_{Ls} = \pi \bullet D_L \bullet L \bullet K_{L1} \bullet I_L$$

Where:

Q_{Ls} = ultimate axial loading capacity (in kN).

D_L = nominal diameter of the pile (in m).

L = length of pile (in m).

K_{Ll} = coefficient that represents the average bond between the pile and the soil for the whole length (in kPa).

I_L = non-dimensional coefficient of form, which depends on the nominal diameter of the pile.

He reported about micropiling with steel pipes and preloading of micropiles, a technique that he rejects for the following reasons:

a) The pre-loading introduces stresses, into both the soil and the building, which constitute a striking disturbance to the existing stability, the consequences of which can be very severe.
b) The factor of safety is only $n = n_{pile}$, and relies on the bearing capacity of the piles, without the essential contribution of the existing subsoil.
c) The building is transferred on to the piling, losing its contact with the soil.
d) The connection between the piles and the structure has to be postponed until the time when the piling is complete, a long period of distress for the building would occur.

These concerns are no long applicable according to FHWA (1997), because recent tests and case histories are proving that preloading is in fact a very efficient technique.

FHWA (1997) stated that one of the basic applications of micropiles is structural support, probably 95% of total world applications (Figure 2.4). They were actually originally devised for underpinning in the restoration of weakened, historic buildings, and were primarily installed as Case I pile groups.

In the report the authors listed their use for underpinning to:

a) Prevent or arrest structural settlements (also through preloading).

b) Repair or replace deteriorating or inadequate foundations.

c) Upgrade the load-bearing capacity of an existing foundation to permit, for example, the extension or rising of a structure.

Some factors influencing the choice of micropiles are listed as (FHWA, 1997):

I. Physical constraints: the manipulation and compactness of conventional, small-scale drilling, and grouting equipment can permit piles to be installed in confined, awkward, or otherwise physically constraining work spaces. In places such as with low overhead clearance, or in close proximity to existing walls, columns, footings, or other structures, and with buried services or other facilities, allowing fully functional facilities with minimal disruptions to normal operations.

II. Environmental constraints: the drilling and grouting techniques are selected to impart minimal disturbance on the soil, structure, and surrounding environment. Thus micropiles have been selected when installation is required near structures sensitive to vibration-induced damage, in areas with soils susceptible to vibration-induced settlement or to slopes of marginal stability, in populated areas where vibrations, noise, dust, or disposal of cuttings or flushing are problematic.

III. Difficult ground conditions: the range of available drilling techniques allows installation through any type of fill, soil, rock, obstruction, or through existing structures. Depth and orientation also are virtually unrestricted.

IV. Load/movement criteria: micropiles can sustain relatively high loads with only small movement or complex loading conditions. In extremely sensitive structures, preloading of Case I piles can be adopted to fully eliminate pile compression.

V. Connection to structure: micropiles can be incorporated and fixed directly into an existing foundation.

VI. Cost: it is important to evaluate micropiles' cost-effectiveness for every different kind of situation. The costs can escalate due to very conservative designing, one more reason for the review of design guidelines available.

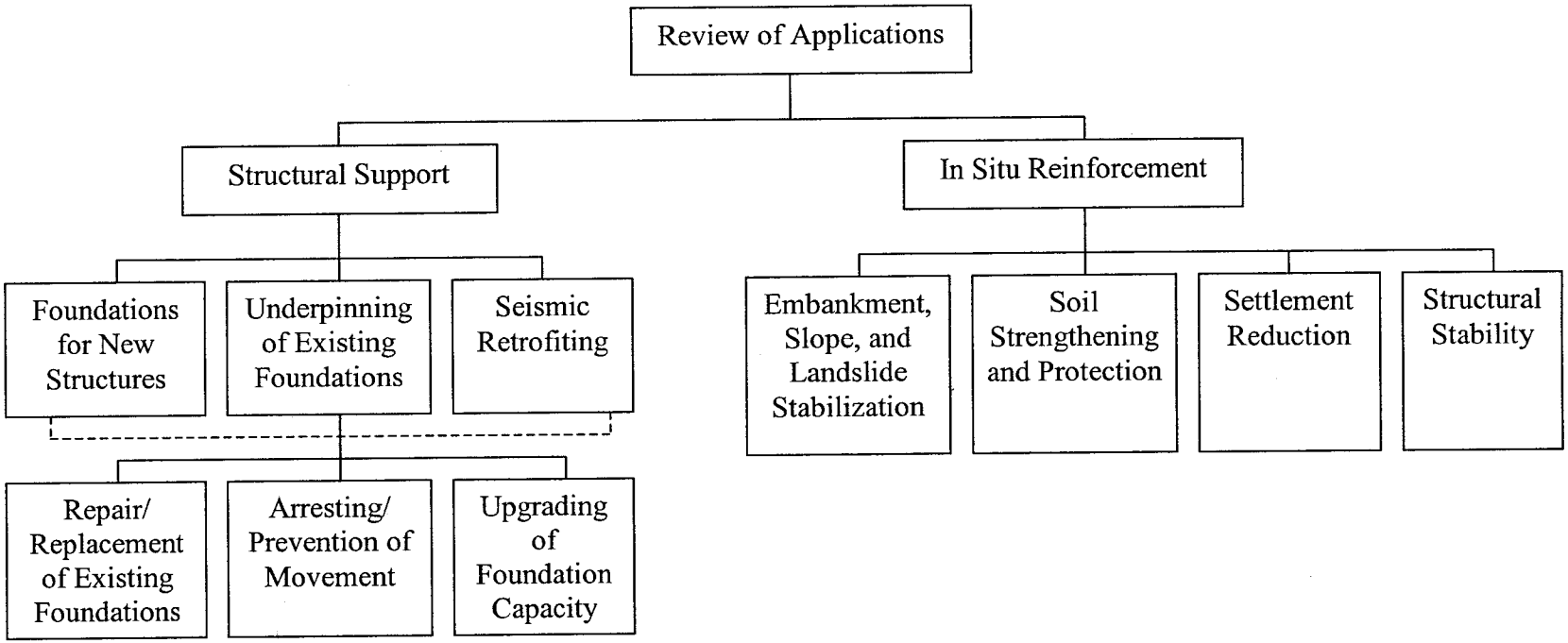

Figure 2.4. Applications of Micropiles (FHWA, 1997).

2.2.3. GEOTECHNICAL DESIGN

FHWA (1997) acknowledged that the load-transfer mechanism and the ultimate unit shaft resistance of micropiles depend upon several parameters, including installation technique; drilling and grouting pressure; loading type; initial state of stresses; engineering properties of the soil; and specifically its relative density (or over-consolidation ratio), permeability, and shear strength characteristics.

Load transfer from the micropile to the surrounding ground requires some relative movement (Ghaly and Hanna, 2003). The movement due to compressive loading is controlled by the elastic modulus of the composite-reinforced micropile and the load-transfer mechanism (Figure 2.5).

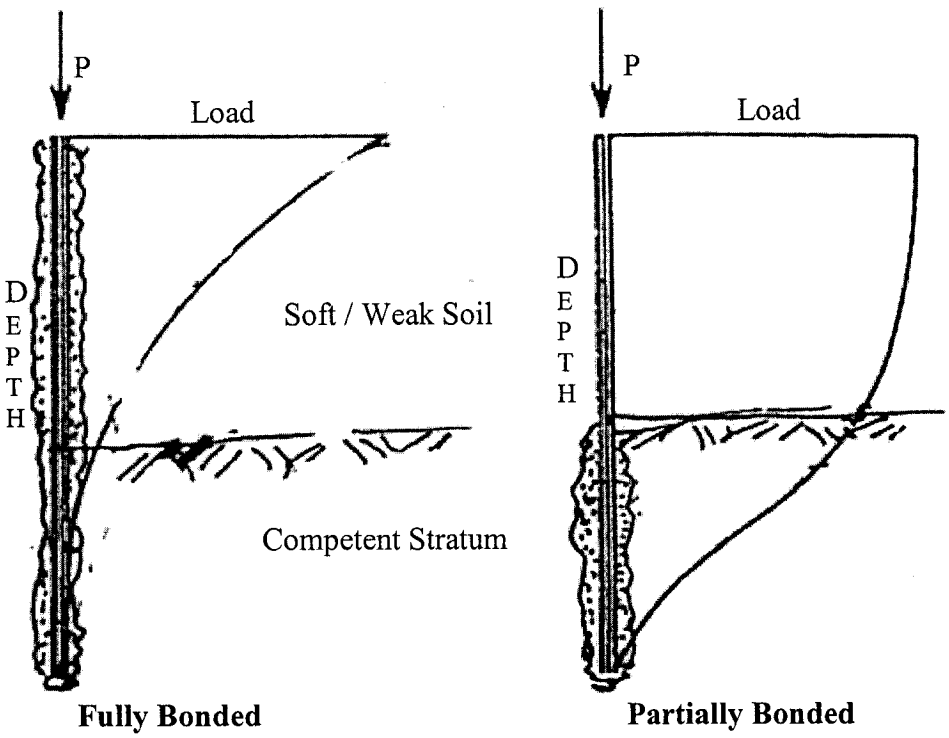

Figure 2.5. Typical load-transfer from micropile to soil (FHWA, 1997).

For the pile capacity evaluation, it is very important to define correctly the extension of the bonded zone because the "partially bonded" design concept generally results in an over conservative design and leads to overestimating head movement under applied loadings.

The prime objective of establishing grout/ground interface parameters is to provide the design engineer with rational methods for:

a) Estimating the capacity of the individual micropile and the micropile system under both axial and lateral loading.
b) Short-term movement control.
c) Evaluation of time-dependent (creep) effects on the long-term performance of the individual micropile and the micropile system.

Modeling the load-displacement behavior of micropiles in soils involves knowledge of the mechanical characteristics and constitutive equations of the soil and the micropile, a realistic estimation of the initial state of stresses in the ground after micropile installation, the effect of micropile installation on the properties of the surrounding soil, and a rational approach to select representative grout/ground interface parameters.

In the general case, when micropiles are subjected to compressive axial loading, the load carrying capacity Q will be transferred to the soil by both the shaft resistance Q_S and the end-bearing Q_P (Hanna and Nguyen, 2003).

$$Q = Q_S + Q_P$$

Many studies on load test demonstrated that micropiles transfer the load mostly through the shaft (Koreck, 1978; Massad et al., 1981; Sabini and Sapio, 1981; Rocha et al., 1985; Brandl, 1988; Carvalho et. al, 1991).

Niyama et al. (1981) suggested that small displacements are enough for the mobilization of the maximum resistance through unit shaft resistance for micropiles, in opposition to the tip that is mobilized totally only after major displacements.

Koreck (1978) stated that due to their small diameter, micropiles have very small or no resistance mobilized at the tip, which causes an abrupt failure when the maximum resistance is reached, even after small displacements. For micropiles with diameter inferior to 30 cm the load transfer is mostly through the shaft. According to Bustamante and Doix (1985) the tip resistance, in general, doesn't exceed 15% to 20% of the shaft resistance.

Sabini and Sapio (1981) analyzed the results of two instrumented load tests on micropiles installed in volcanic ground with two support conditions: floating and fixed in the tip. They acknowledged that both of them presented the same behavior in relation to the curve load versus displacement and distribution of load along the shaft and tip; the shaft resistance surpassed by far the tip resistance; and under the maximum test load (700 kN) the tip resistance was not, yet mobilized.

According to Das (1999) the pile tip must attain a displacement of 10 to 25% of the pile diameter for full mobilization of the point resistance; and according to Niyama et al. (1981) small displacements are enough for the mobilization of the maximum unit shaft resistance while the unit point resistance is only mobilized totally after bigger displacements.

FHWA (1997) declared that due to the slenderness of the micropiles, any end-bearing effect is negligible and the total applied load is considered to be transferred to the soil only through the shaft resistance Q_S, generated through the unit shaft resistance and/or adhesion mobilized at the grout/ground interface, and estimated as:

$$Q_S = \pi \bullet D \bullet \sum_{i=1}^{m} f_{si} \bullet dl_i$$

Where:

f_{si} = ultimate unit shaft resistance for the soil layer i (in kPa).

D = effective diameter of the micropile (in m).

m = number of soil layers.

dl_i = depth of considered layer (in m).

In accordance with the micropile type and soil type the following methods are available for the geotechnical evaluation of the ultimate axial loading capacity of micropiles.

For micropiles type A in cohesionless soils the unit shaft resistance along drilled shafts is commonly evaluated using the β method (FHWA, 1997):

$$f_s = \beta \bullet \sigma'_{vz}$$

Where σ'_{vz} is the vertical effective stress at depth z and the general expression for β is:

$$\beta = K \bullet \tan\delta$$

Where:

β = proportionality coefficient.

K = coefficient of earth pressure at the wall of the drilled shaft at side shear failure.

δ = angle of soil/pile friction.

Several relationships of β vs. depth have been proposed (FHWA, 1997; and Jeon and Kulhawy, 2001), however there is no unique relation because the results are strongly affected by various factors.

Referring to a fine silty sand initially normally consolidated with an effective angle of shearing strength of $\phi = 30^{\circ}$, Hassan and O'Neill (1994) assumed that $K = K_o$ (coefficient of earth pressure at rest) and $\delta = \phi$, and proposed the following relationship:

$$\beta = K_o \bullet \tan\phi$$

Where the profile K_o is computed using the method proposed by Mayne and Kulhawy (1982), in which for simple loading/unloading:

$$K_o = (1 - \sin\phi) \bullet OCR^{\sin\phi}$$

Where OCR refers to the over-consolidation ratio.

Touma and Reese (1974) suggested that for drilled shafts of a diameter of 0.6 m or greater in fine to medium sand, a K value of about 0.7 would correspond to O'Neill and Hassan's recommendations and to a conservative envelope of the β values reported by various authors. The design of micropiles (with a smaller diameter) requires an appropriate database for a proper determination of the adequate K (or β) value.

For micropiles type A in cohesive soils and soft rocks, the unit shaft resistance for large-diameter drilled shafts can be evaluated from a total stress analysis using the α concept introduced by Tomlinson (1957). In general practice in the United States, the ultimate unit shaft resistance f_s is evaluated from a single soil parameter, the undrained shear strength s_u as:

$$f_s = \alpha \bullet s_u$$

Where α is a lumped constant of proportionality that depends on several factors. There are many empirical correlations between α and s_u proposed by various authors with great disparity and they have been established for large-diameter drilled shafts.

The effect of micropile construction techniques and the scale effect, due to small diameters, have not yet been sufficiently investigated. However, as indicated by Bruce (1994), micropiles are often designed satisfactorily with α values between 0.6 and 0.8.

For micropiles type B in cohesionless soils the shaft resistance is commonly estimated using:

$$Q_S = \pi \bullet D \bullet \sum_{i=1}^{m} f_{si} \bullet dl_i$$

Where:

f_{si} = ultimate unit shaft resistance for the soil layer i.

D = effective diameter of the micropile.

m = number of soils layers.

dl_i = depth of considered layer.

With the following expression for the ultimate unit shaft resistance:

$$f_s = p_g \bullet \tan\phi'$$

Where:

p_g = grout pressure.

ϕ' = effective angle of shearing resistance of the soil, usually obtained from empirical correlations of SPT vs. ϕ.

The β method used for Type A micropiles has been generalized to account for pressure grouting in Type B micropiles. The generalized β expression is given by:

$$\beta = K_1 \bullet K_2 \bullet \tan\phi'$$

Where:

K1 = earth pressure coefficient.

K2 = coefficient representing the increase in effective diameter of the pile shaft due to grouting pressure.

Littlejohn (1970) has suggested values for K_1 that range between 1.4 and 1.7 for compact dune sand ($\phi'= 35^o$) and compact sandy gravel ($\phi'= 40^o$), with K_2 varying between 1.2 and 1.5 for very dense sand, 1.5 and 2 for medium sand, and 3 and 4 for coarse sand and gravels.

Littlejohn (1980) suggests a combined K' factor as K_1 x K_2. FHWA (1997) recommends combined K' values ranging from 4 to 7 for Type B micropiles installed in fine to medium sands to fine to coarse sands and gravels, of the normal range of densities, using low-pressure Type B techniques with grouting pressures around 0.2 to 0.35 Mpa.

For micropiles type B in cohesive soils and weak rocks the design rules used for Type A apply.

For micropiles types C and D high-pressure grouted micropiles are installed under effective grout pressures exceeding 1 Mpa using regrouting or selective grouting techniques. The high-pressure grouting may result conceptually in a grout root (or fissure) system that mechanically interlocks with the surrounding ground, increasing substantially the axial loading capacity of the micropile.

The effect of pressure injection on the grout/ground is difficult to evaluate, and some empirical relationships were developed by Ostermayer and Sheele (1978).

In cohesionless soils the shaft resistance Q_s of micropiles with a grouted diameter of 0.10 to 0.16 m is obtained by the curves published by Ostermayer and Sheele (1978).

In the French specification (CCTG, 1993), the ultimate unit shaft resistance is determined by the following equation:

$$f_s = \min\left(\frac{q_c}{\beta_c}, q_{s\max}\right)$$

Where:

f_s = unit shaft resistance.

q_c = CPT resistance at the depth considered.

β_c, q_{smax}= coefficients given in Table 2.1 as a function of the soil and pile type.

The pullout capacity and shaft side resistance of the high-pressure post-grouted anchors or micropiles is estimated using the relevant Q_i curve given in Table 2.3 for different types of soil.

To estimate the unit shaft resistance, at a depth z below the ground surface, for axially loaded vertical drilled piles from pressuremeter test results, the CCTG specifies that, the modified limit pressure p_l^* must be calculated as follows:

$$p_l^* = p_l - u - K_o \bullet \sigma'_{vz}$$

Where:

p_l = limit pressure given by pressuremeter test.

u = pore-water pressure.

σ'_{vz} = effective vertical stress at the depth considered.

K_o = coefficient of earth pressure at rest.

Table 2.1.Choice of β_c and q_{smax} coefficients (CCTG, 1993).

Pile Type		**Silts – Clays**					**Sands - Gravel**	
		A	**B**		**C**		**B**	**C**
Bored	β	-	-	75[1]	-	-	200	200
	q_{smax} (kPa)	15	40	80[1]	40	80[1]	-	120
Bored with casing (withdrawn)	β	-	100	100[2]	-	100[2]	250	300
	q_{smax} (kPa)	15	40	60[2]	40	80[2]	40	120

Note: [1]Reaming and grooving before pouring concrete.

[2]Drilling in the dry, without rotating the casing.

The notation A, B, C indicates different types of soil according to Table 2.2.

The f_s value can then be obtained for a given modified limit pressure p_l^* considering the relevant Q_i curve as illustrated in Figure 2.6.

These design guidelines have been incorporated in the FHWA (1984) recommendations for the use of pressuremeter test results in pile design practices.

Table 2.2. Soil classification after CCTG (1993).

Soil Type		**Pressuremeter p_l (MPa)**	**CPT resistance q_c (MPa)**
Clays, Silts	A – Soft Clays and Silts	< 0.7	< 0.3
	B – Stiff Clays and Silts	1.2 – 2.0	3.0 – 6.0
	C – Very Stiff Clay	> 2.5	> 6.0
Sand, Gravel	A – Loose	< 0.5	< 5
	B - Dense	1.0 – 2.0	8.0 – 15.0
	C – Very Dense	> 2.5	> 20.0
Marls	A - Soft	1.5 – 4.0	-
	B - Compact	> 4.5	-

Table 2.3. Determination of Q_i curve after CCTG (1993).

Micropile Type		**Clay, Silt**			**Sand, Gravel**			**Chalk**			**Marls**		**Rocks**
		A	**B**	**C**	**A**	**B**	**C**	**A**	**B**	**C**	**A**	**B**	
Type A	drilled - dry	Q1	Q1 Q2	Q2 Q3	-			Q1	Q3	Q4 Q5	Q3	Q4 Q5	Q6
	drilled – with mud	Q1	Q1 Q2		Q1	Q1 Q2	Q2 Q3	Q1	Q3	Q4 Q5	Q3	Q4 Q5	Q6
	drilled – with casing retrieved	Q1	Q1 Q2		Q1	Q1 Q2	Q2 Q3	Q1	Q2	Q3 Q4	Q3	Q4	-
	drilled – with casing left in place	Q1			Q1		Q2		-		Q2	Q3	-
Type B	injected – low pressure	Q1			Q3			Q2	Q3	Q4	Q5		-
Type C	injected – high pressure	-	Q4	Q5	Q5		Q6	-	Q5	Q6	Q6		Q7

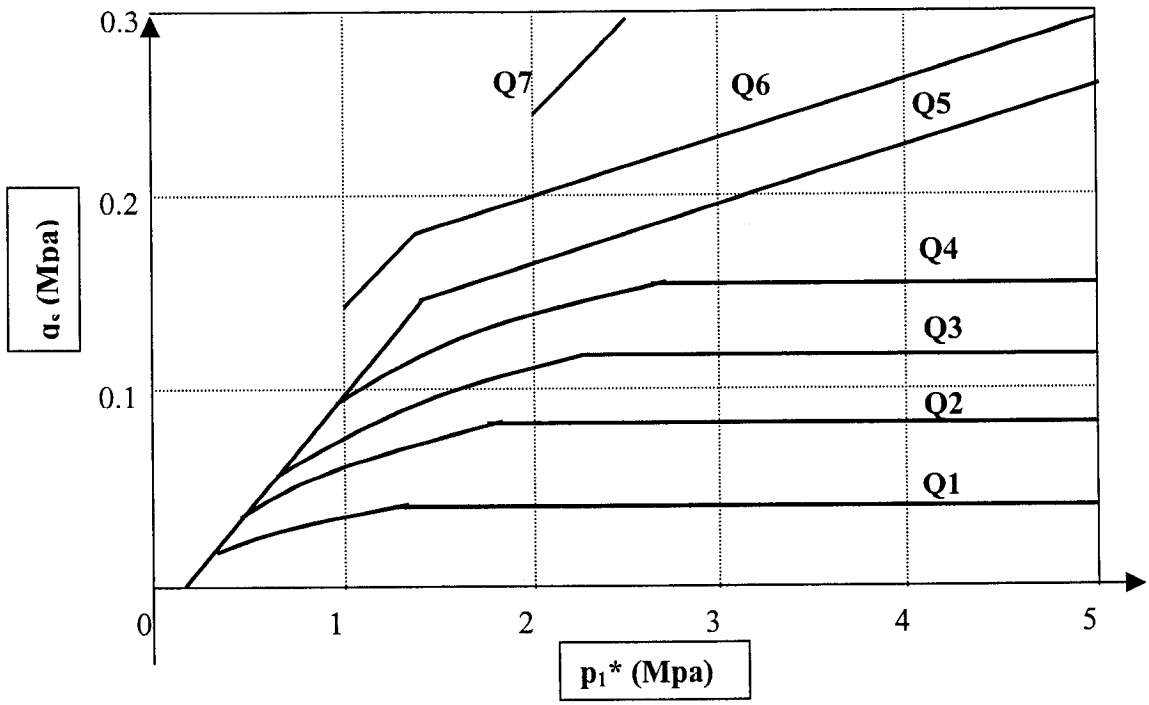

Figure 2.6. Limit unit shaft resistance, $q_s = f_s$ (after CCTG, 1993).

In cohesive soils the unit shaft resistance f_s may be determined as follows:

$f_s = \min [f_{s(p)} \text{ or } f_{s(s)}]$

Where:

$f_{s(p)}$ = ultimate unit shaft resistance in kN/m^2 due to primary grouting pressure extrapolated from the curves published by Ostermayer (1975).

$f_{s(s)}$ = ultimate unit shaft resistance in kN/m^2 due to secondary grouting pressure extrapolated from Ostermayer's (1975) curves.

For Types C and D piles installed in clays, there is no readily available or recognized method of design that enables the axial loading capacity of micropiles to be theoretically determined taking into account the post-grouting effect.

Table 2.4 attempts to summarize the available recommendations outlined by different authors for the preliminary estimate of the axial loading capacity of different types of micropiles in cohesionless and cohesive soils and rocks.

Table 2.4. Recommendations for preliminary design of micropiles.

Soil Type	**Type A** **Tremie-grouted**	**Type B** **Pressure-grouted**	**Types C and D** **Post-grouted**
Cohesionless	β method $f_s = \beta \cdot \sigma'_{vz}$ $\beta = K \cdot \tan\phi$ $K = K_o = (1-\sin\phi) \cdot OCR^{\sin\phi}$ K = 0.7 (Touma and Reese, 1974)	$f_s = p_g \cdot \tan\phi'$ $f_s = \beta \cdot \sigma'_{vz}$ $\beta = K_1 \cdot K_2 \cdot \tan\phi'$ K_1 = 1.4 to 1.7 K_2 = 1.2 to 4 → 1.2 – 1.5 DS; 1.5 – 2.0 MS; 3 – 4 G K = 4 to 7	Ostermayer and Scheele, 1978 CCTG, 1993
Cohesive	α method $f_s = \alpha \cdot s_u$ α = 0.6 to 0.8 (Bruce, 1994)	Similar to Type A	Ostermayer, 1975 with and without post-grouting. CCTG, 1993.

Note: DS = dense sand, MS = medium sand and G = gravel.

Jeon and Kulhawy (2001) examined twenty-one full-scale field tests on micropiles and synthesized the results in a convenient design procedure that incorporates both estimated axial displacements and soil properties (for cohesive and cohesionless soils).

The database was used to estimate the load-displacement behaviour by modeling with the following hyperbolic curve:

$$P = \frac{\Delta}{a + m_c \bullet \Delta}$$

Where:

P = applied load.

Δ = butt displacement.

a & m_c = curve fitting parameters.

The undrained shaft resistance in cohesive soils was evaluated by the alpha method:

$$Q_s = \pi \bullet D_s \bullet \alpha \bullet \int_0^D s_u(z)dz$$

Where:

α = lumped constant of proportionality.

D_s = shaft diameter.

s_u = undrained shear strength.

z = depth.

The axial compression capacity is given by the L_2 method (Hirany and Kulhawy, 1988,1989), and the value of α is back calculated from the load test results as follows:

$$\alpha = \frac{Q_{s(L2)}}{\pi \bullet D_s \bullet L_s \bullet s_u}$$

Where:

$Q_{s(L2)}$ = interpreted shaft resistance using L_2 method.

D_s = shaft diameter.

L_s = shaft depth.

s_u = mean undrained shear strength over depth D.

For cohesionless soils the drained shaft resistance was given by the β method:

$$Q_s = \pi \bullet D_s \bullet \left(\frac{K}{K_0}\right) \bullet \int_0^D \sigma'_{vz}(z) \bullet K_0(z) \bullet \tan\left[\frac{\phi' \bullet \delta}{\phi'}\right] dz$$

Where:

$\frac{K}{K_0}$ = factor that represents the change in the in-situ stress by construction method.

$\frac{\delta}{\phi'}$ = interface roughness factor.

σ'_{vz} = vertical effective stress.

ϕ' = effective angle of shear strength.

The coefficient of earth pressure at rest was calculated as:

$$K_0 = (1 - \sin\phi') \bullet OCR^{\sin\phi'}$$

The value of K/K_0 has not been calibrated for micropiles (Jeon and Kulhawy, 2001), so a value of 1.0, which is based on good quality construction for drilled shafts, was used for first-order estimation.

The field average proportionality coefficient (β_m) was computed as:

$$\beta_m = \frac{Q_{s(L2)}}{\pi \bullet D_s \bullet L_s \bullet \sigma'_{vm}}$$

Where:

σ'_{vm} = mean vertical effective stress.

And the predicted beta (β_p) was computed as:

$$\beta_p = K_0 \bullet \left(\frac{K}{K_0}\right) \bullet \tan\left[\frac{\phi' \bullet \delta}{\phi'}\right]$$

The results showed that micropiles can have a significant increase in capacity over larger-diameter drilled shafts at shallower depths with $L_s/D_s < 100$. At greater depths where L_s/D_s is approximately greater than 100, micropiles and drilled shafts appear to have similar capacity.

The predicted unit shaft resistance by drilled shaft calculations was compared to the calculated field average, but there was no test of the model with a different database, finite element or model tests.

According to FHWA (1997), the grouting operation has substantial control over subsequent micropile capacity. Its effects may extend beyond the confines of the drill hole by permeation, densification, or fissuring, or a combination of all these processes.

The load-transfer mechanism for types B and D is commonly assumed similar to those governing the performance of ground anchors (Ghaly and Hanna, 1994). Better geotechnical evaluation requires appropriate determination of the grout/ground interface parameters and the initial state of stress in the ground after micropile installation.

The grain size and porosity govern the grout penetrability. In sands, gravel and weathered rocks, with permeabilities of 10^{-3} to 10^{-4} m/s, grout will permeate through the pores or natural fractures of the ground. In fine-grained cohesionless soils (silt and fine sands), with permeability less than 10^{-5} m/s, the grout cannot penetrate the small pores, but rather compacts locally, under pressure, in the surrounding ground. Increasing the grout pressure will induce a greater radius of grout permeation into the ground and/or a more effective ground densification, that combined with the beneficial effect that such grouting pressure might have on the interface conditions, can result in a significant improvement of the grout/ground interface properties. Consequently, under high-pressure grouting, high radial stresses are locked into the soil surrounding the micropile, increasing its axial capacity. (FHWA, 1997)

Frank (1971), Bruce and Yeung (1984), Salioni (1985) and, Moreno and Marco (1989) pointed out that as a consequence of the construction method, mostly due to the pressure injection, there is an increase on the cross-section of micropiles. Salioni (1985) considers that the final diameter of the micropile is between 20% and 25% greater than the diameter of the perforation tube. For Bustamante & Doix (1985), this value changes according to the type of soil, and can be between 10% and 40%.

FHWA (1997) acknowledged that on micropiles type B additional grouting is injected (after the primary grout) with pressures usually between 0.3 Mpa and 1 Mpa through the casing, to enhance subsequent grout/soil bond characteristics. The operation may be limited to the load transfer length or be extended to the full length of the pile.

When pressure grouting in granular soils, a certain amount of permeation and replacement of loosened soil takes place. In addition a phenomenon known as "pressure filtration" occurs, wherein the applied grout pressure forces some of the integral mixing water out of the cement suspension and into the surrounding soil. This process leaves behind a grout of lower water content than what was injected; it's thus quicker setting and has a higher strength. It also causes the formation of a cake-like cement paste along the grout/soil interface that improves bond. In cohesive soils, some lateral displacement, compaction, or localized improvement of the soil can occur around the bond zone, although the effect is generally less well marked than for cohesionless soils.

Pressure grouting also appears to cause a recompaction or redensification of the soil around the borehole and increases the effective diameter of the pile in the bond zone. These mechanisms effectively enhance grout/soil contact, leading to higher unit shaft resistance values and improved load/movement performance.

Bustamante & Doix (1985) presented a table with correction factors (α_c) for the final diameter of the micropiles according to the type of soil (Table 2.5).The effective micropile diameter is estimated using a correction factor α_c that allows for radial expansion due to pressure grouting:

$$D = \alpha_c \bullet D_o$$

Where:

D = effective pile diameter.

α_c = diameter correction factor.

D_o = diameter of the drilled hole.

Table 2.5. Correction coefficient α_c for micropiles type B (Bustamante & Doix, 1985).

Type of soil	α_c
Gravel	1.3-1.4
Sandy gravel	1.2-1.4
Gravely sand	1.2-1.3
Coarse sand	1.1-1.2
Medium sand	1.1-1.2
Fine sand	1.1-1.2
Silty sand	1.1-1.2
Silt	1.1-1.2
Clay	1.2
Marl	1.1-1.2

FHWA (1997) indicated that in case of type D micropiles during installation is applied a post-grouting technique where additional grout can be injected, with pressures between 2 Mpa and 8 Mpa, via special grout tubes some time after the placing of the primary grout.

It is reasoned that excess water from these mixes is expelled by pressure filtration during passage into the soil, and so the actual placed grout has a lower water content, and therefore higher strength. Three or four phases of injection are not uncommon,

contributing additional grout volumes up to 50 percent of the primary volume. A double packer is used to grout through the tubes from the bottom sleeve upwards.

The high-pressure grouting may result conceptually in a grout root (or fissure) system that mechanically interlocks with the surrounding ground, increasing substantially the axial loading capacity of the micropile. In addition, pressure grouting may increase the nominal cross-section, particularly in the weaker soil layers or near ground level, where natural in situ horizontal stresses are small. The effect of pressure injection on the grout/ground interaction is difficult to evaluate.

The effective micropile diameter is estimated using a correction factor α_c (from Bustamante & Doix , 1985) that allows for radial expansion due to pressure grouting (Table 2.6) as:

$$D = \alpha_c \bullet D_o$$

Where:

D = effective pile diameter.

α_c = diameter correction factor.

D_o = diameter of the drilled hole.

Table 2.6. Correction coefficient α_c for micropiles type D (Bustamante & Doix, 1985).

Soil Type	α_c
Gravel	1.8
Sandy gravel	1.6-1.8
Gravely sand	1.5-1.6
Coarse sand	1.4-1.5
Medium sand	1.4-1.5
Fine sand	1.4-1.5
Silty sand	1.4-1.5
Silt	1.4-1.6
Clay	1.8-2.0
Marl	1.8

2.2.4. INTERNAL STRUCTURAL DESIGN

FHWA (1997) declared that the ultimate axial capacity of a micropile is dictated by the minimum combination of reinforcement and grout shaft diameter. The internal or structural capacity depends mainly on the area of the composite reinforced micropile and strength of the reinforcement provided. The structural analysis is usually based upon available design specifications for steel or for composite construction. An alternative and simplistic approach, which is commonly adopted, is to limit the working stresses. Many codes limit the working structural stresses that can be carried by a micropile. The design in compression is usually given by the equation:

$$Q_W = g \bullet f'_c \bullet A_c + s \bullet f_y \bullet A_y$$

Where:

Q_w = design ultimate axial load.

f'_c = characteristic unconfined compressive strength of the grout (after 28 days).

A_c = area of pile grout.

f_y = characteristic yield stress of reinforcing steel.

A_y = area of steel reinforcement.

g and s = partial factors for the materials that ensure that the mobilized stress levels in the steel and grout are limited to acceptable values (values specified by the design code).

Consistent with Dringenberg and Craizer (1990) research on load tests, there are three different causes for the failure of a pile (Figure 2.7):

- Failure of the ground – Curve 1.
- Buckling of the pile – Curve 2.
- Internal failure of the pile – Curve 3.

In general the buckling of the pile depends of the geometric characteristics and material of the pile, the ground characteristics where the pile stands (mostly the shear resistance) and the load eccentricity. Also, according to Poulos and Davis (1980), the connection conditions on the pile boundaries will be very important in the process of buckling.

Dringenberg and Craizer (1990) acknowledged that micropiles have high slenderness ratios and are submitted to very high loads (due to the high capacity), this can

cause buckling when the pile is poorly confined in the ground. It is therefore important to investigate this behavior.

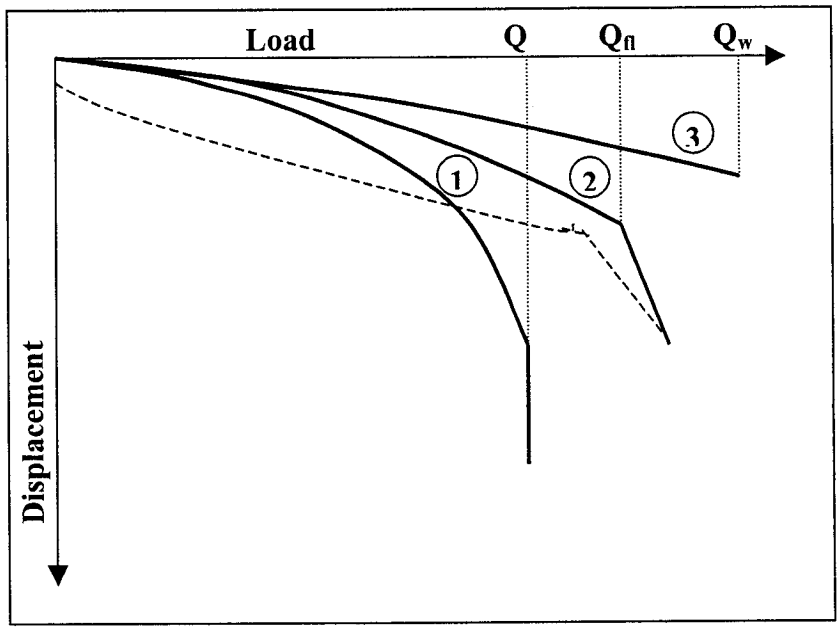

Figure 2.7. Characteristics curves of pile failure (after Dringerberg and Craizer, 1990).

Dringenberg and Craizer (1990) proposed that for micropiles, if not confined, they would buckle when the "Euler Load" is reached on the elastic behavior or failure with the ultimate load. The buckling load will increase, when the pile is confined, because of the lateral support that the ground offers. On this work the authors mentioned two ways of estimating the buckling critical load.

The first method defined the critical buckling load of a column completely compressed with an elastic support C, as "Forsell Load":

$$Q_{fl} = 2\sqrt{C \bullet E_p \bullet I_p}$$

Where:

C = relation load-displacement transversally.

E_p = Young's modulus of the pile.

I_p = moment of inertia of the pile.

For clays or weak soils, without elastic reaction, it offered a relation between C and the undrained cohesion c_u as $C = 20*c_u$.

The second method suggested, for piles with finite length, that the buckling load of a pile fixed at both ends is the sum of the "Euler Load" and the "Forsell Load":

$$Q_{fl} = \frac{4 \bullet \pi^2 \bullet E_p \bullet I_p}{l_{fl}^{\ 2}} + 9\sqrt{c_u \bullet E_p \bullet I_p}$$ (for plastic clays).

And $$Q_{fl} = \frac{4 \bullet \pi^2 \bullet E_p \bullet I_p}{l_{fl}^{\ 2}} + 2\sqrt{C_t \bullet E_p \bullet I_p}$$ (for soils with elastic-plastic reactions).

Where:

E_p = Young's modulus of the pile.

I_p = moment of inertia of the pile.

c_u = undrained cohesion.

l_{fl} = distance between the connections of the pile.

C_t = coefficient of lateral elastic-plastic support.

The length l_{fl} is determined according to:

$$l_{fl} = h + L_1^{\ *} + L_2^{\ *}, \quad \text{being } L_i^{\ *} = \sqrt[4]{\frac{E_p \bullet I_p}{1.4 \bullet E_l}}$$

Where:

h = thickness of the low resistance layer.

$L_1^{\ *}$ = thickness of the layer over the low resistance layer.

L_2^* = thickness of the layer under the low resistance layer.

E_l = deformability modulus of the layers over and under the low resistance layer.

For soft or very soft clays the relationship between c_u and the number of blows N (from SPT tests) is close to linear. For sands or sandy clays the coefficient C is shown in Table 2.7 (where D_L = nominal diameter of the pile).

Table 2.7. Coefficient of lateral elastic-plastic support C (Dringenberg and Craizer,1990).

N	C (kN/m^2)
15	$2,000*D_L$
30	$6,500*D_L$
45	$18,000*D_L$

In accordance with Dringenberg and Craizer (1990) after the buckling by the "Euler-Forsell Load" the gain of load is very small and therefore the limit is really this load.

Mathematical models can be called upon to investigate the stability of micropiles with respect to buckling where the soil Young's modulus E is less than 0.5Mpa. Regarding the former, early work by Bjerrum (1957) is supported by the detailed analyses of Mascardi (1970, 1982) and Gouvenot (1975). These authors conclude that only in soils of the very poorest mechanical properties, such as loose silts, peat, and

unconsolidated clay, is there even a possibility of failure through insufficient lateral restraint.

Stability analysis with respect to buckling can be conducted by adopting the Winkler model for the soil, defined by a horizontal subgrade reaction modulus. This analysis yields the following expression for the critical buckling load:

$$Q_{fl} = n_e^{\,2} \bullet F_{ce} + \frac{l}{n_e^{\,2}} \bullet \frac{f_e^{\,2}}{F_{ce}}$$

Where:

$F_{ce} = \dfrac{\pi^2 \bullet E_p \bullet I_p}{4L^2}$, for micropiles with a free end.

$F_{ce} = \dfrac{\pi^2 \bullet E_p \bullet I_p}{L^2}$, for micropiles with a fixed end.

$f_e = \sqrt{E_p \bullet I_p \bullet E_s}$

$l_0 = \sqrt[4]{\dfrac{4 \bullet E_p \bullet I_p}{E_s}}$

F_{ce} = critical Euler buckling force.

E_p = Young's modulus of the pile.

I_p = moment of inertia of the pile.

E_s = modulus of horizontal subgrade reaction.

L = pile length.

l_0 = transfer length.

n_e = the integer number defining the solution for the elastic deformation of the micropile under the applied load P, which has to be selected to yield to the minimum value of Q_{fl}.

Mandel's (1936) solutions are given by the relationships between the variables ($\phi = P/f_e$) and ($\eta = L/l_0$) for different boundary conditions, as in Table 2.8.

Table 2.8. Solution of Mandel (1936).

Number of curve	**Boundary conditions at the ends**	**Approximate formula for small values of η**	**Approximate formula for high values of η**
1	zero lateral displacement at both ends	$\phi = \frac{\pi^2}{4 \bullet \eta^2} + \frac{4 \bullet \eta^2}{\pi^2}$	$\phi = 2 + \left[\frac{ar\cos(\cos 2\eta)}{\eta}\right]^2$
2	fixed at both ends	$\phi = \frac{\pi^2}{\eta^2} + \frac{3 \bullet \eta^2}{\pi^2}$	$\phi = 2 + \frac{\pi^2}{\eta^2}\left[1 - \frac{\sin 2\eta}{\eta}\right]^2$
3	free	$\phi = \frac{1}{3} \bullet \eta$	$\phi = 1 - \frac{4}{\sqrt{3}}\left[\frac{\sin \eta\sqrt{3}}{e^{\eta}}\right]^2$
4	pile fixed at one end and free at the other end	$\phi = \frac{\pi^2}{16 \bullet \eta^2} + \frac{16 \bullet \eta^2}{\pi^2}\left(3 - \frac{8}{\pi}\right)$	$\phi = 1 + \frac{4}{3}\left[2 + \frac{\cos 2\eta\sqrt{3}}{e^{2\eta}}\right]^2$

According to Nilson and Winter (1979), a member of great slenderness will collapse under a smaller compression load than a robust member of the same cross-sectional dimensions.

Collapse will be caused by buckling, i.e., by lateral bending of the member, with consequent overstressing of steel and concrete by the bending stresses, which superpose on the axial compression stresses.

In the case of exposed micropiles, where there is no support from the soil, Euler's formula for the behavior of straight, concentrically loaded slender columns can be applied as follows:

$$P_{cr} = \frac{\pi^2 \bullet E_c \bullet I_p}{(k \bullet l_c)^2}$$

Where:

P_{cr} = critical load.

E_c = Young's modulus (for columns made of elastic material).

k = coefficient that depends on the kind of connection between the column and the structure.

I_p = moment of inertia.

l_c = length of column.

2.2.5. UNDERPINNING DESIGN

Makarchian and Poulos (1996) developed a design method based on the concepts of pile-raft interaction. They acknowledged that the methods of designing piled-raft foundations can be classified in two broad categories: the conservative, which ignores the presence of the strip or raft, and assumes that the piles carry the total applied load; and the realistic, in which account is taken of the load sharing between the piles and the raft or strip.

This second approach can be classified as:

a) Approximate hand-calculation methods based on the theoretical solution for analysis of a raft and for a pile group in an elastic continuum.

b) Idealization of piles by springs for modified analysis of a plate or a strip on an elastic soil mass.

c) Idealization of the raft and the piles by boundary element analysis, and consideration of the interaction between them based on solutions from the theory of elasticity.

d) Finite element analysis, representing the raft and pile group by a stiffer block (pile-reinforced material) within the soil mass.

e) Finite element analysis, by modeling the raft as a series of plate elements and piles, either as discrete piles or as a series of equivalent concentric rings.

The basic problem is shown in Figure 2.8. The anticipated future settlement, S_{TF}, of a foundation is excessive, and it is desired to underpin the foundation so that its final settlement will be reduced to a tolerable value, S_{TFP}. This approach requires the designer to estimate the stiffness of the existing and the underpinned foundation, the interaction factors among the various foundation elements, and the load distribution among these elements.

The final settlement after underpinning can be estimated by the following equation:

$$S_{TFP} = S_{ti} + \chi(S_{TF} - S_{ti})$$

Where:

S_{TFP} = total final settlement of foundation underpinned by piles.

S_{ti} = total settlement of existing foundation at time t_i of underpinning.

S_{TF} = total final settlement of existing foundation if no underpinning is carried out.

χ = ratio of stiffness of existing foundation to underpinned foundation.

$$\chi = \frac{K_r}{K_{pr}}$$

Where:

K_r = existing raft foundation stiffness, that is, foundation stiffness before underpinning.

K_{pr} = piled-raft stiffness, that is, foundation stiffness after underpinning.

For the total proportion of load in piles after underpinning the following equation is suggested:

$$P_P = \frac{\lambda(S_{TF} - S_{ti})}{S_{TF}} \bullet P_{tot}$$

Where:

P_P = pile load taken by the underpinning piles (at the end of consolidation).

λ = proportion of load carried by underpinning piles in the underpinned foundation, can be obtained by Randolph's equation (Randolph, 1983).

P_{tot} = total applied load on foundation.

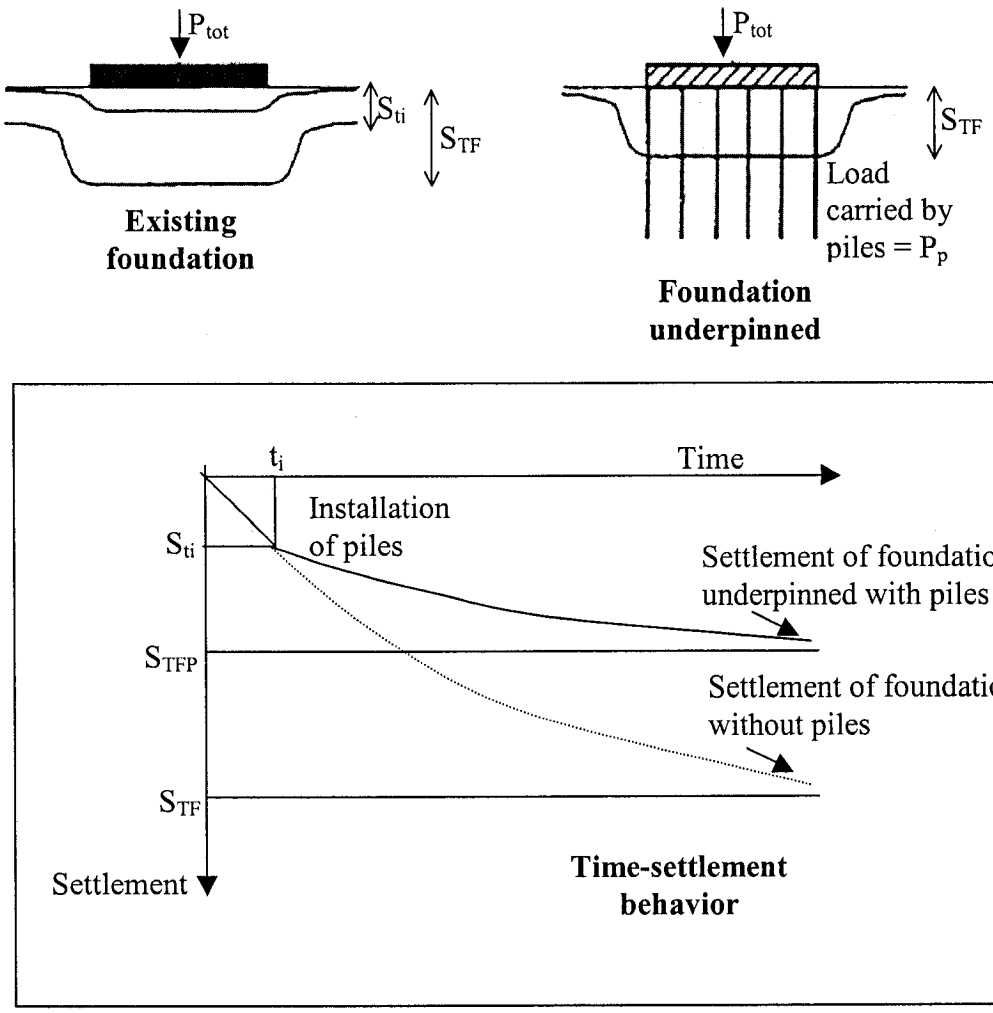

Figure 2.8. Definition of underpinning problem (Makarchian and Poulos, 1996).

For the calculation of stiffness of foundation elements, generally, foundation displacement or pile deformation may be related to the applied load on the foundation by the following equation:

$P_F = K_F \bullet S_F$ or in the matrix form $\{P_F\} = [K_F] \bullet \{S_F\}$

Where:

P_F = footing or pile load.

K_F = footing or pile stiffness.

S_F = foundation displacement.

The footing or pile stiffness can be obtained in different ways according to several authors, among them by computer programs and pile load tests.

Makarchian and Poulos (1994 a & b) have carried out finite element analyses on underpinning of strip foundations, both rigid and flexible (under plane-strain conditions), by piles at either the center or the edge of the foundation (for cohesive soils). Some of these examples have been analyzed by the simplified method described above, and it was found that the method could be used for calculation of settlement reduction by piles and the proportion of load transferred to the piles with reasonable accuracy. Realistic agreement was also found with the results of model footing underpinning tests.

This study was made for piles and not for micropiles, and considerations have to be made for their use in the second case, mostly due to the fact that there is still not a good knowledge concerning groups of micropiles. The method is based on a lengthy research with finite element modeling and controlled model underpinning tests; there are no examples with field load tests. The process is simple and can be hand calculated as affirmed. It was developed for cohesive soils only and there is no mention for cohesionless soils.

CHAPTER 3

NUMERICAL MODELING

3.1. GENERAL

The shaft resistance is the major contributor for the micropiles resistance in carrying the applied load. Micropiles have by definition very small diameters and the tip resistance is almost negligible. Because they are classified as bored piles the design methods of this category has been applied, although they were developed for greater shaft diameters.

There are different methods of execution of micropiles. In North America the most common, are types B and D where pressure is applied during grouting or on post grouting. How the grouting mechanism affects the micropile capacity is still relatively unknown and incorporated in the design, the methodologies available are empirical and based on anchor figures.

This study investigates the applicability and efficiency of the empirical formulations for large diameters bored piles and anchors, evaluates the parameters affecting the shaft resistance and presents a new design procedure.

The research focuses on micropiles that fall under the following specifications (for definitions of pile types, see Section 2.2.1):

a) Pile/soil interaction:

   Type 1, or individual directly loaded piles for axial loading conditions.

b) Grouting technique:

   Type A, grout is placed in the pile under gravity head only.

Type B, when the neat cement grout is injected into the drilled hole as the temporary steel drill casing is withdrawn, and pressures are typically in the range of 0.3 to 1Mpa.

Type D, when neat cement grout is placed in the hole under gravity head, some hours later, when this primary grout has hardened, similar grout is injected via a pre-placed sleeved grout pipe. In this case, a packer is used inside the sleeved pipe so, that specific horizons can be treated several times if necessary, at pressures usually of 2 to 8MPa.

3.2. FINITE ELEMENT MODELS

Micropiles can have different cross-section resultants of different construction methods, and to numerically study them with accuracy it is necessary to account for all the possibilities in the definition of the micropile geometry.

Section 3.2.1 presents in detail the finite element model proposed to study the interaction pile/soil. This model will consider micropiles with uniform cross-sections or with expanded bulbs, and will be validated with field tests and theory.

Section 3.2.2 presents another finite element model, which simulates a cavity expansion caused by grouting pressure. This model will be used to study the relationships between pressure, expansion of diameter, length of expansion, and soil properties; and to validate Table 2.6, necessary for the design of micropiles type D.

3.2.1. MICROPILES SUBJECTED TO AXIAL LOAD

Numerical analysis using finite element techniques is well accepted in the field of geotechnical engineering today as the behavior of the soil can be approximated by the use of an appropriate stress-strain rule applied to discrete elements, and so provides an analytical tool to specify a realistic simplified model.

Program PLAXIS version 8 developed by Delft University of Technology (Brinkgreve, R. B. J., 2001) used in this investigation is a special purpose two-dimensional finite element computer program used to perform deformation and stability analyses for various types of geotechnical applications.

The first step in the numerical analysis with this software is to generate a geometry model and finite element mesh based on a representative vertical cross-section of the situation.

The case of a single pile can be described as a circular structure, with a relative uniform radial cross-section and loading scheme around the central axis, where the deformations and stress state are assumed to be identical in any radial direction (Hanna and Nguyen, 2002). In the 2-dimensional program there are two options of model: plane strain and axisymmetric; in the single pile condition the axisymmetric model where the axis coincides with the axis of the pile is the most adequate and it will have only two degrees of freedom per node (Figure 3.1).

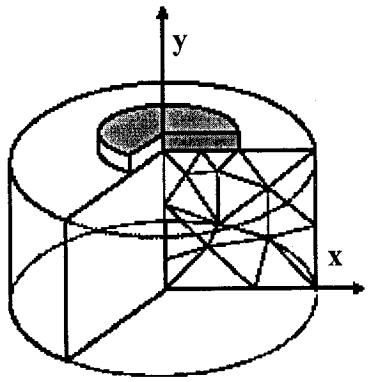

Figure 3.1. Axisymmetrical model of a micropile.

The cross-section of the geometry model was designed in accordance with Randolph and Wroth's (1978) recommendations for the boundary: at least 50 times the pile radius in the lateral direction, and 1.5 times the pile length below the tip in the vertical direction. These boundary conditions are necessary to minimize the boundary effect on the zone around the shaft, not affecting the deformations and providing sufficient accuracy for the analyses.

There are two options presented for the definition of the cross-section, uniform radius (Figure 3.2) and micropile with expanded bulb (Figure 3.3), where L is the pile length, l is the length of the expanded diameter, R is the pile radius and r is the expanded radius.

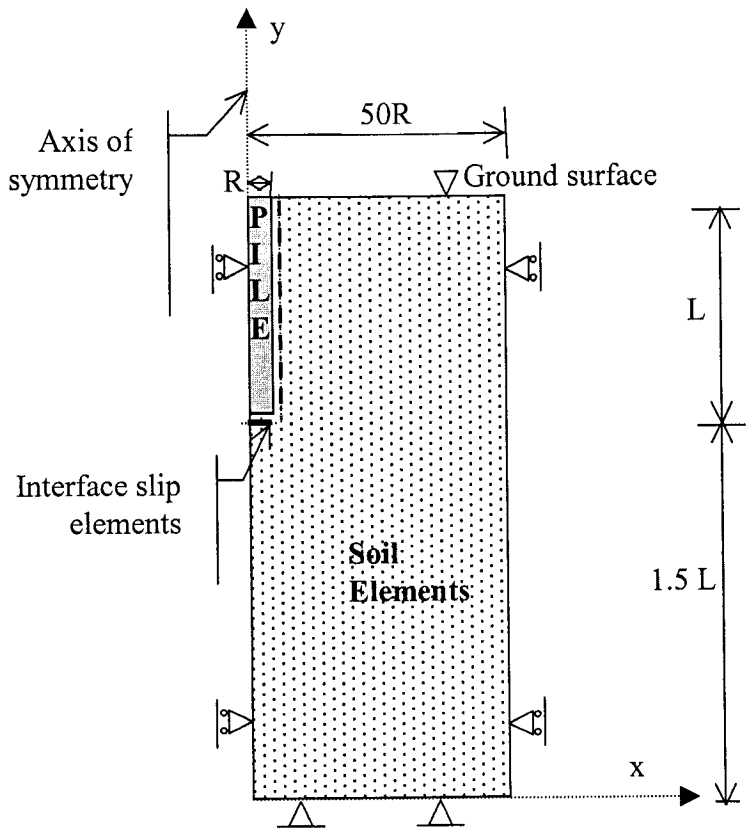

Figure 3.2. Numerical model for pile with a uniform radius.

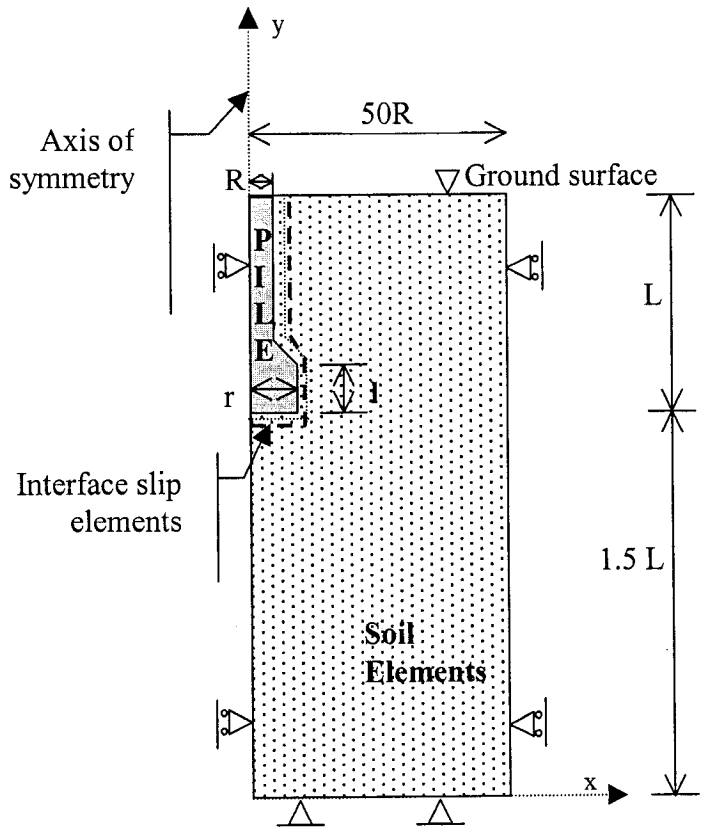

Figure 3.3. Numerical model for pile with an expanded bulb.

It is necessary to impose on the mesh (of an axisymmetric model) that the nodes belonging to the periphery are fixed against displacement in the horizontal direction, but free in the vertical direction; and the nodes on the bottom of the mesh are fixed in both horizontal and vertical directions.

For the mesh, there are two options available, 6-node or 15-node triangular elements to model soil layers. For the 6-node element the order of interpolation for displacements is two and the numerical integration involves three Gauss points (for the stress calculations). The 15-node triangle provides a fourth order interpolation for displacements and the numerical integration involves twelve Gauss (or stress) points.

In this study the 15-node element was chosen because it is a very accurate element that can produce high quality stress results for difficult problems, more adequate for axisymmetric models and failure situations.

The generation of the mesh is based on a robust triangulation procedure, which results in unstructured meshes. These meshes may look disorderly, but the numerical performance of such meshes is usually better than for regular (structured) meshes.

There are five levels of global coarseness for the mesh generation: very coarse, coarse, medium, fine, and very fine. It was chosen a medium global coarseness with around 150 elements in order to have a balance between accuracy and calculation time. The mesh was refined around the pile to be more accurate, where major variations of deformations and stresses are expected (Figure 3.4).

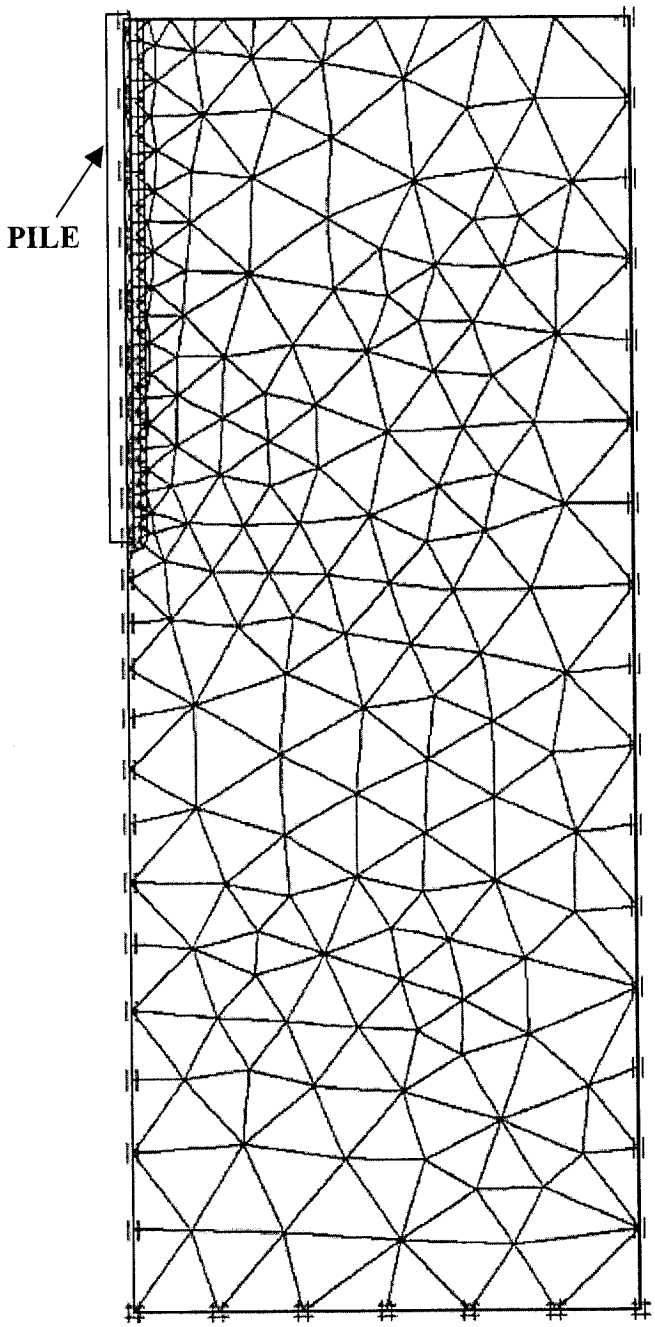

Figure 3.4. Typical finite element mesh.

The interface between soil and pile is modeled with interface elements to allow a relative slippage when the shear stress mobilized on the shaft exceeds the limiting values; Figure 3.5 shows how these elements are connected to soil elements. When using 15-node soil elements, the corresponding interface elements are defined by five pairs of nodes. In the figure, the interface elements are shown to have a finite thickness, but in the finite element formulation the coordinates of each node pair are identical, which means that the element has a zero thickness.

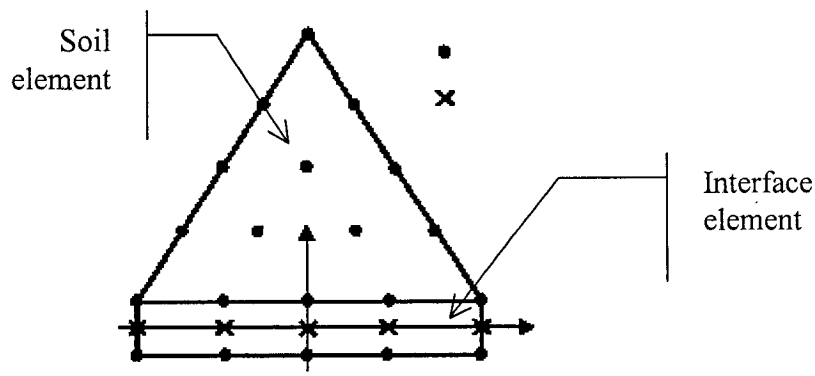

Figure 3.5. Soil/interface elements.

Each interface has assigned to it a 'virtual thickness' which is an imaginary dimension used to define the material properties of the interface. In the model was used a virtual thickness of 0.1 in order to have very little elastic deformations on the interface elements.

The roughness of the interaction pile-soil is modeled by choosing a suitable value for the strength reduction factor in the interface, R_{inter}. This factor relates the interface strength (wall friction and adhesion) to the soil strength (friction angle and cohesion).

The interface properties are calculated from the soil properties in the associated data set and the strength reduction factor by applying the following rules:

$c_{interface} = R_{inter} * c$

$\tan\phi_{interface} = R_{inter} * \tan\phi$

Where:

c = cohesion of the soil.

ϕ = angle of shearing strength of the soil.

$c_{interface}$ = cohesion at the interface soil/pile.

$\phi_{interface}$ = angle of shearing strength at the interface soil/pile.

For rough interface between concrete and soil R_{inter} can be considered 1 and between steel and soil 0.67.

The soil was modeled as Mohr-Coulomb (Brinkgreve, R. B. J., 2001), a model that can be considered as a first order approximation of real soil behavior. This elastic perfectly plastic model requires five basic input parameters: Young's modulus (E), Poisson's ratio (ν), cohesion (c), angle of shearing strength (ϕ), and dilatancy angle (ψ). This model was chosen after its simplicity and facility to adapt when there is little soil data available, the program supports more sophisticated models but they require different soil parameters from more complex laboratory tests.

The pile was modeled as linear elastic non-porous, a model that represents Hooke's law of isotropic linear elasticity. The model involves two elastic stiffness parameters, Young's modulus and Poisson's ratio, that were chosen as $E = 7.e^7$ kN/m^2, a value high enough to assure that the pile will not fail before the soil and $\nu = 0.1$.

For the simulation of load tests a point load (in the negative y-direction) was applied on the top of the pile, exactly on the axis of symmetry. In axisymmetric models, point loads are in fact line loads on a circle section of 1 radian.

After the definition of the model comes the generation of initial effective stress where the pile is deactivated and there is only soil material. The procedure considers only soil weight and calculates effective stresses in soil elements and interfaces. The initial horizontal effective stress $\sigma'_{h,0}$ is related to the initial vertical effective stress by the coefficient of earth pressure at rest, K_0 ($\sigma'_{h,0} = K_0.\sigma'_{v,0}$). The default K_0 value is based on Jaky's formula ($1-\sin\phi$) for normally consolidated soils. When the K_0 procedure is adopted, vertical stresses are generated in equilibrium with the self-weight of the soil.

The next step is the calculation process, which is divided into calculation phases, much like project phases. Each calculation phase is divided into a number of calculation steps because the non-linear behavior of the soil requires loadings to be applied in small proportions, called load steps.

There are many options available for calculations phases in the program; the most appropriate for the case studied is the staged construction where the user can specify a new state that is to be reached at the end of the calculation phase. It is possible to change the geometry and load configurations (activate pile and activate loads).

The load-displacement curves were obtained with two staged construction phases. On the first one the properties of the material on the pile cluster is changed from soil to concrete to simulate the execution of the pile with minimum disturbance of the stresses in the soil. On the second phase the value of the point load is input high enough to assure a satisfactory load versus displacement curve.

During each load step, the equilibrium errors in the solution are successively reduced using a series of iterations. The iteration procedure is based on an accelerated initial stress method. Each phase was executed with as many steps as the program found necessary to keep small the number of iterations required for equilibrium.

In this study, the failure point was determined following the procedure proposed by Davisson (1972). Referring to Figure 3.6:

1. Drawn the load-displacement curve.
2. Drawn a tangent line through the initial points of the load-displacement curve.
3. Drawn a line parallel to the tangent line, at an offset equal to 0.15 + D/120 (where D is the pile diameter in inches).
4. The load corresponding to the intersection of the load-displacement curve and this offset line is the slope tangent load (L_{st}).

Hirany and Kulhawy (1988, 1989) have proposed for micropiles that the failure load should be taken at L_2, estimated as 1.18 L_{st}. There is on average a consistent relationship between L_{st} (the slope tangent value from Davisson, 1972) and L_2 for drilled shafts (Hirany and Kulhawy, 1988), augured cast-in-place piles (Chen, 1998), and pressure-injected footings (Chen, 1998).

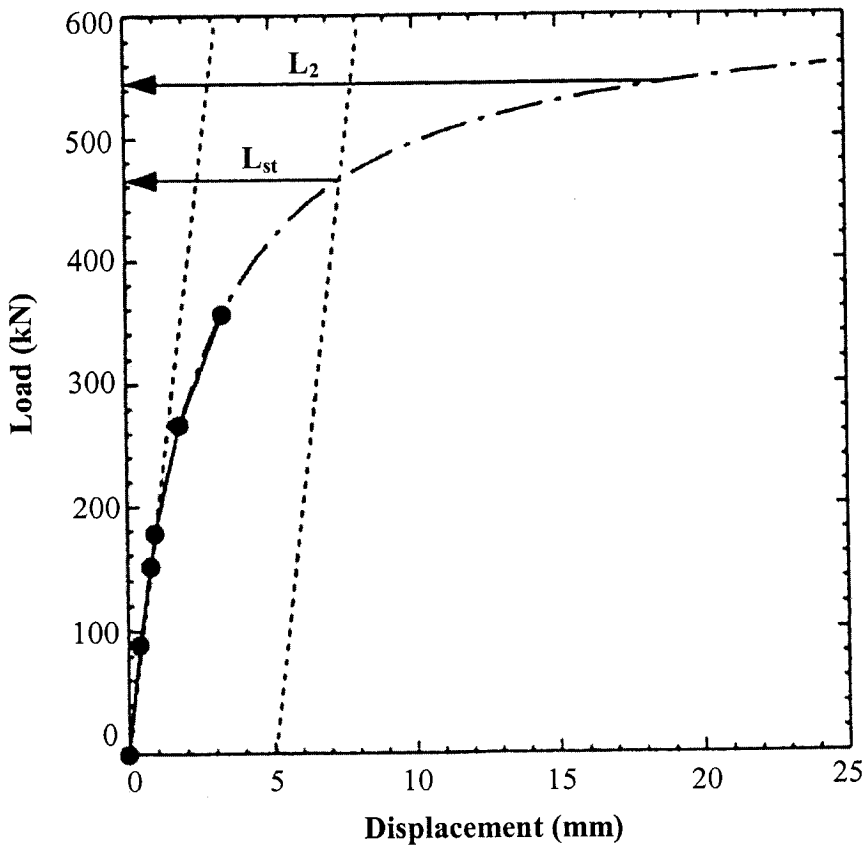

Figure 3.6. Load versus displacement curve. (Davisson, 1972).

3.2.1.1. MODEL VALIDATIONS

To validate the model, 5 full-scale test results (Jeon and Kulhawy, 2001) were used. Tables 3.1 and 3.2 summarize the parameters and the results of these tests. Jeon and Kulhawy (2001) have collected results for type B and D micropiles, where pressure is applied during grouting; as a result the diameter expands. The effective diameter of the piles ($D = D_o * \alpha_c$) was determined in accordance with the recommendations by Bustamante and Doix (1985) in Tables 2.5 and 2.6.

For test number 1 and 2, the micropiles are constructed with the Gewi procedure, where the pressure is not applied on the first 5 to 6 m. The first half of the piles were modeled with diameter 0.15 m and the last half with 0.270 m (coefficient $\alpha_c = 1.8$).

For test number 3, the pressure was applied through the entire depth and therefore the pile was modeled with effective diameter of 0.216 m (coefficient $\alpha_c = 1.2$).

For test number 4, the pressure was only applied on the last 5m, where in the numerical model the diameter was 0.219 m (coefficient $\alpha_c = 1.5$).

For test number 5, the pressure was only applied on the last 3m, where in the numerical model the diameter was 0.204 m (coefficient $\alpha_c = 1.2$).

The material of the soils was modeled with Mohr-Coulomb behavior and the properties according to the data given by Jeon and Kulhawy (2001) (Table 3.1). Since the actual soil properties were limited the average values of effective angle of shearing strength (ϕ'), coefficient of earth pressure at rest (K_o), cohesion (c) and soil unit weight (γ) were estimated by the authors.

The Young's modulus of the soil (E) and Poisson's ratio are necessary input on the numerical model and were estimated according to Das (1999).

The slope tangent values (L_{st}) were obtained graphically at the load versus displacement curves with the same methodology employed by Jeon & Kulhawy (2001) for comparison. The maximum value of the load on these curves is presented on Table 3.1 as test load.

Table 3.1. Soil Parameters used for validation of the numerical model.

Test		Diameter (m)	Shaft Depth (m)	Pile Type	L_{st} (kN)	γ_{unsat} (kN/m^3)	γ_{sat} (kN/m^3)	E (kN/m^2)	ν	c (kN/m^2)	ϕ' (^{o})	K_o	Test Load (kN)
Jones & Turner (1980)	1	0.15	9.0	D	769	19.4	21	6.0.e4	0.30	117	0.0	0.98	1037
	2	0.15	12.0	D	932	19.4	21	7.0.e4	0.30	138	0.0	1.00	1397
Koreck (1978)	3	0.18	10.0	B	476	18.2	20	9.0.e4	0.25	1	32.4	1.30	720
	4	0.15	16.0	D	979	19.2	21	7.0.e4	0.25	1	38.5	1.73	1469
Bruce (1987, 1988)	5	0.17	10.7	B	463	17.3	20	2.0.e4	0.30	1	33.0	1.15	695

Table 3.2. Validation of the numerical model.

Test		Diameter (m)	Shaft Depth (m)	Grout Pressure (kPa)	Pile Type	L_{st} (kN)	L_{st} from Numerical Model (kN)	Error
Jones & Turner (1980)	1	0.15	9.0	1000-1500	D	769	861	-12%
	2	0.15	12.0	1000-1500	D	932	1145	-23%
Koreck (1978)	3	0.18	10.0	600-1000	B	476	509	-7%
	4	0.15	16.0	1500-2000	D	979	1138	-16%
Bruce (1987, 1988)	5	0.17	10.7	414	B	463	361	22%

The results in Table 3.2 show that for micropiles type B, test number 3, the value of the slope tangent load (L_{st}) were very close (7%) to the value obtained by Jeon and Kulhawy (2001), for test number 4 there was a bigger difference (22%) probably because the soil parameters were underestimated by Jeon & Kulhawy (2001), and the effective diameter and respective length were underestimated.

For type D micropiles, the results from the model were higher possibly because of the overestimation of the soil parameters by Jeon & Kulhawy (2001). Overall a difference between the results from the model test results and the values given in the literature is expected due to the difficulties encountered in duplicating the field conditions in the numerical model.

To identify the failure pattern on the numerical model it is necessary to plot the stresses around the pile after the load tests were conducted and the program stopped to increase the load on the calculation phase because the failure was reached. In PLAXIS

there are different outputs of effective stresses; one of them is the relative shear stress (τ_{rel}), which can be plotted as shadings over the geometry model. The relative shear stress, τ_{rel}, option gives an indication of the proximity of the stress point to the Coulomb failure envelope, and is defined as:

$$\tau_{rel} = \frac{\tau}{\tau_{max}}$$

Where τ is the maximum value of shear stress (i.e. the radius of the Mohr stress circle). The parameter τ_{max} is the maximum value of shear stress for the case where the Mohr's circle is expanded to touch the Coulomb failure envelope keeping the intermediate principal stress constant.

Figures 3.7, 3.8, 3.9 and 3.10 show the results of relative shear stresses on intermediary steps of the calculation phase and the final failure state. The figures show the vertical section of the axisymmetric model and the coloured areas representing the values of relative shear stress, when the color is red, τ_{rel} is equal to 1, and can be assumed that failure was reached.

There are two ways for the pile to transfer the load to the ground: through the shaft and through the tip; they are functions of the movement of the pile that generates shear tensions.

In the cohesive soil the failure starts on the tip and expanded upward and laterally around the shaft. In the cohesionless soil, on the other hand the failure started at the top and then at the tip and around the shaft. The different performances can be explained by the fact that on the cohesionless soils the shear strength increases with depth.

It can be noted in case of cohesive soil that the bulb of the failure zone reached the boundary of the finite element mesh. This is due to the fact that in this test the load has exceeded the failure load.

In the entire loading test a large amount of movement was required to generate failure, one of the reasons why micropiles are highly appreciated. In general the failure results confirm the theoretical and experimental observations by FHWA (1997) presented in Chapter 2, Sections 2.2.2 and 2.2.3.

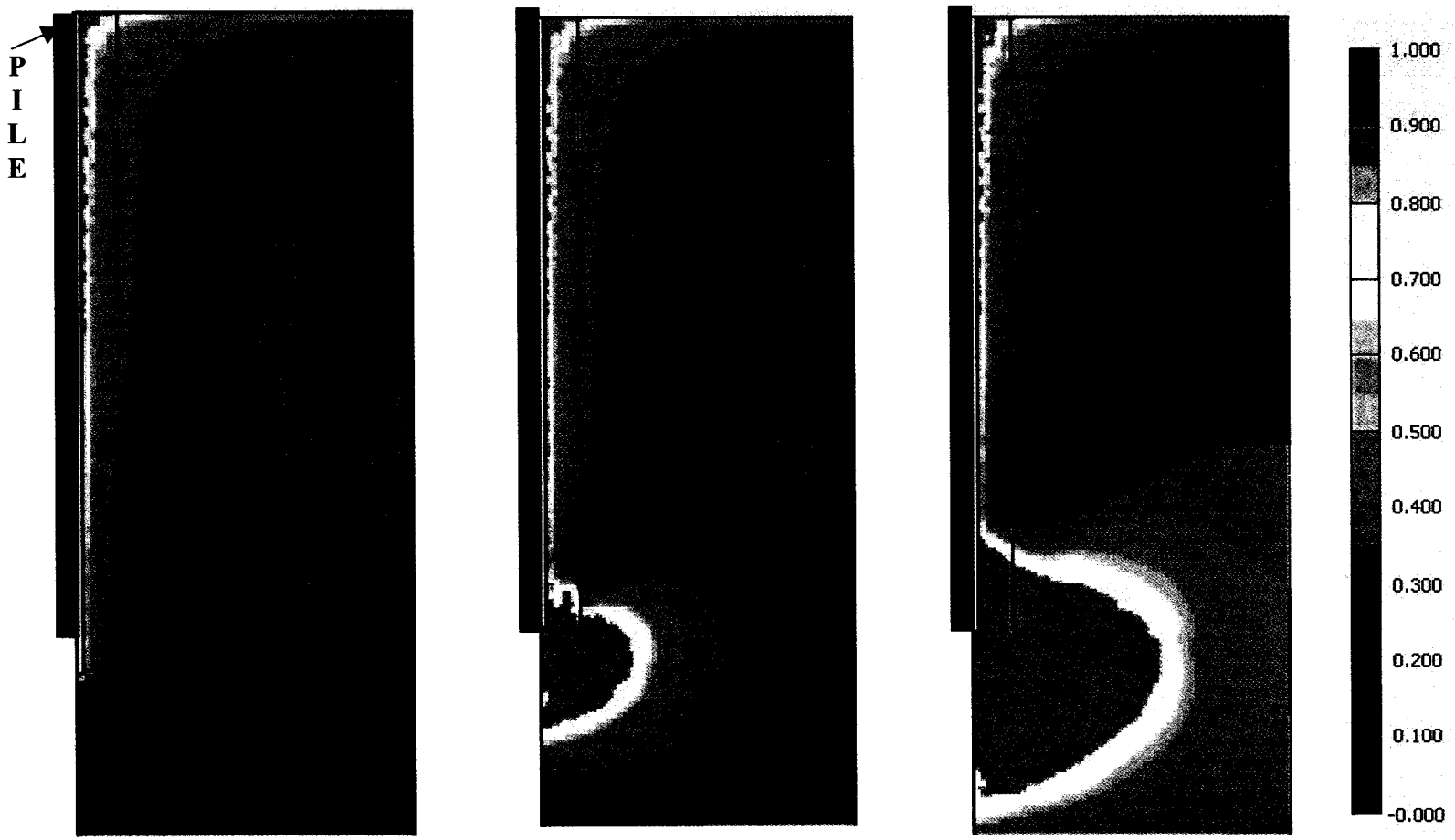

Figure 3.7. Shear stress evolution on sand.

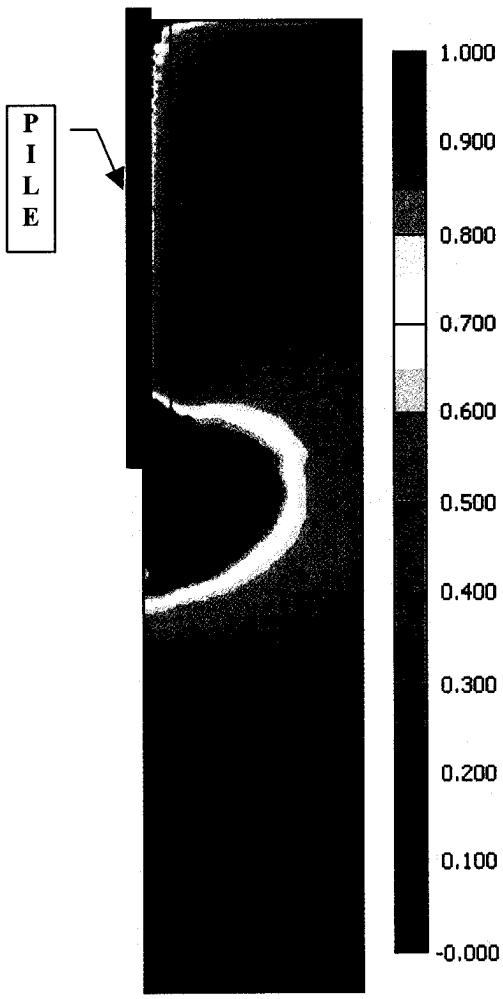

Figure 3.8. Failure pattern on sand.

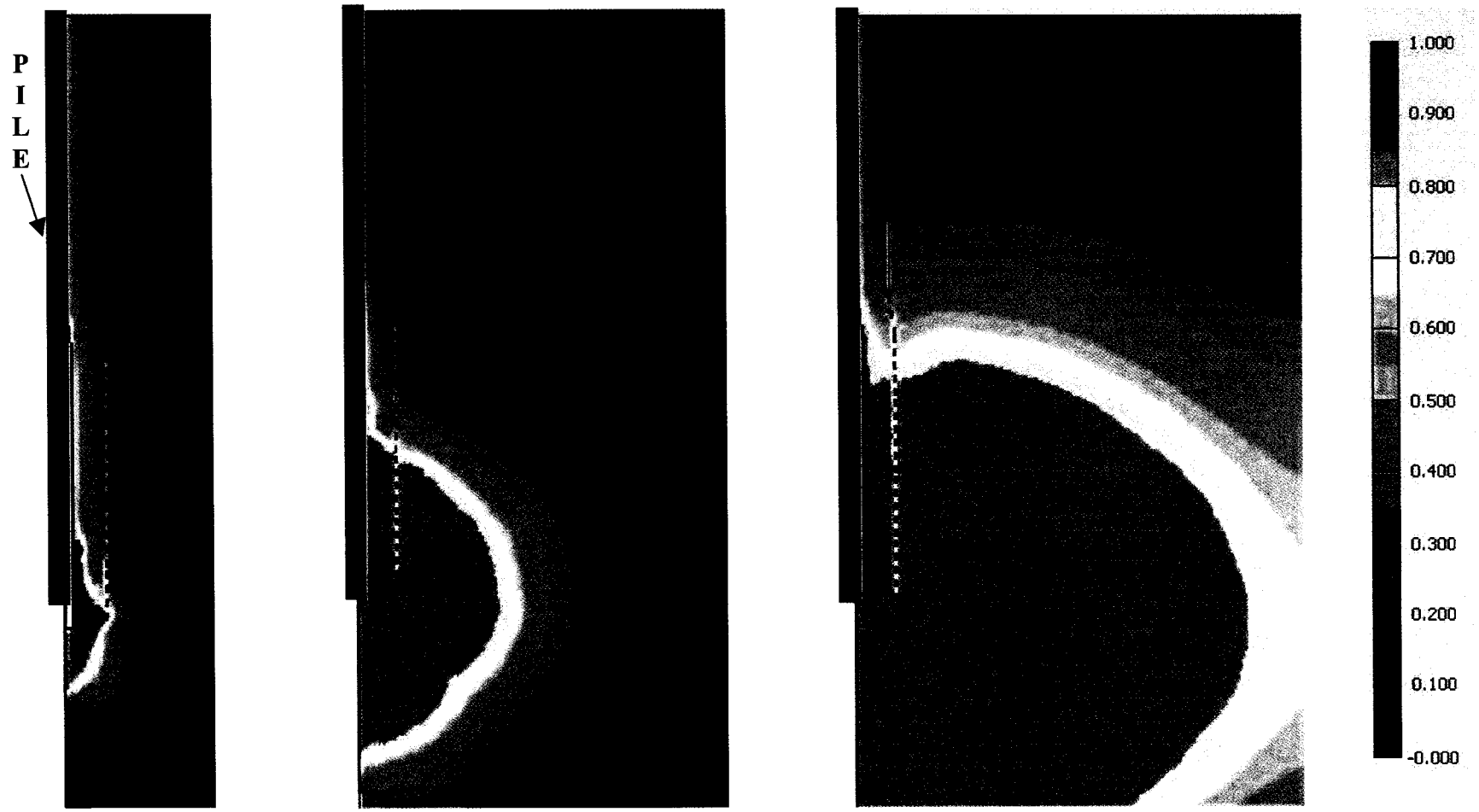

Figure 3.9. Shear stress evolution on clay.

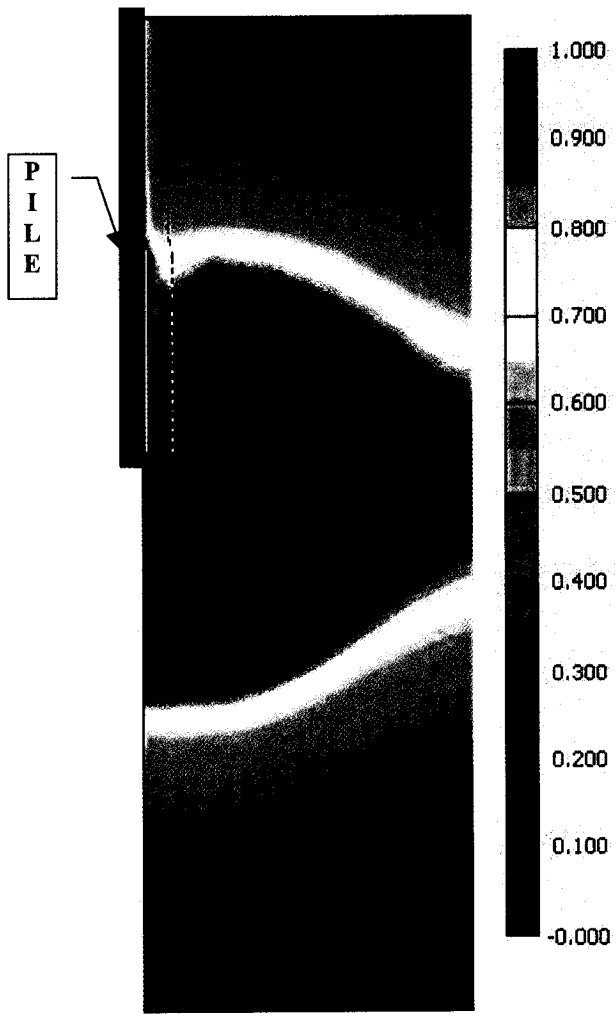

Figure 3.10. Failure pattern on clay.

3.2.2. BULB EXPANSION SUBJECTED TO PRESSURE

A finite element model was developed in this section to analyze the expansion of the micropile's diameter due to the grout pressure and to compare the values of pressure, p, and diameter correction factor, α_c ($D = \alpha_c * D_0$), with the values available from Bustamante and Doix (1985) in Table 2.6.

The problem of expansion of a cylindrical cavity in a finite soil mass has been analyzed for a long time and one of the most accepted theories was developed by Vesic (1972). In this work he presents the problem as an axially symmetrical cavity of initial radius R_i expanded by a uniform internal pressure p. When this pressure is increased, a spherical zone around the cavity will pass into the state of plastic equilibrium. This plastic zone will expand until the pressure reaches an ultimate value p_u. At this moment the cavity will have a radius, R_u, and the plastic zone around the cavity will extend to a radius R_p. Beyond that radius, the rest of the mass remains in a state of elastic equilibrium (Figure 3.11).

The finite element software PLAXIS models the problem of the cylindrical cavity with an axisymmetric mesh as in Figure 3.12. The axisymmetrical model consists of an initial cavity with radius R_i, that is expanded with pressure p to a final radius R_u. The boundary conditions are: on the horizontal limits fixed to vertical displacements, on the vertical right limit fixed for horizontal and vertical displacements and at a distance of at least 128 times R_i.

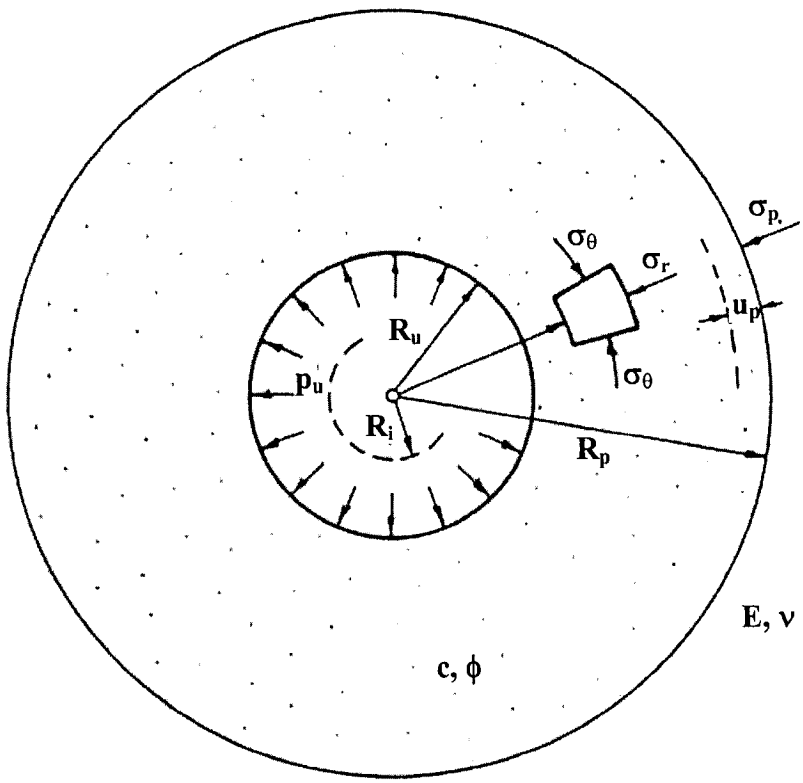

Figure 3.11. Expansion of cavity (after Vesic, 1972).

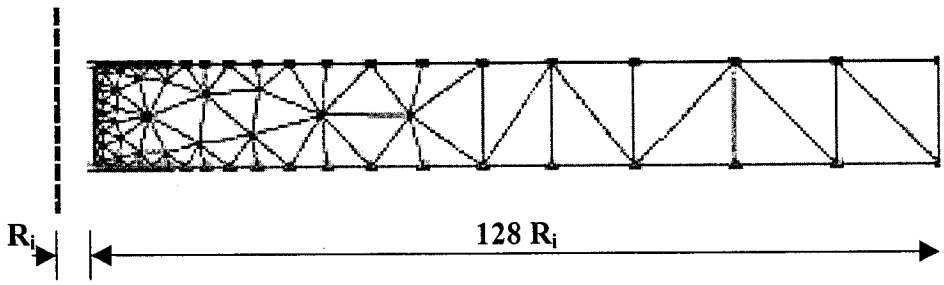

Figure 3.12. Mesh for cavity expansion from numerical model.

The model was calculated for small and large displacements (due to theoretical differences) and the normalized pressure versus normalized radial displacement curve

plotted for comparison with theory. The computed relationships between cavity pressure and radial displacement are given in Figure 3.13. It can be seen that the computed results agree very well with the analytical solutions, therefore this same model adapted for the micropile design will be employed to study the effects of grouting pressure in the expansion of the pile diameter, as a result of compaction originated from the grouting pressure on type D piles.

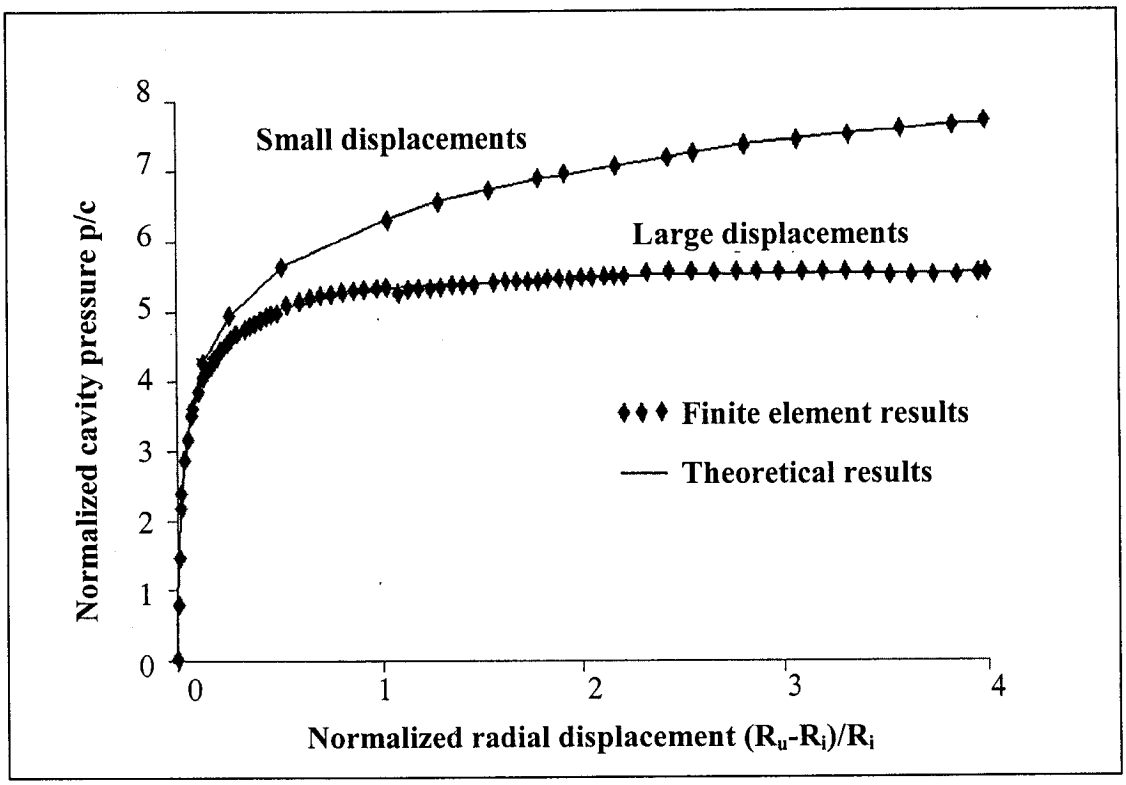

Figure 3.13. Radial displacement versus cavity pressure.

Figure 3.14 presents a sketch of the geometry model employed for this analysis. It is similar to the finite element model described in Section 3.2.1, and consists of an axisymmetrical vertical cross-section that follows the boundary specifications of the

model in Figure 3.12 that was validated with the theory of cavity expansion by Vesic (1972).

The model has a cavity, on the axis of symmetry, of initial radius R = 0.10m and length L = 15m that are the dimensions of the vertical cross-section of the pile. This cavity will be expanded along the length l = 5m to a final diameter r, this is an attempt to reproduce the results from micropiles on site that are usually expanded at the bottom 1/3 of their lengths. To simulate the expansion in the numerical model will be used a tool called prescribed displacements that by definition are special conditions, always with linear distribution, that can be imposed on the model to control the displacements of certain points.

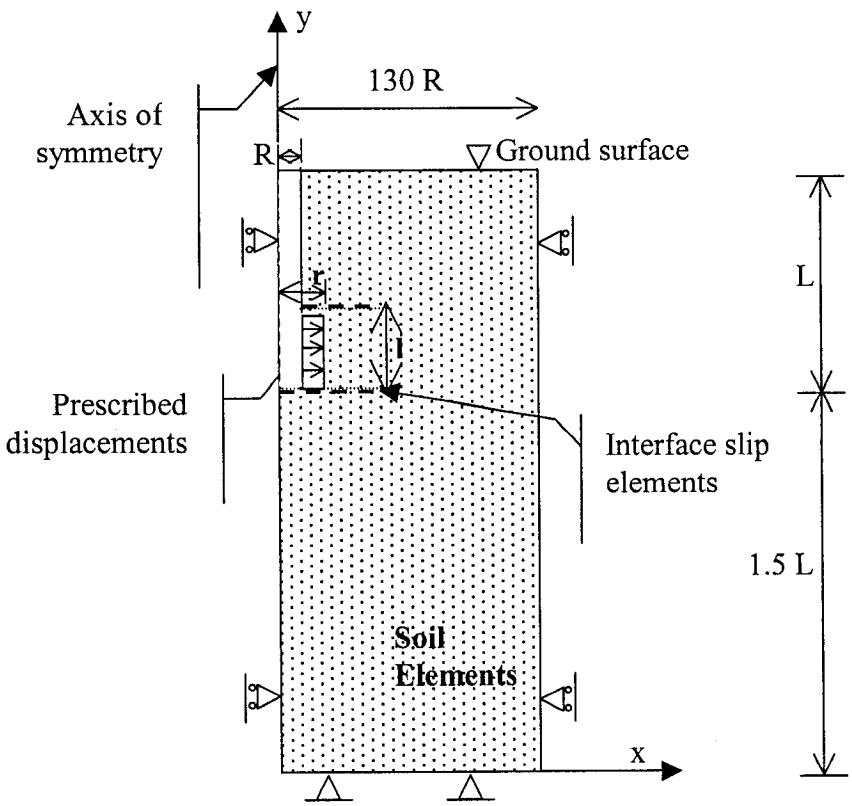

Figure 3.14. Finite element model for grouting pressure study.

For the mesh, 15-node triangle elements were chosen because they provide a fourth order interpolation for displacements and the numerical integration involves twelve Gauss (or stress) points. This proven to provide accurate elements and produce high quality stress results for the problem state. The mesh was defined with medium global coarseness and refined along the length of expansion to be more accurate, where major variations of deformations and stresses are expected.

On the top and bottom of the expansion length there are horizontal lines of interface elements to allow relative slippage between the soil particles without local rupture. Each interface has assigned to it a 'virtual thickness' which is an imaginary dimension used to define the material properties of the interface. A virtual thickness of 0.1 was used in the model in order to have small elastic deformations on the interface elements.

The strength reduction factor in the interface, R_{inter}, was chosen as 1, so as to not affect the properties of the soil in that region. This factor relates the interface strength (wall friction and adhesion) to the soil strength (friction angle and cohesion). For the soil properties it was chosen Mohr-Coulomb model, after its simplicity and facility to adapt when there is few soil data available.

The next step is the calculation process, which for this analysis consists of only one stage of the construction phase where the prescribed displacement value was defined in accordance with the expansion desired. As a result, the numerical model presents the force per unit radian (kN/rad) necessary to reach the displacement desired. In order to obtain the cavity pressure it is necessary to divide the computed force per unit radian

acting on the cavity surface by the thickness of the soil subjected to expansion (l) and the cavity final radius (r).

3.3. PARAMETRIC ANALYSIS

In order to examine the sensitivity of the parameters governing the shaft resistance of micropiles, the first numerical model for micropiles subjected to axial load was used to generate results for a wide range of these parameters (pile length L, pile diameter D, slenderness ratio L/D, angle of shear strength of the soil ϕ, cohesion c, coefficient of earth pressure K_o, and strength reduction factor at the interface soil/pile R_{inter}); and the second numerical model for bulb expansion was used to generate results for grouting pressure p.

Figure 3.15 presents typical load versus settlement curves deduced from the present numerical investigations. It can be noted from this figure that at the ultimate point L_{st} the pile settlement is small, but not enough to mobilize the tip resistance according to Das (1999) and Niyama et al. (1981). Accordingly, in this analysis it was reasonable to assume that the load carrying capacity Q is equal to the shaft resistance Q_s and the end-bearing Q_p is negligible.

The average unit shaft resistance was obtained as:

$$f_{sav} = \frac{Q}{\pi \bullet D \bullet L}$$

Where:

Q = failure load obtained from the curve load versus displacement with the recommendations by Hirany and Kulhawy (1988, 1989) on Figure 3.6.

D = effective diameter.

L = pile length.

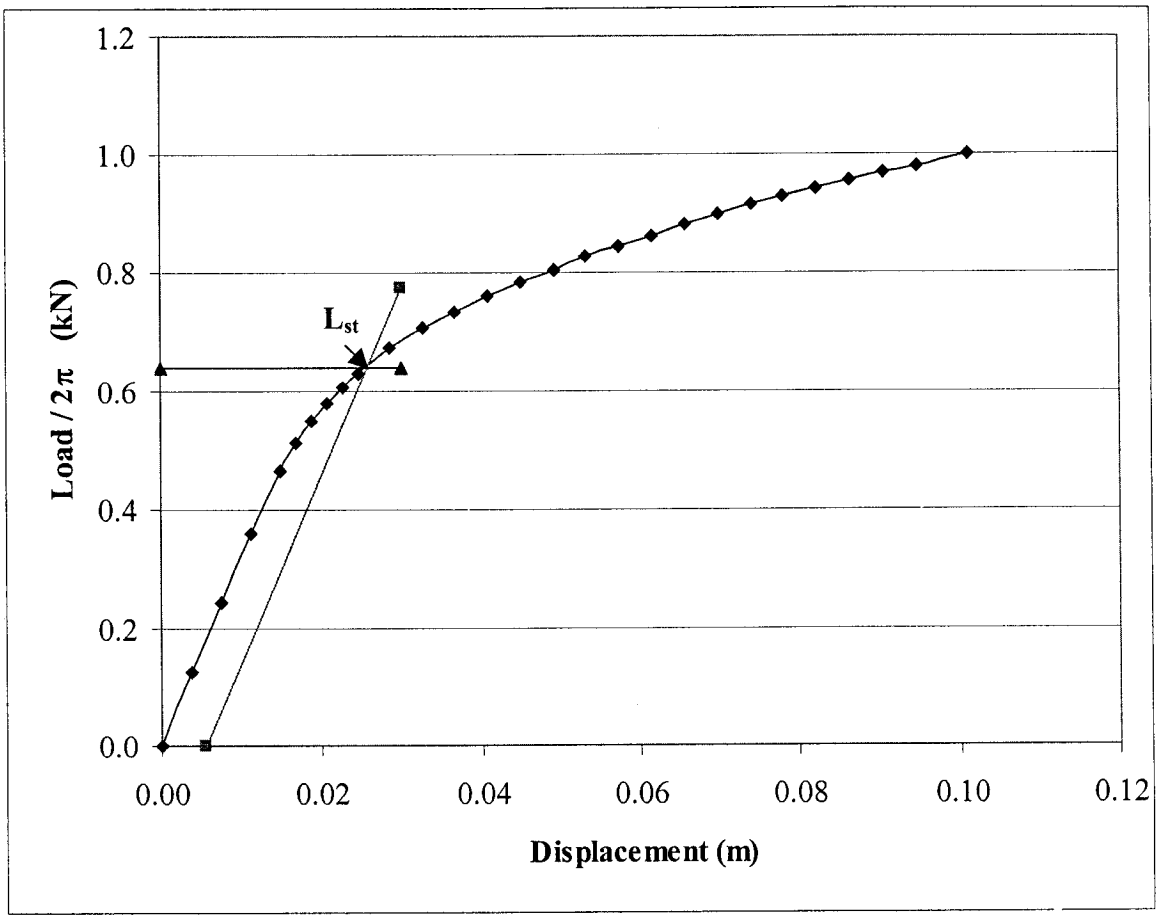

Figure 3.15. Typical load versus displacement curve from the numerical model.

For the case of cohesionless soil, load tests were carried out on the numerical models for pile diameters, D = 0.18 m and 0.25 m, and shaft depths, L = 10.9 m and 18.0 m. The properties of the sand were: unit weight of 19.1 kN/m^3, Young's modulus of 35,000 kN/m^2, Poisson ratio of 0.3 and angles of shearing strength of 30°, 35° and 41.5° (Tables 3.3 and 3.4).

When there is no value for the parameter R_{inter}, it was considered that there was no slippage between the pile and the soil.

Table 3.3. Load tests results - numerical model for cohesionless soils.

Test	L (m)	D (m)	L/D	ϕ (°)	K_o	R_{inter}	Q (kN)	f_{sav} (kPa)
1	10.9	0.18	60.6	30.0	0.5	0.9	235	38.1
2	10.9	0.18	60.6	30.0	0.5	1.0	267	43.3
3	10.9	0.18	60.6	30.0	0.5	-	644	104.5
4	10.9	0.18	60.6	30.0	1.0	0.9	441	71.6
5	10.9	0.18	60.6	30.0	1.0	1.0	599	97.3
6	10.9	0.18	60.6	30.0	1.0	-	929	150.7
7	10.9	0.18	60.6	30.0	1.5	0.9	640	103.8
8	10.9	0.18	60.6	30.0	1.5	1.0	599	97.3
9	10.9	0.18	60.6	30.0	1.5	-	1160	188.2
10	10.9	0.18	60.6	35.0	0.5	0.9	512	83.1
11	10.9	0.18	60.6	35.0	0.5	1.0	322	52.3
12	10.9	0.18	60.6	35.0	0.5	-	738	119.7
13	10.9	0.18	60.6	35.0	1.0	0.9	530	86.0
14	10.9	0.18	60.6	35.0	1.0	1.0	605	98.2
15	10.9	0.18	60.6	35.0	1.0	-	1061	172.1
16	10.9	0.18	60.6	35.0	1.5	0.9	761	123.5
17	10.9	0.18	60.6	35.0	1.5	1.0	833	135.2
18	10.9	0.18	60.6	35.0	1.5	-	1306	211.9
19	10.9	0.18	60.6	41.5	0.5	0.9	347	56.3
20	10.9	0.18	60.6	41.5	0.5	1.0	402	65.3
21	10.9	0.18	60.6	41.5	0.5	-	848	137.7
22	10.9	0.18	60.6	41.5	1.0	0.9	654	106.1
23	10.9	0.18	60.6	41.5	1.0	1.0	750	121.8
24	10.9	0.18	60.6	41.5	1.0	-	1195	193.9
25	10.9	0.18	60.6	41.5	1.5	0.9	925	150.1
26	10.9	0.18	60.6	41.5	1.5	1.0	1029	166.9
27	10.9	0.18	60.6	41.5	1.5	-	1497	242.9
28	18.0	0.25	72.0	30.0	0.5	0.9	827	58.5
29	18.0	0.25	72.0	30.0	0.5	1.0	935	66.1
30	18.0	0.25	72.0	30.0	0.5	-	2283	161.5
31	18.0	0.25	72.0	30.0	1.0	0.9	1599	113.1

Test	L (m)	D (m)	L/D	ϕ (°)	K_o	R_{inter}	Q (kN)	f_{sav} (kPa)
32	18.0	0.25	72.0	30.0	1.0	1.0	1807	127.8
33	18.0	0.25	72.0	30.0	1.0	-	3277	231.8
34	18.0	0.25	72.0	30.0	1.5	0.9	2349	166.2
35	18.0	0.25	72.0	30.0	1.5	1.0	2595	183.6
36	18.0	0.25	72.0	30.0	1.5	-	4210	297.8
37	18.0	0.25	72.0	35.0	0.5	0.9	988	69.9
38	18.0	0.25	72.0	35.0	0.5	1.0	1127	79.7
39	18.0	0.25	72.0	35.0	0.5	-	2629	186.0
40	18.0	0.25	72.0	35.0	1.0	0.9	1920	135.8
41	18.0	0.25	72.0	35.0	1.0	1.0	2192	155.1
42	18.0	0.25	72.0	35.0	1.0	-	3725	263.5
43	18.0	0.25	72.0	35.0	1.5	0.9	2803	198.2
44	18.0	0.25	72.0	35.0	1.5	1.0	3116	220.4
45	18.0	0.25	72.0	35.0	1.5	-	4670	330.4
46	18.0	0.25	72.0	41.5	0.5	0.9	1224	86.6
47	18.0	0.25	72.0	41.5	0.5	1.0	1422	100.6
48	18.0	0.25	72.0	41.5	0.5	-	3011	213.0
49	18.0	0.25	72.0	41.5	1.0	0.9	2387	168.9
50	18.0	0.25	72.0	41.5	1.0	1.0	2762	195.4
51	18.0	0.25	72.0	41.5	1.0	-	4289	303.4
52	18.0	0.25	72.0	41.5	1.5	0.9	3447	243.8
53	18.0	0.25	72.0	41.5	1.5	1.0	3848	272.2
54	18.0	0.25	72.0	41.5	1.5	-	5375	380.2

Table 3.4. Load tests results - numerical model for cohesionless soils.

Test	L (m)	D (m)	L/D	ϕ (°)	K_o	R_{inter}	Q (kN)	f_{sav} (kPa)
23	10.9	0.18	60.6	42	1	1	745	120.8
55	10.9	0.20	54.5	42	1	1	843	123.0
56	10.9	0.23	47.4	42	1	1	974	123.6
50	18.0	0.25	72.0	42	1	1	2753	194.7
57	15.0	0.25	60.0	42	1	1	1930	163.9
58	10.0	0.25	40.0	42	1	1	899	114.5

For the case of cohesive soils, load tests were carried out on the finite element models for pile diameters, D = 0.18 m and 0.25 m, and shaft depths, L = 10.9 m and 18.0 m. The properties of the clay were: unit weight of 17 kN/m^3, Young's modulus of 30,000 kN/m^2, Poisson ratio of 0.3 and cohesions of 20kPa, 36 kPa and 70 kPa (Tables 3.5 and 3.6). The first 18 tests were for undrained conditions and the last 18 for drained.

Table 3.5. Load tests results - numerical model for cohesive soils.

Test	L (m)	D (m)	L/D	c (kPa)	K_o	R_{inter}	Q (kN)	f_{sav} (kPa)
1	10.9	0.18	60.6	20	1	0.8	130	21.1
2	10.9	0.18	60.6	20	1	0.9	144	23.4
3	10.9	0.18	60.6	20	1	1.0	158	25.7
4	10.9	0.18	60.6	36	1	0.8	231	37.5
5	10.9	0.18	60.6	36	1	0.9	258	41.9
6	10.9	0.18	60.6	36	1	1.0	284	46.1
7	10.9	0.18	60.6	70	1	0.8	445	72.2
8	10.9	0.18	60.6	70	1	0.9	497	80.6
9	10.9	0.18	60.6	70	1	1.0	549	89.0
10	18.0	0.25	72.0	20	1	0.8	296	21.0
11	18.0	0.25	72.0	20	1	0.9	329	23.3
12	18.0	0.25	72.0	20	1	1.0	362	25.6
13	18.0	0.25	72.0	36	1	0.8	529	37.4
14	18.0	0.25	72.0	36	1	0.9	590	41.7
15	18.0	0.25	72.0	36	1	1.0	650	46.0
16	18.0	0.25	72.0	70	1	0.8	1014	71.7
17	18.0	0.25	72.0	70	1	0.9	1130	80.0
18	18.0	0.25	72.0	70	1	1.0	1250	88.4
19	10.9	0.18	60.6	20	1	0.8	125	20.3
20	10.9	0.18	60.6	20	1	0.9	140	22.8
21	10.9	0.18	60.6	20	1	1.0	156	25.3
22	10.9	0.18	60.6	36	1	0.8	223	36.2
23	10.9	0.18	60.6	36	1	0.9	250	40.6
24	10.9	0.18	60.6	36	1	1.0	277	45.0
25	10.9	0.18	60.6	70	1	0.8	428	69.5
26	10.9	0.18	60.6	70	1	0.9	480	77.9

Test	L (m)	D (m)	L/D	c (kPa)	K_o	R_{inter}	Q (kN)	f_{sav} (kPa)
27	10.9	0.18	60.6	70	1	1.0	532	86.3
28	18.0	0.25	72.0	20	1	0.8	283	20.0
29	18.0	0.25	72.0	20	1	0.9	319	22.5
30	18.0	0.25	72.0	20	1	1.0	354	25.0
31	18.0	0.25	72.0	36	1	0.8	504	35.6
32	18.0	0.25	72.0	36	1	0.9	569	40.2
33	18.0	0.25	72.0	36	1	1.0	629	44.5
34	18.0	0.25	72.0	70	1	0.8	968	68.4
35	18.0	0.25	72.0	70	1	0.9	1093	77.3
36	18.0	0.25	72.0	70	1	1.0	1214	85.9

Table 3.6. Load tests results - numerical model for cohesive soils.

Test	L (m)	D (m)	L/D	c (kPa)	K_o	R_{inter}	Q (kN)	f_{sav} (kPa)
23	10.9	0.18	60.6	36	1	1	283	46.0
55	10.9	0.20	54.5	36	1	1	317	46.4
56	10.9	0.23	47.4	36	1	1	373	47.3
50	18.0	0.25	72.0	36	1	1	649	45.9
57	15.0	0.25	60.0	36	1	1	551	46.8
58	10.0	0.25	40.0	36	1	1	384	48.8

3.3.1. PILE GEOMETRY

In micropiles, the ratio of the circumference to the cross-sectional area is extremely high, so it derives its capacity solely from the perimetric area. The end bearing capacity is almost negligible.

For cohesionless soils it is reasonable to expect that the length of the pile, and consequently the slenderness ratio L/D, will have a much stronger influence on the pile capacity than the diameter. This increase is due to the increase in the overburden pressure

with the embedment in depth that generates the horizontal earth pressure that acts as a normal force on the pile shaft.

From the analysis based on numerical data it is found that the unit shaft resistance increases with length and slenderness ratio L/D. In the case of two piles with equal slenderness ratio, the one with higher length presented a higher unit shaft resistance (Figures 3.16, 3.18 and 3.20).

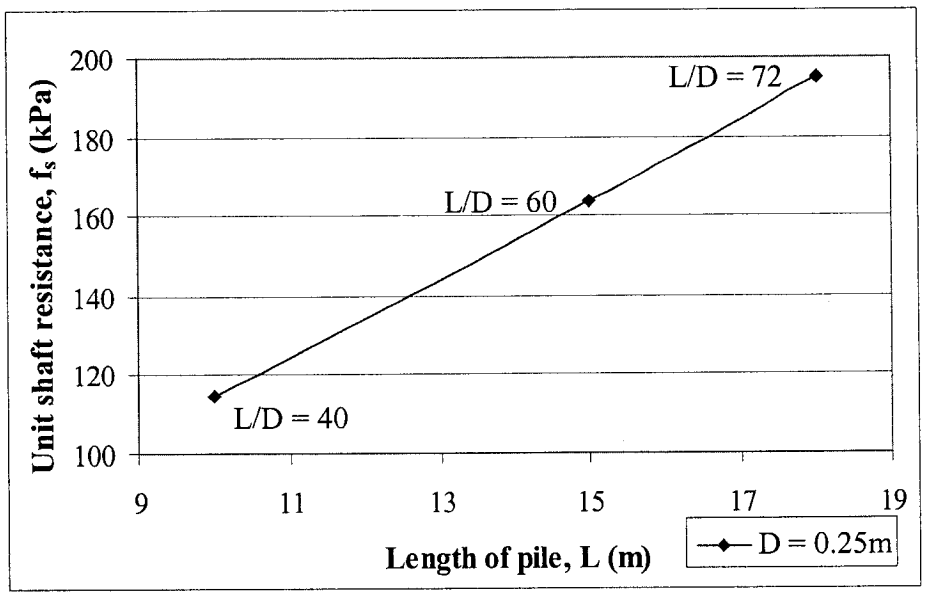

Figure 3.16. Unit shaft resistance versus pile length – cohesionless soil.

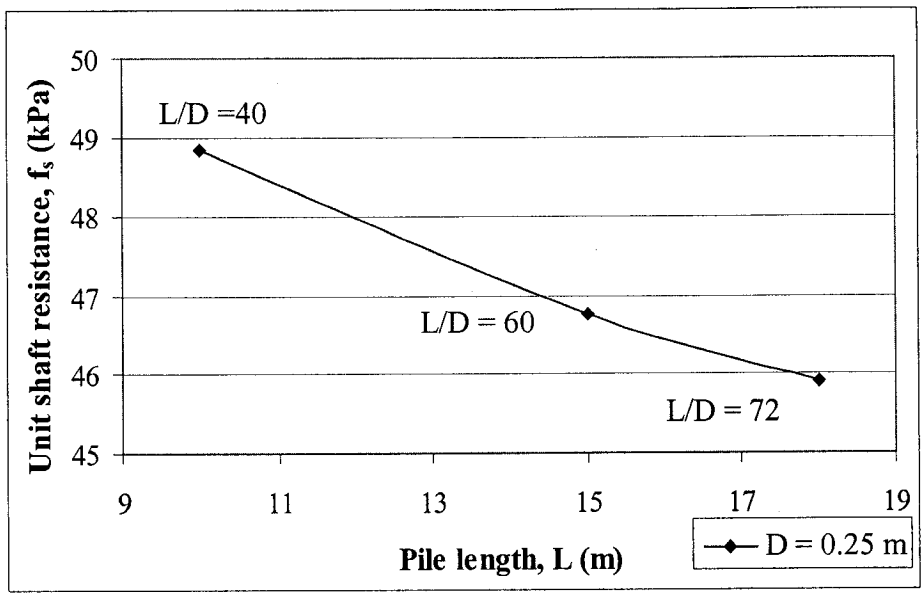

Figure 3.17. Unit shaft resistance versus pile length – cohesive soil.

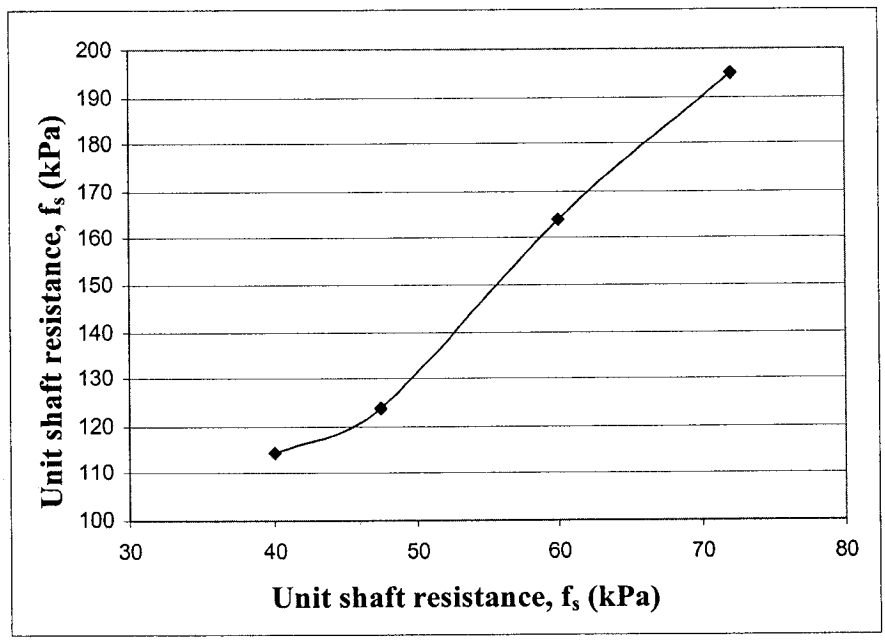

Figure 3.18. Unit shaft resistance versus slenderness ratio- cohesionless soil.

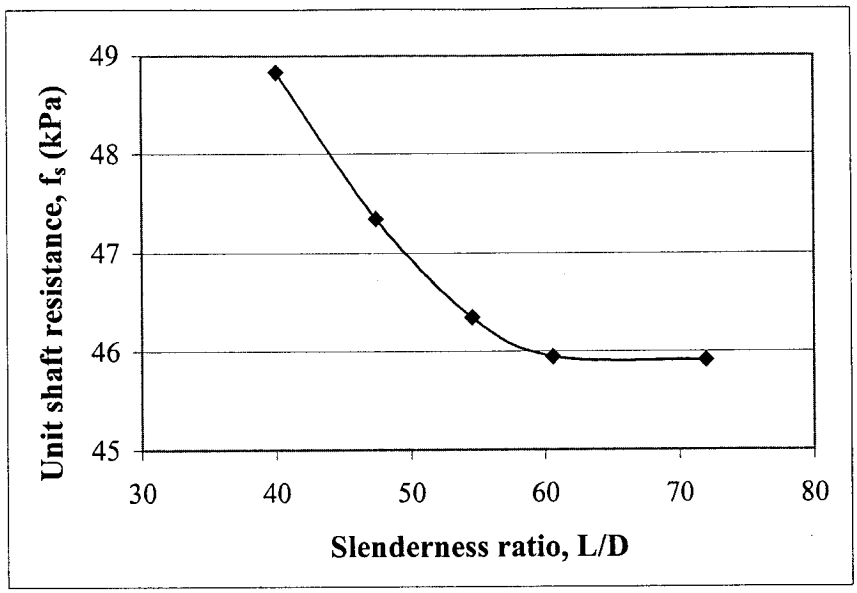

Figure 3.19. Unit shaft resistance versus slenderness ratio- cohesive soil.

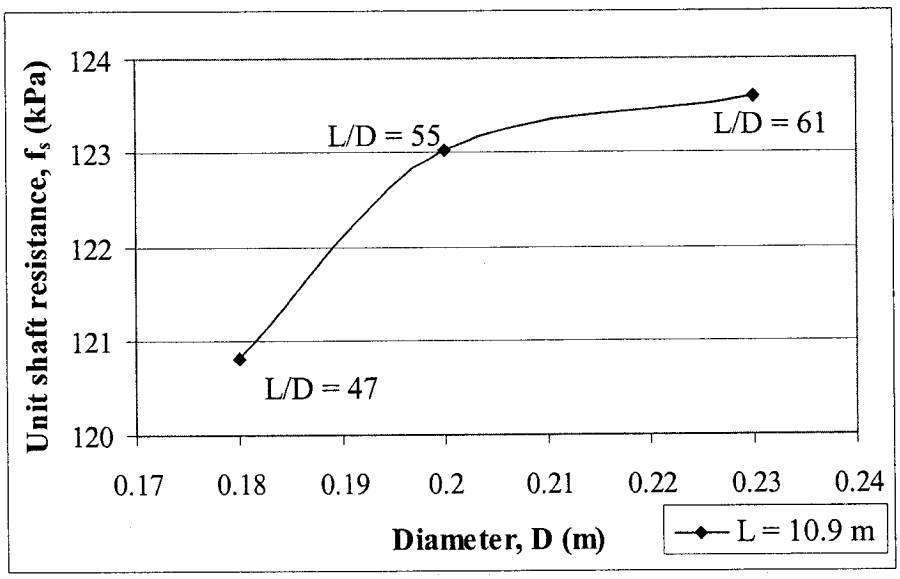

Figure 3.20. Unit shaft resistance versus pile diameter – cohesionless soil.

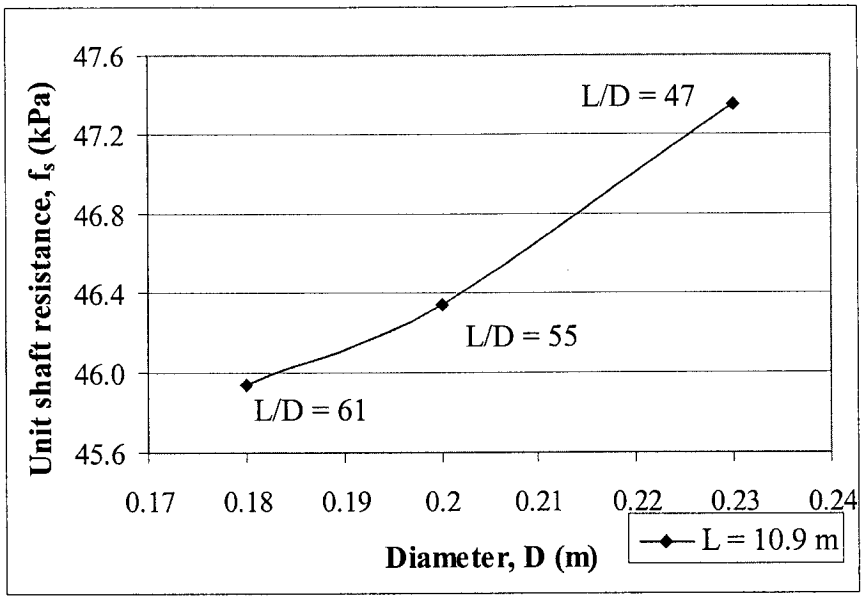

Figure 3.21. Unit shaft resistance versus pile diameter – cohesive soil.

For cohesive materials the diameter had a stronger influence over the capacity of the pile than the length, with the unit shaft resistance decreasing with a decrease in slenderness ratio L/D. This behavior can be explained by the phenomenon of arching in cohesive soils, when the shear strength actually decreases with greater lengths (Figures 3.17, 3.19 and 3.21).

3.3.2. ANGLE OF SHEAR STRENGTH OF THE SOIL

The angle of shear strength is expected to have a major effect on the unit shaft resistance because the soil (modeled as Mohr-Coulomb material) is considered to have negligible cohesion, and the shear strength will be derived from the effective vertical stress, σ'_{vz}, and $\tan\phi$.

The unit shaft resistance is influenced by the amount of mobilization of the angle of shear strength. It is reasonable to expect higher influence for longer piles because the overburden pressure increases with depth and makes it more difficult for the soil particles to move.

Figures 3.22 and 3.23 show how the increase in unit shaft resistance is more accentuated with greater L/D.

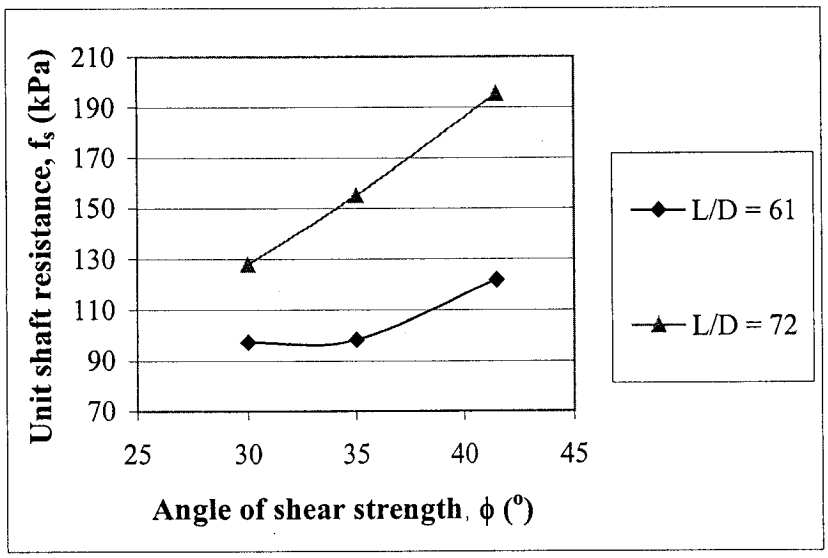

Figure 3.22. Unit shaft resistance versus angle of shear strength.

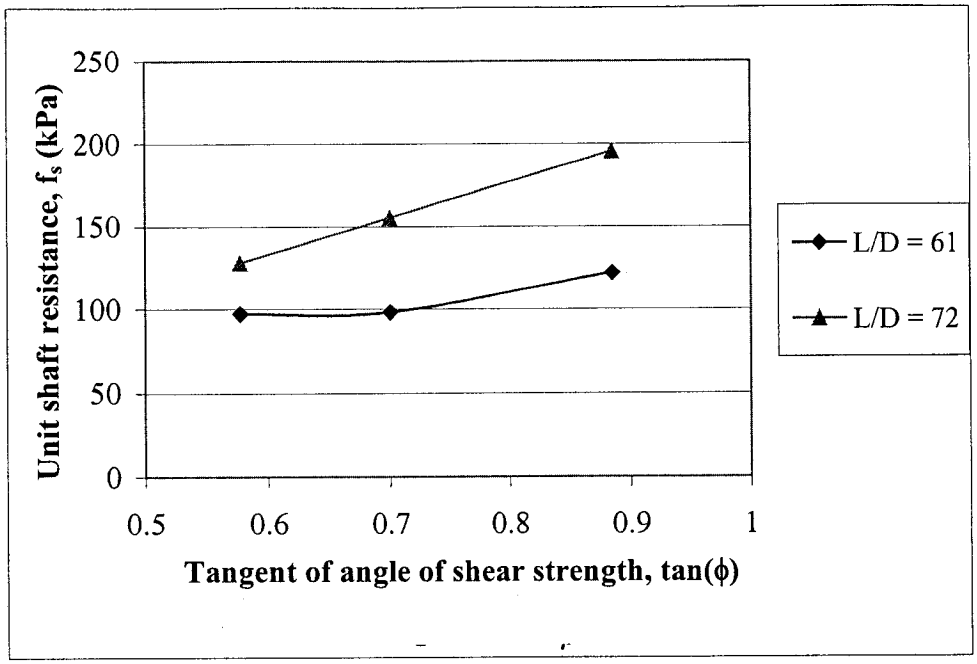

Figure 3.23. Unit shaft resistance versus tangent of angle of shear strength.

3.3.3. COHESION

Cohesion is also expected to have a great influence on the unit shaft resistance because the cohesive soil has an angle of shear strength $\phi = 0^{\circ}$, and so derives its shear strength solely from the cohesion. The influence is independent of the slenderness ratio because the cohesion was considered constant along the length of the pile (Figure 3.24).

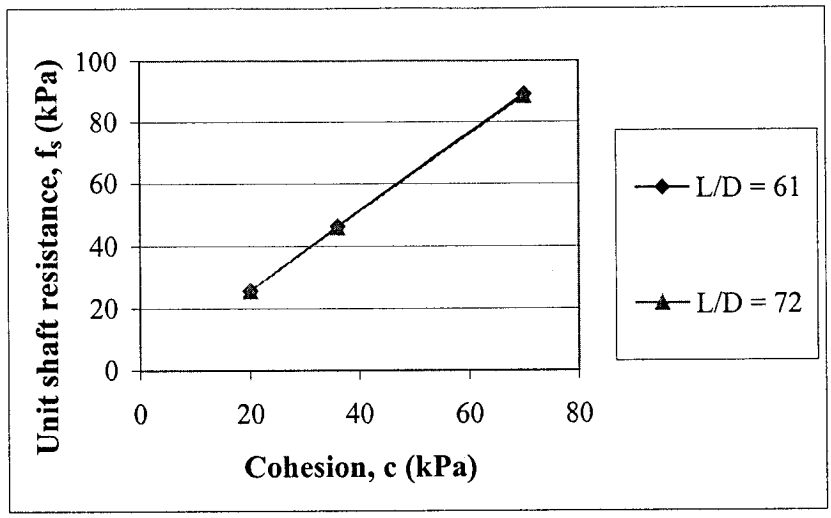

Figure 3.24. Unit shaft resistance versus cohesion.

3.3.4. COEFFICIENT OF EARTH PRESSURE

For high quality construction drilled shafts, a good estimation is to consider $K = K_o$ (Jeon and Kulhawy, 2001), which means that the soil coefficient of earth pressure at rest will not be strongly affected by the construction technique. In the numerical model the value of the coefficient K before and after the simulation of the construction of the pile was almost the same, with changes at the top or tip of the pile.

Figures 3.25 and 3.26 are typical data obtained from the finite element model where the coefficient of earth pressure was calculated along the pile as the horizontal effective stress divided by the vertical effective stress.

Higher coefficients of earth pressure at rest means higher shaft capacity because of the higher pressure exerted by the soil. The effect will be stronger for longer piles due to the increase in the effective stress for cohesionless soils (Figure 3.27).

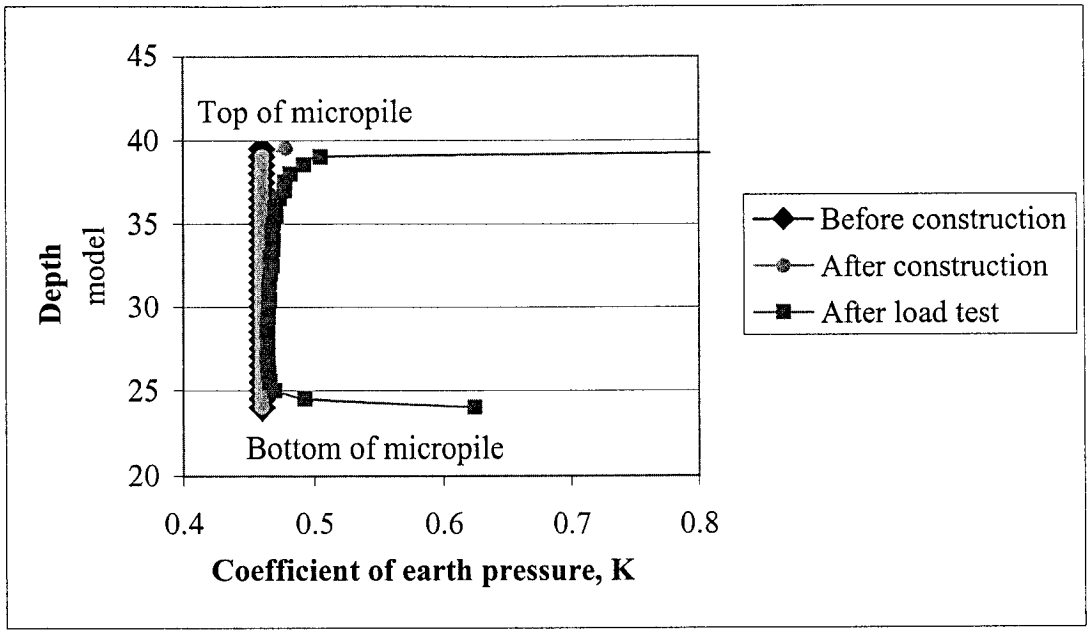

Figure 3.25. Coefficient of earth pressure at different phases– cohesionless soil.

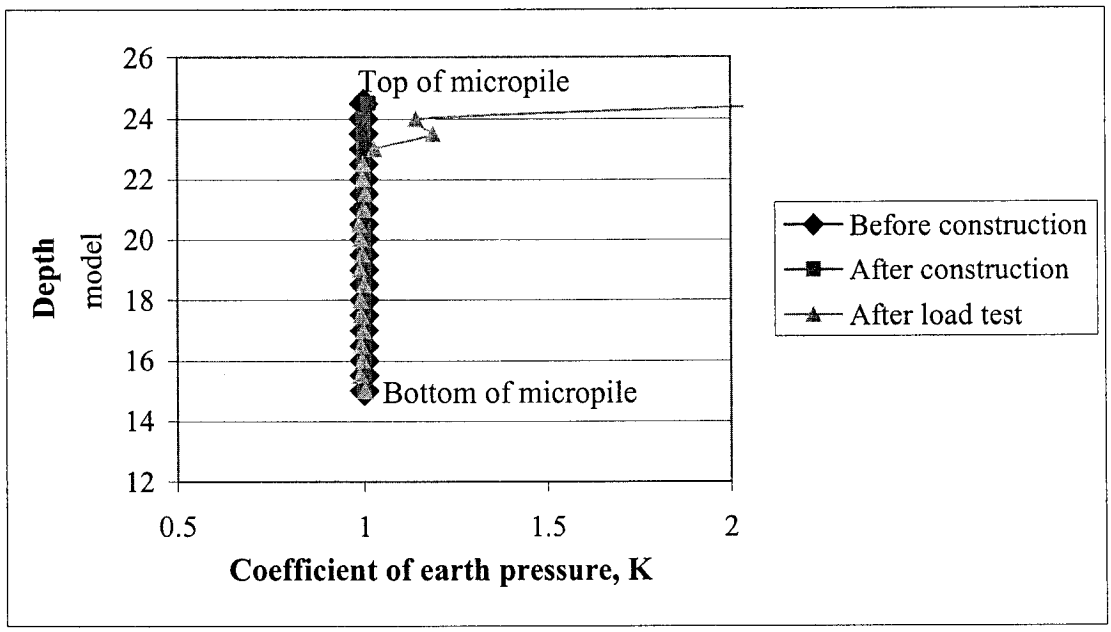

Figure 3.26. Coefficient of earth pressure at different phases– cohesive soil.

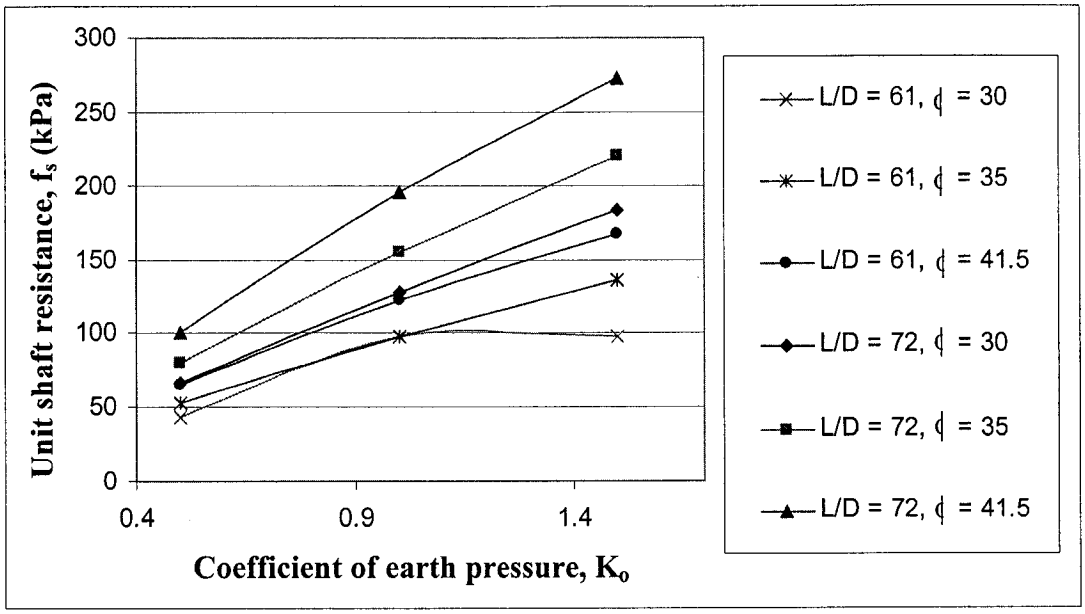

Figure 3.27. Unit shaft resistance versus coefficient of earth pressure.

3.3.5. STRENGTH REDUCTION FACTOR AT INTERFACE SOIL/PILE

The factor R_{inter} defines the properties of the soil around the pile. As an example, for R_{inter} = 0.9, $\tan\phi_{interface}$ = 0.9* $\tan\phi$, $c_{interface}$ = 0.9 * c, and angle of soil/pile friction on the interface $\delta = 0.92\phi$. When there is no factor R_{inter} there is no slippage between pile and soil, and the load will be much higher than for $R_{inter} \leq 1$. Higher factors R_{inter}, mean more resistance against the movement of the pile and higher unit shaft resistance, as can be seen on Figures 3.28 and 3.29.

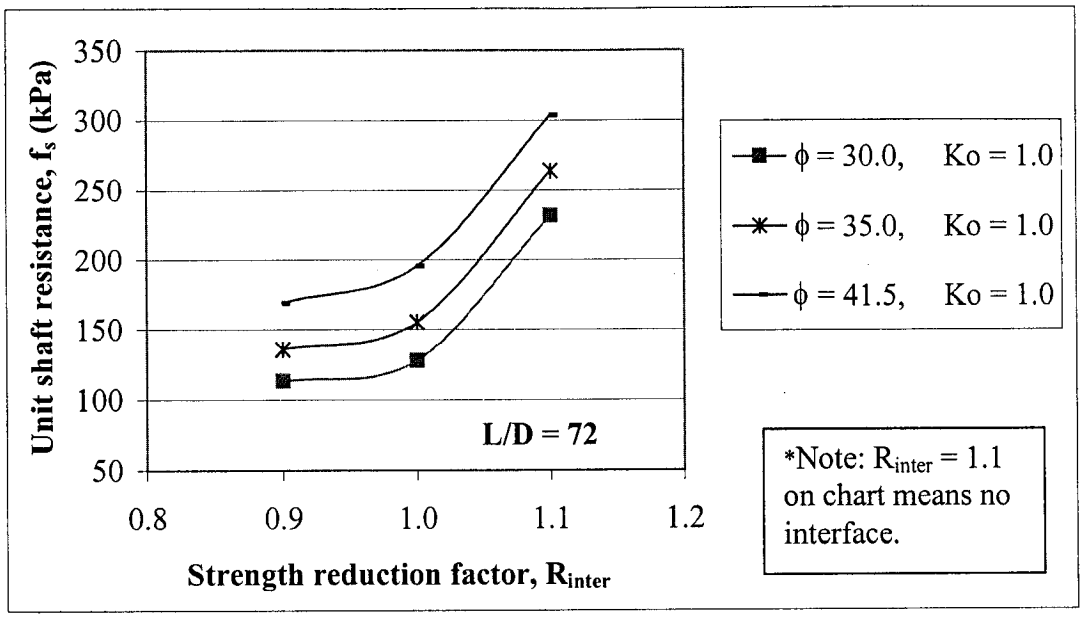

Figure 3.28. Unit shaft resistance versus strength reduction factor -cohesionless soil.

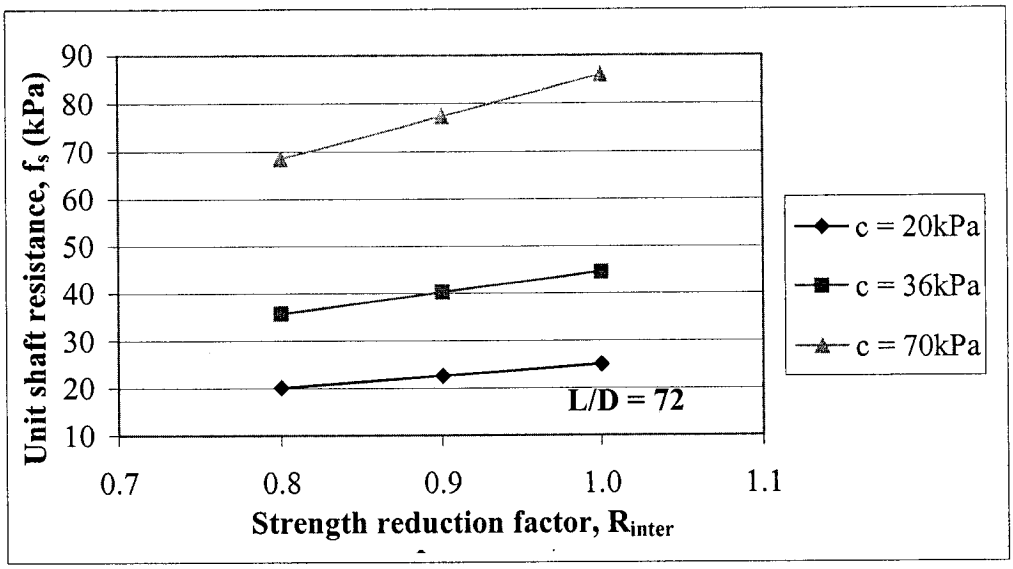

Figure 3.29. Unit shaft resistance versus strength reduction factor -cohesive soil.

3.3.6. GROUTING PRESSURE

One of the challenges in the design of micropiles is the definition of the effective diameter ($D = \alpha_c D_o$). As previously presented in Tables 2.5 and 2.6, Bustamante and Doix (1985) attempted to establish the coefficients α_c for anchors depending on the injection method and the soil type. Those same α_c's are employed in the design of micropiles because of its similarity to anchors and its injection methods that can be compared to types B and D micropiles. It is well accepted that there is a strong correlation between anchors and micropiles but there is a deficiency of studies, mainly experimental modeling, on the effects of pressure on micropiles.

Sodré (1994) presented the results of 20 field load tests on type B micropiles in different kinds of soils (sands and clay) where the effective diameter on the bond zone was determined by supervision on site (Table 3.7). The bond zone is the length of the pile, in total or in part, where the load transfer is expected because the upper layers are too weak, or because part of the steel casing is left in place, and consequently is the only length where expansion of the diameter with grouting pressure occurred.

Table 3.7. Coefficients α_c for micropiles type B from Sodré (1994).

Pile	Nominal diameter (m)	Effective diameter (m)	Pressure (Mpa)	α_c
1	0.22	0.25	0.4	1.14
2	0.27	0.30	0.4	1.11
3	0.27	0.30	0.4	1.11
4	0.22	0.25	0.4	1.14
5	0.10	0.12	0.2	1.20
6	0.22	0.25	0.4	1.14
7	0.22	0.25	0.4	1.14
8	0.22	0.25	0.4	1.14
9	0.22	0.25	0.4	1.14
10	0.22	0.25	0.4	1.14
11	0.17	0.20	0.4	1.18
12	0.22	0.25	0.4	1.14
13	0.22	0.25	0.4	1.14
14	0.22	0.25	0.4	1.14
15	0.22	0.25	0.4	1.14
16	0.17	0.20	0.4	1.18
17	0.22	0.25	0.2	1.14
18	0.22	0.25	0.2	1.14
19	0.22	0.25	0.2	1.14
20	0.22	0.25	0.2	1.14

On type B micropiles the pressures are low and a large increase in the effective diameter at the bond zone by permeation and/or local compaction of the ground is not expected. The α_c coefficients obtained by Sodré (1994) therefore are in accordance with the proposed values on Table 2.5, and even if there are differences on the site conditions between micropiles and anchors, resulting in different effective diameters, they will be of little importance because of the dimension of the coefficient α_c.

For the method of grouting D neat cement grout is placed in the hole under gravity head only. Hours later, when this primary grout has hardened, a similar grout is injected via a pre-placed sleeved grout pipe. A packer is used inside the sleeved pipe so, that specific horizons can be treated several times if necessary, at pressures of 2 to 8 MPa.

There are many empirical correlations between grout pressure and diameter for anchors available in the literature but none seem to be offered specifically for micropiles type D.

Tables 3.8 and 3.9 presents the data obtained with the numerical model designed to study the bulb expansion subjected to pressure. The results appear to be in good agreement with the values proposed in Table 2.6, for the range of pressures on type D micropiles, for both cohesive and cohesionless soils.

Table 3.8. Values of pressure and α_c on cohesionless soils.

Soil Type	γ (kN/m^3)	ν	E (Mpa)	ϕ (^{o})	K_o	Pressure (MPa)	α_c
Dense Sand	20.0	0.31	30	34	0.44	5.55-5.92	1.4-1.5
	20.0	0.29	35	36	0.41	5.94-6.43	1.4-1.5
	20.0	0.28	40	38	0.38	6.30-6.93	1.4-1.5
	20.0	0.26	45	40	0.36	6.70-7.85	1.4-1.5
	20.0	0.25	55	42	0.33	8.18	1.4
Medium Sand	18.5	0.32	20	32	0.47	4.38-4.60	1.4-1.5
	18.5	0.31	23	33	0.46	4.68-5.02	1.4-1.5
	18.5	0.31	25	34	0.44	4.84-5.25	1.4-1.5
	18.5	0.30	25	35	0.43	4.90-5.48	1.4-1.5
	18.5	0.28	30	37	0.40	5.30-5.64	1.4-1.5
Loose Sand	17.5	0.34	20	29	0.52	4.09-4.61	1.4-1.5
	17.5	0.33	20	30	0.50	4.56-4.74	1.4-1.5
	17.5	0.33	20	31	0.48	4.23-4.71	1.4-1.5
	17.5	0.32	22	32	0.47	4.40-4.78	1.4-1.5
	17.5	0.31	25	33	0.46	5.02-5.27	1.4-1.5

Table 3.9. Values of pressure and α_c on cohesive soils.

Soil Type	γ (kN/m^3)	ν	E (MPa)	c (kPa)	K_o	Pressure (MPa)	α_c
Stiff Clay	19	0.495	41	48	1	4.33-4.58	1.8-2.0
	19	0.495	55	60	1	4.87-4.91	1.8-2.0
	19	0.495	70	73	1	5.29-5.33	1.8-2.0
	19	0.495	85	85	1	5.92-5.97	1.8-2.0
	19	0.495	97	96	1	6.11-6.16	1.8-2.0
Medium Clay	17	0.495	21	24	1	2.84-3.06	1.8-2.0
	17	0.495	25	30	1	3.07-3.09	1.8-2.0
	17	0.495	31	36	1	3.41-3.24	1.8-2.0
	17	0.495	35	42	1	3.64-3.52	1.8-2.0
	17	0.495	41	48	1	3.97-3.83	1.8-2.0
Sof Clay	15	0.495	13	12	1	2.23-2.32	1.8-2.0
	15	0.495	15	15	1	2.40-2.45	1.8-2.0
	15	0.495	17	18	1	2.57-2.60	1.8-2.0
	15	0.495	19	21	1	2.54-2.67	1.8-2.0
	15	0.495	21	24	1	2.61-2.78	1.8-2.0

The pressure necessary to expand the cavity can be considered a function of the soil properties, mainly cohesion (c) and angle of shear strength (ϕ), and the deepth of the cavity, among others. Figures 3.30 and 3.31 present the variation of the pressure necessary to expand a cavity to 1.5 times its radius on cohesionless soils and 2 times its radius on cohesive soils, against the length of the cavity (l). As expected higher values of pressure are obtained for smaller lengths (l) because the lower the cavity into the ground the higher is the vertical and horizontal pressures acting on the soil mass, due to the increase of the overburden pressure.

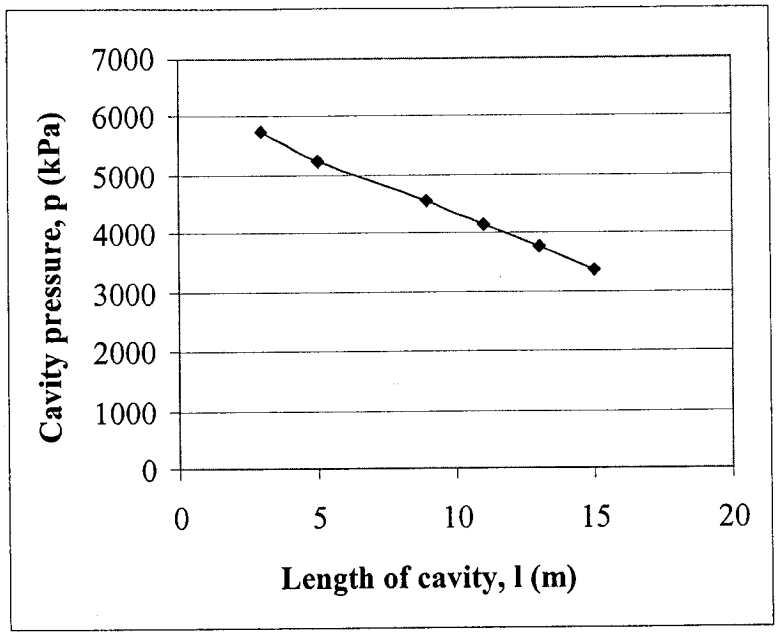

Figure 3.30. Variation of pressure versus length of cavity for cohesionless soils.

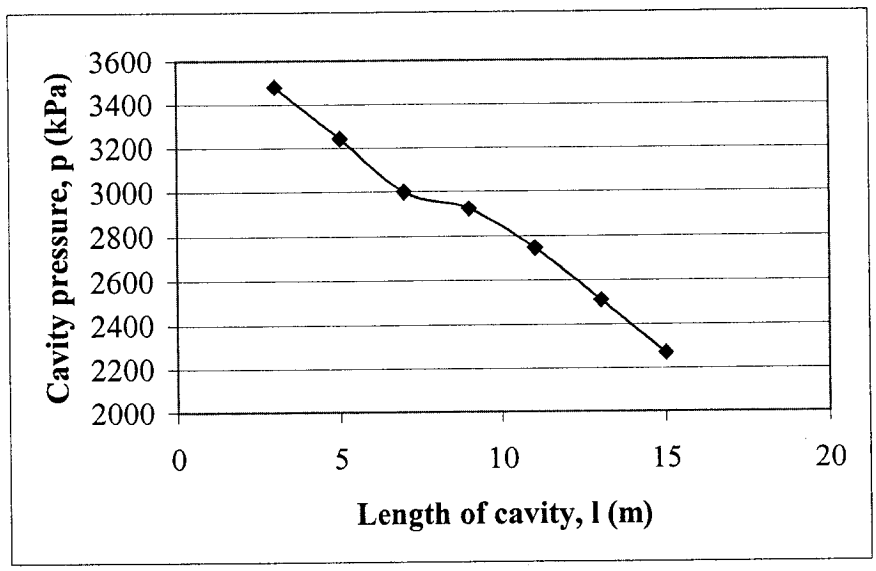

Figure 3.31. Variation of pressure versus length of cavity for cohesive soils.

Figures 3.32 and 3.33 present the variation of cavity pressure with the soil properties angle of shear strength (ϕ) and cohesion (c) for a cavity length of 5m to expand

to 1.5 and 1.4 times its radius on cohesionless soil and; 2 and 1.8 times its radius on cohesive soil. As expected the higher the shear strength, the higher the pressure because of the difficulty in moving the particles and the increase of resistance of the soil.

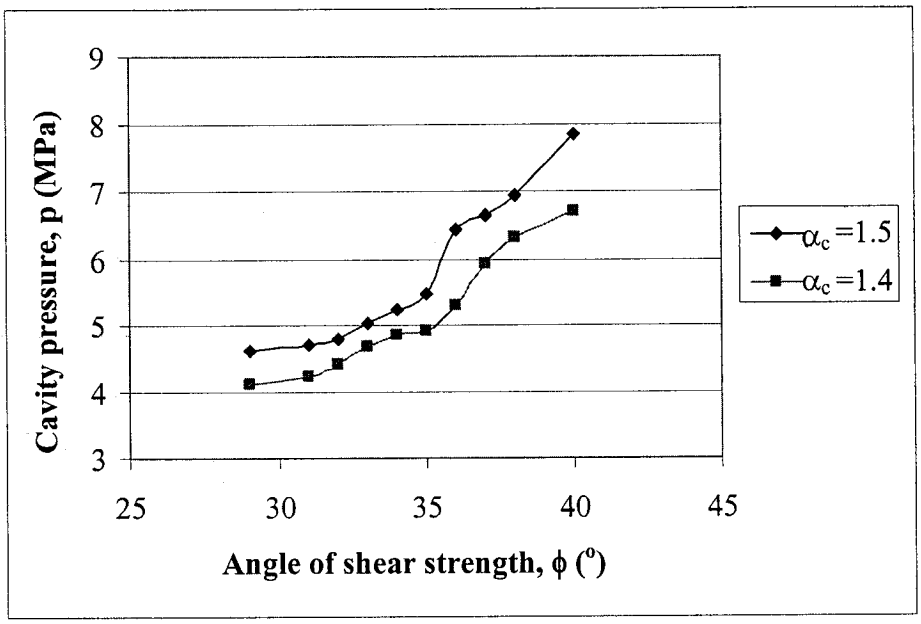

Figure 3.32. Variation of cavity pressure with angle of shear strength.

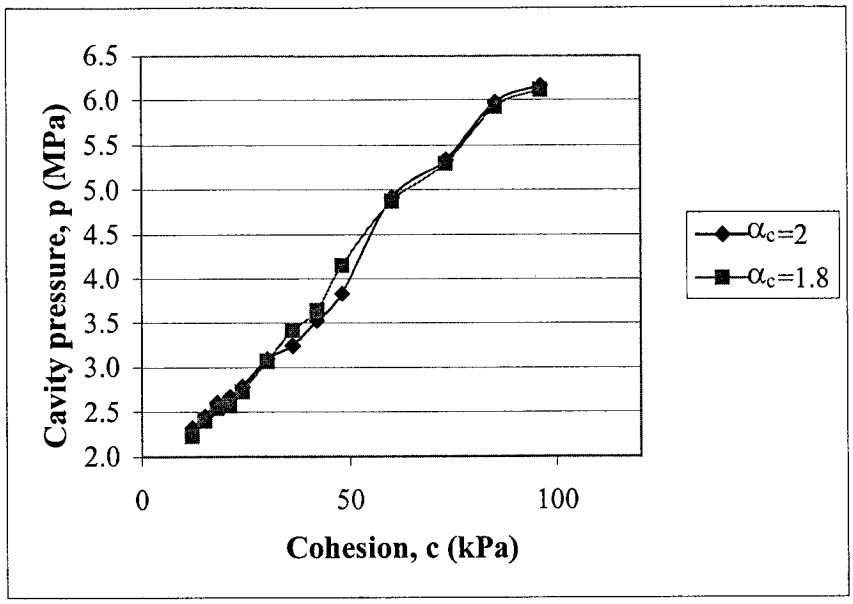

Figure 3.33. Variation of cavity pressure versus cohesion.

3.4. DESIGN PROCEDURE

According with Das (1999), any pile may be designed with the following equations:

a) Ultimate load carrying capacity (Q)

$$Q = Q_s + Q_p$$

Where:

Q_s = shaft resistance.

Q_p = end-bearing resistance.

b) End-bearing resistance – on clays (Q_p)

$$Q_p = N_c^* \bullet c_u \bullet A_p = 9 \bullet c_u \bullet A_p$$

Where:

N_c^* = bearing capacity factor.

c_u = undrained cohesion.

A_p = area of pile tip.

c) Shaft resistance (Q_s)

$$Q_s = \pi \bullet D \bullet \sum_{i=1}^{m} f_{si} \bullet dl_i$$

Where:

f_{si} = ultimate unit shaft resistance for the soil layer i.

D = effective diameter of pile.

m = number of soil layers.

dl_i = depth of considered layer.

d) Unit shaft resistance (f_s) on sands

$$f_s = \beta \bullet \sigma'_{vz} = K \bullet \tan\delta \bullet \sigma'_{vz}$$

Where:

β = proportionality coefficient.

σ'_{vz} = vertical effective stress.

K = coefficient of earth pressure.

δ = angle of soil/pile friction.

e) Unit shaft resistance (f_s) on clays

$$f_s = \alpha \bullet s_u$$

Where:

α = lumped constant of proportionality.

s_u = undrained shear strength.

In Section 3.3 an analysis was conducted to study the parameters affecting the unit shaft resistance and in summary the following could be concluded:

I. It increases with length and diameter for cohesionless soils, and decreases with length but increases with diameter for cohesive soils.

II. It increases linearly with the tangent of the angle of shear strength and with cohesion.

III. It increases with the coefficient of earth pressure at rest.

These observations confirm that the theory of Das (1999), which can be applied to micropiles, in addition:

I. The coefficient of earth pressure after construction can be considered the same as the coefficient of earth pressure at rest (K=Ko), as a result of the construction method.

II. The angle of soil/pile friction, due to construction method and roughness on the interface soil/pile can be considered equal to the angle of shear strength of the soil ($\phi = \delta$).

III. The coefficients α were back calculated with the data in Tables 3.3 and 3.5, and the results were higher than the ones proposed on the literature. For micropiles, Bruce (1994) proposes values between 0.6 and 0.8, and the numerical model obtained values between 1.02 and 1.04 for cohesions between 20 and 70 kPa.

IV. The end-bearing resistance wasn't mobilized until the end of the load test, therefore it can be considered neglectful (Q = Qs).

Figures 3.34 and 3.35 show a very good agreement between the theoretical values of unit skin friction, with the definitions above incorporated, and the numerical ones.

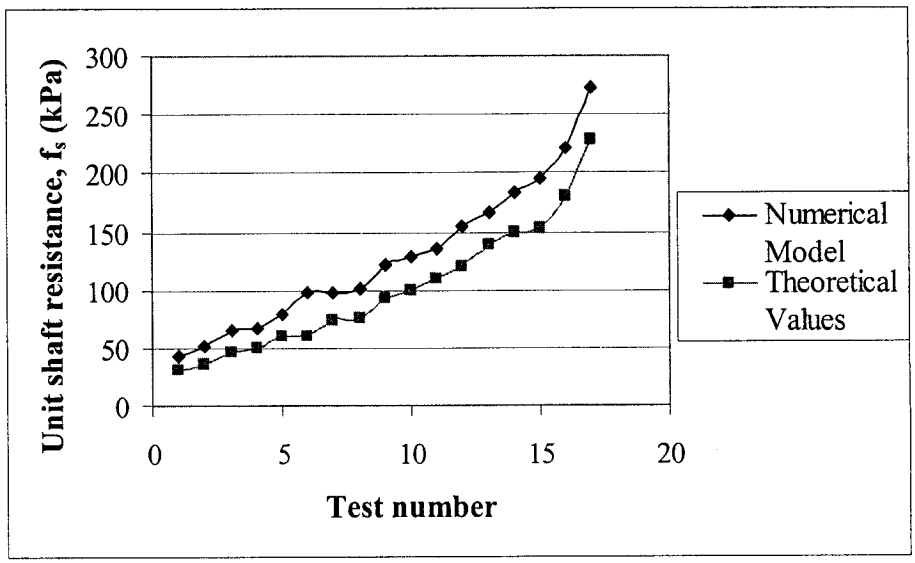

Figure 3.34. Unit shaft resistance in cohesionless soils.

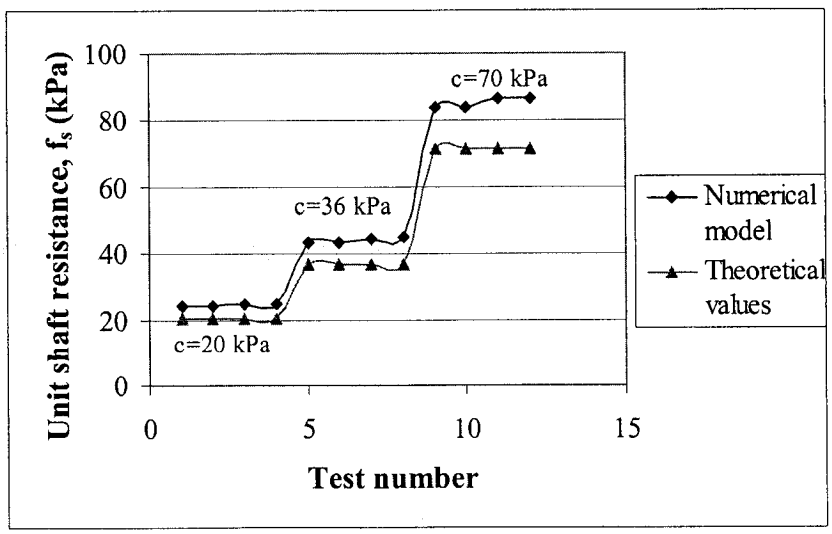

Figure 3.35. Unit shaft resistance in cohesive soils.

This formulation can be employed for type A micropiles but it will underestimate the capacity of types B and D micropiles, because on this type of pile pressure is applied while grouting to increase the effective diameter. To incorporate this effect in the design procedure another database was obtained with the numerical model developed in Section 3.2.1 for micropiles with non uniform cross-section, and the results together with soil properties are presented on Tables 3.10 and 3.11.

Table 3.10. Results from numerical model on cohesionless soils.

Test	L (m)	D (m)	d (m)	γ (kN/m^3)	ν	E (Mpa)	ϕ (^{o})	K_o	Q (kN)
1	15	0.15	0.210	20.0	0.31	30	34	0.44	480
2	15	0.15	0.225	20.0	0.31	30	34	0.44	518
3	15	0.15	0.240	20.0	0.31	30	34	0.44	551
4	15	0.15	0.210	20.0	0.28	40	38	0.38	735
5	15	0.15	0.225	20.0	0.28	40	38	0.38	788
6	15	0.15	0.240	20.0	0.28	40	38	0.38	842
7	15	0.15	0.210	20.0	0.25	55	42	0.33	967
8	15	0.15	0.225	20.0	0.25	55	42	0.33	1037
9	15	0.15	0.240	20.0	0.25	55	42	0.33	1102
10	15	0.15	0.210	18.5	0.32	20	32	0.47	238
11	15	0.15	0.225	18.5	0.32	20	32	0.47	256
12	15	0.15	0.240	18.5	0.32	20	32	0.47	273
13	15	0.15	0.210	18.5	0.31	25	34	0.44	361
14	15	0.15	0.225	18.5	0.31	25	34	0.44	387
15	15	0.15	0.240	18.5	0.31	25	34	0.44	410
16	15	0.15	0.210	18.5	0.28	30	37	0.40	479
17	15	0.15	0.225	18.5	0.28	30	37	0.40	517
18	15	0.15	0.240	18.5	0.28	30	37	0.40	550
19	15	0.15	0.210	17.5	0.34	20	29	0.52	119
20	15	0.15	0.225	17.5	0.34	20	29	0.52	127
21	15	0.15	0.240	17.5	0.34	20	29	0.52	136
22	15	0.15	0.210	17.5	0.33	20	31	0.48	179
23	15	0.15	0.225	17.5	0.33	20	31	0.48	191
24	15	0.15	0.240	17.5	0.33	20	31	0.48	204

Test	L (m)	D (m)	d (m)	γ (kN/m^3)	ν	E (Mpa)	ϕ (^{o})	K_o	Q (kN)
25	15	0.15	0.210	17.5	0.31	25	33	0.46	239
26	15	0.15	0.225	17.5	0.31	25	33	0.46	256
27	15	0.15	0.240	17.5	0.31	25	33	0.46	272
28	10	0.18	0.252	20.0	0.31	30	34	0.44	461
29	10	0.18	0.270	20.0	0.31	30	34	0.44	508
30	10	0.18	0.288	20.0	0.31	30	34	0.44	553
31	10	0.18	0.252	20.0	0.28	40	38	0.38	707
32	10	0.18	0.270	20.0	0.28	40	38	0.38	778
33	10	0.18	0.288	20.0	0.28	40	38	0.38	846
34	10	0.18	0.252	20.0	0.25	55	42	0.33	931
35	10	0.18	0.270	20.0	0.25	55	42	0.33	1023
36	10	0.18	0.288	20.0	0.25	55	42	0.33	1117
37	10	0.18	0.252	18.5	0.32	20	32	0.47	229
38	10	0.18	0.270	18.5	0.32	20	32	0.47	250
39	10	0.18	0.288	18.5	0.32	20	32	0.47	273
40	10	0.18	0.252	18.5	0.31	25	34	0.44	343
41	10	0.18	0.270	18.5	0.31	25	34	0.44	378
42	10	0.18	0.288	18.5	0.31	25	34	0.44	412
43	10	0.18	0.252	18.5	0.28	30	37	0.40	460
44	10	0.18	0.270	18.5	0.28	30	37	0.40	504
45	10	0.18	0.288	18.5	0.28	30	37	0.40	549
46	10	0.18	0.252	17.5	0.34	20	29	0.52	113
47	10	0.18	0.270	17.5	0.34	20	29	0.52	124
48	10	0.18	0.288	17.5	0.34	20	29	0.52	136
49	10	0.18	0.252	17.5	0.33	20	31	0.48	171
50	10	0.18	0.270	17.5	0.33	20	31	0.48	186
51	10	0.18	0.288	17.5	0.33	20	31	0.48	204
52	10	0.18	0.252	17.5	0.31	25	33	0.46	227
53	10	0.18	0.270	17.5	0.31	25	33	0.46	250
54	10	0.18	0.288	17.5	0.31	25	33	0.46	271

Table 3.11. Results from numerical model on cohesive soils.

Test	L (m)	D (m)	d (m)	γ (kN/m^3)	ν	E (Mpa)	c (kPa)	K_o	Q (kN)
1	15	0.15	0.270	19.0	0.495	41	48	1	567
2	15	0.15	0.300	19.0	0.495	41	48	1	612
3	15	0.15	0.330	19.0	0.495	41	48	1	650
4	15	0.15	0.270	19.0	0.495	70	73	1	867
5	15	0.15	0.300	19.0	0.495	70	73	1	930
6	15	0.15	0.330	19.0	0.495	70	73	1	994
7	15	0.15	0.270	19.0	0.495	97	96	1	1141
8	15	0.15	0.300	19.0	0.495	97	96	1	1224
9	15	0.15	0.330	19.0	0.495	97	96	1	1300
10	15	0.15	0.270	17.0	0.495	21	24	1	281
11	15	0.15	0.300	17.0	0.495	21	24	1	302
12	15	0.15	0.330	17.0	0.495	21	24	1	322
13	15	0.15	0.270	17.0	0.495	31	36	1	426
14	15	0.15	0.300	17.0	0.495	31	36	1	457
15	15	0.15	0.330	17.0	0.495	31	36	1	484
16	15	0.15	0.270	17.0	0.495	41	48	1	565
17	15	0.15	0.300	17.0	0.495	41	48	1	610
18	15	0.15	0.330	17.0	0.495	41	48	1	649
19	15	0.15	0.270	15.0	0.495	13	12	1	140
20	15	0.15	0.300	15.0	0.495	13	12	1	150
21	15	0.15	0.330	15.0	0.495	13	12	1	160
22	15	0.15	0.270	15.0	0.495	17	18	1	211
23	15	0.15	0.300	15.0	0.495	17	18	1	225
24	15	0.15	0.330	15.0	0.495	17	18	1	241
25	15	0.15	0.270	15.0	0.495	21	24	1	282
26	15	0.15	0.300	15.0	0.495	21	24	1	302
27	15	0.15	0.330	15.0	0.495	21	24	1	321
28	10	0.18	0.324	19.0	0.495	41	48	1	544
29	10	0.18	0.360	19.0	0.495	41	48	1	599
30	10	0.18	0.396	19.0	0.495	41	48	1	653
31	10	0.18	0.324	19.0	0.495	70	73	1	834
32	10	0.18	0.360	19.0	0.495	70	73	1	918
33	10	0.18	0.396	19.0	0.495	70	73	1	998
34	10	0.18	0.324	19.0	0.495	97	96	1	1099
35	10	0.18	0.360	19.0	0.495	97	96	1	1207
36	10	0.18	0.396	19.0	0.495	97	96	1	1318

Test	L (m)	D (m)	d (m)	γ (kN/m^3)	ν	E (Mpa)	c (kPa)	K_o	Q (kN)
37	10	0.18	0.324	17.0	0.495	21	24	1	270
38	10	0.18	0.360	17.0	0.495	21	24	1	295
39	10	0.18	0.396	17.0	0.495	21	24	1	322
40	10	0.18	0.324	17.0	0.495	31	36	1	405
41	10	0.18	0.360	17.0	0.495	31	36	1	446
42	10	0.18	0.396	17.0	0.495	31	36	1	486
43	10	0.18	0.324	17.0	0.495	41	48	1	543
44	10	0.18	0.360	17.0	0.495	41	48	1	595
45	10	0.18	0.396	17.0	0.495	41	48	1	648
46	10	0.18	0.324	15.0	0.495	13	12	1	133
47	10	0.18	0.360	15.0	0.495	13	12	1	146
48	10	0.18	0.396	15.0	0.495	13	12	1	160
49	10	0.18	0.324	15.0	0.495	17	18	1	202
50	10	0.18	0.360	15.0	0.495	17	18	1	219
51	10	0.18	0.396	15.0	0.495	17	18	1	241
52	10	0.18	0.324	15.0	0.495	21	24	1	268
53	10	0.18	0.360	15.0	0.495	21	24	1	295
54	10	0.18	0.396	15.0	0.495	21	24	1	320

The shaft resistance obtained with the model above is illustrated in Figures 3.36 and 3.37, together with the theoretical values for two cases: considering the pile to have a nominal diameter D throughout its length, and considering the expansion on the last 5m to diameter d.

Figure 3.37 show that for cohesive soils the theoretical formulation had again a very good agreement with α coefficients between 1.02 and 1.04 for cohesions between 20 and 70 kPa. Because the diameter was considerably expanded on the bulb it was observed that the end-bearing resistance has a stronger influence and it was considered on the calculation of the shaft resistance.

In Figure 3.36 new theoretical values were added because the theory wasn't close enough to the numerical ones; therefore a new coefficient K_2 was back calculated with the database. This coefficient represents the increase in pile capacity due to the increase in diameter, and is a function of the ratio l/L (expansion length/pile length). For l/L = 0.33, K_2 is equal to 1.22; and for l/L = 0.50, K_2 is equal to 1.35.

According to Das (1999), the unit shaft resistance in the field for piles embedded in sand is considered to increase with depth approximately linearly to a depth called critical depth and to remain constant thereafter. In the numerical model, because of the diameter expansion, the load distribution along the pile is changed; explaining the development of coefficient K_2 as a function of l/L.

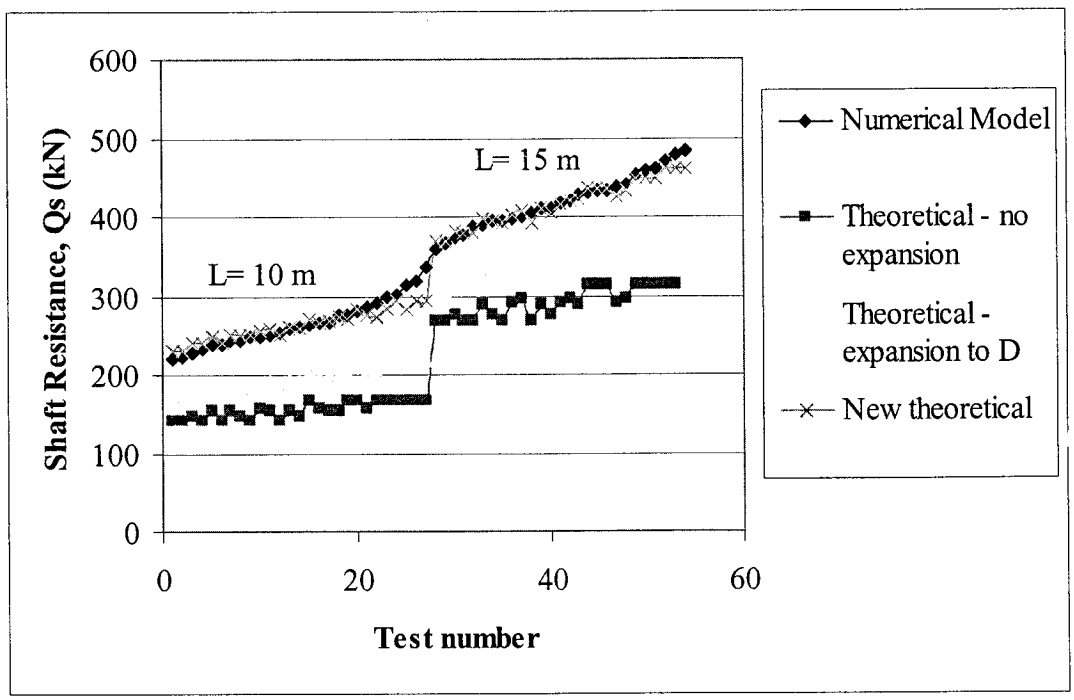

Figure 3.36. Shaft resistance from numerical model and theory, cohesionless soil.

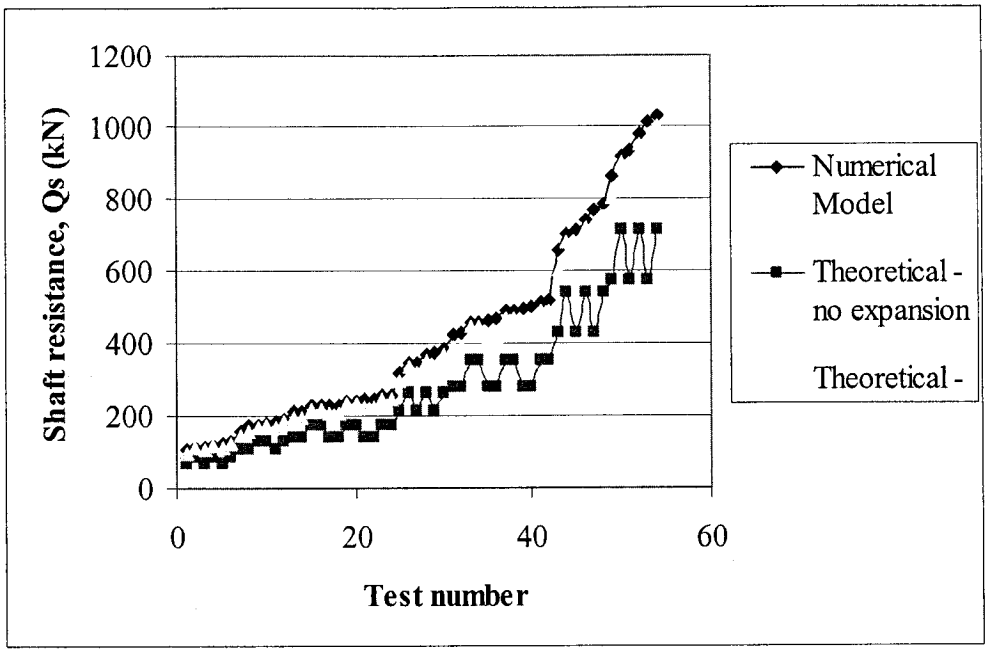

Figure 3.37. Shaft resistance from numerical model and theory, cohesive soil.

Based on the findings of the numerical model, a new design procedure can be proposed as follow:

For micropiles embedded in sand:

a) Ultimate load carrying capacity

$$Q = Q_s$$

Where:

Q_s = shaft resistance.

b) Shaft resistance

$$Q_s = \pi \bullet \sum_{i=1}^{m} D_i \bullet f_{si} \bullet dl_i$$

Where:

f_{si} = ultimate unit shaft resistance for the soil layer i.

D_i = effective diameter of micropile on layer i.

m = number of soil layers.

dl_i = depth of considered layer.

The effective diameter can be determined with Table 2.5 for type B micropiles and with Table 3.8 for type D, where with the pressure to be applied in the field can be obtained the coefficient α_c, depending on the soil kind.

If the designer defines the effective diameter and the length of expansion, the pressure to be applied in the field can be determined with Figures 3.30, and 3.32, based on soil properties.

c) Unit shaft resistance – Type B piles

$$f_s = K_o \bullet \tan\phi \bullet \sigma'_{vz}$$

Where:

σ'_{vz} = vertical effective stress.

K_o = coefficient of earth pressure at rest.

ϕ = angle of shear strength.

d) Unit shaft resistance – Type D piles

$$f_s = K_o \bullet K_2 \bullet \tan\phi \bullet \sigma'_{vz}$$

Where:

σ'_{vz} = vertical effective stress.

K_o = coefficient of earth pressure at rest.

ϕ = angle of shear strength.

K_2 = coefficient representing the increase in diameter.

For l/L = 0.33, K_2 is equal to 1.22; and for l/L = 0.50, K_2 is equal to 1.35.

For micropiles embedded in clay:

a) Ultimate load carrying capacity

$$Q = Q_s + Q_p$$

Where:

Q_s = shaft resistance.

Q_p = end-bearing resistance.

b) End-bearing resistance

$$Q_p = 9 \bullet c \bullet A_p$$

Where:

c = cohesion.

A_p = area of pile tip.

c) Shaft resistance

$$Q_s = \pi \bullet \sum_{i=1}^{m} D_i \bullet f_{si} \bullet dl_i$$

Where:

f_{si} = ultimate unit shaft resistance for the soil layer i.

D_i = effective diameter of micropile on layer i.

m = number of soil layers.

dl_i = depth of considered layer.

The effective diameter can be determined with Table 2.5 for type B micropiles and with Table 3.9 for type D, where with the pressure to be applied in the field can be obtained the coefficient α_c, depending on the soil kind.

If the designer defines the effective diameter and the length of expansion, the pressure to be applied in the field can be determined in Figures 3.31 and 3.33, based on soil properties.

d) Unit shaft resistance

$$f_s = \alpha \bullet s_u$$

Where:

α = lumped constant of proportionality with values between 1.02 and 1.04 for cohesions between 20 and 70 kPa.

s_u = undrained shear strength.

This design procedure was applied to some field test available in literature. The soil data is presented in Table 3.12, where the average values of shear strength angle and over consolidation ratio were estimated by Jeon and Kulhawy (2001). The lengths of the expanded diameter and grout pressures were given by the respective authors and estimated with the site conditions.

The calculation steps are presented in Table 3.13, where every parameter was obtained with the procedure proposed. The field test failure loads were obtained from load versus displacement curves according with the specifications previously proposed in Section 3.2.

Figure 3.38 show graphically the results obtained theoretically and with the curves load versus displacement from field tests. The outcome from the design procedure is in very good agreement with field test values, considering that some soil parameters were estimated and the difficulty in estimating the final geometry of the pile on site.

Table 3.12. Test data for demonstration of design procedure.

Test		Ground water table (m)	Diameter (m)	Shaft Depth (m)	Length of expanded diameter (m)	Pile Type	Pressure (kPa)	γ (kN/m^3)	ϕ (^{o})	K_o	s_u (kN/m^2)	Q (kN)
Bruce (1988)	1	1.2	0.19	13.7	6.1	B	414	17.3	33.0	1.15	-	472
Bruce (1992)	2	10.0	0.18	15.0	9.4	B	450	19.2	41.5	2.03	-	961
Singh & Heine (1984)	3	9.1	0.15	11.4	7.0	B	450	18.8	35.0	1.25	-	502
Ichimura & Ochita (2000)	4	1.0	0.18	21.8	5.2	B	500	18.8	35.0	1.25	-	1245
	5	1.0	0.18	17.6	1.1	B	500	18.8	35.0	1.25	-	658
Jones & Turner (1980)	6	-	0.15	12.0	12.0	B	900	19.4	-	-	138	932
	7	-	0.15	9.0	9.0	B	900	19.4	-	-	119	770

Table 3.13. Calculation of parameters from the design procedure.

Test Number	σ'_{vz} (kN/m^2)	α	f_s (kN/m^2)	α_c	Q_p (kN)	Q_s (kN)	$Q = Q_p + Q_s$ (kN)	Q Field test (kN)	Error (%)
1	56	-	42	1.2	-	372	372	472	-21
2	69	-	124	1.1	-	1117	1117	961	16
3	96	-	84	1.2	-	505	505	502	1
4	101	-	88	1.2	-	1140	1140	1245	-8
5	82	-	72	1.1	-	723	723	658	10
6	-	1.06	126	1.2	27	642	669	932	-11
7	-	1.07	148	1.2	32	1002	1034	770	13

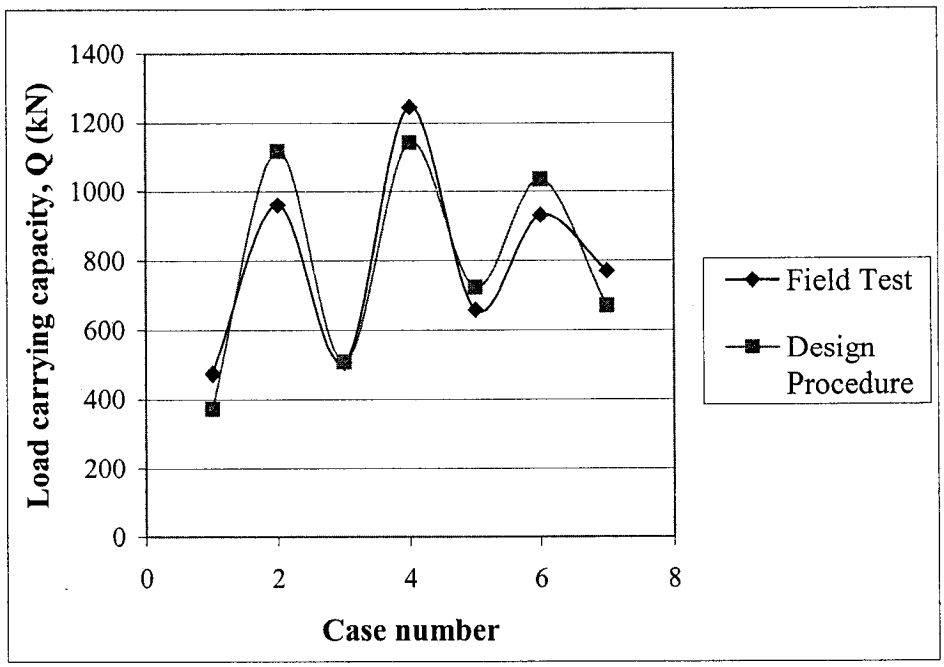

Figure 3.38. Results from design procedure and field tests.

CHAPTER 4

CONCLUSIONS AND RECOMMENDATIONS

4.1. CONCLUSIONS

Numerical models were developed to critically review the existing design methods and to examine the parameters governing the design of micropiles, in clay and sand. A design procedure is proposed to take into account the geometry of the micropiles, the interaction with the soil and to incorporate the parameters, which seemed to be ignored in the previous methods. The proposed design procedure was validated against field tests, where good agreement could be found.

The first model was to simulate the installation techniques of the micropiles and to perform parametric study. The second numerical model was to simulate the cavity expansion caused by grouting pressure and to develop the relationships of pressure versus expansion of the pile diameter, length of expansion and soil properties.

The finite element model proved to be a very powerful tool enabling the following information:

1) Finite element technique together with boundary conditions and pile/soil constitutive laws presented in this thesis proved to be vital numerical model for the problem stated.
2) Pile installation was successfully simulated with finite element technique with almost no disturbance on soil stresses.
3) The numerical model together with cavity expansion theory was successful to simulate the bulb expansion of the pile due to grouting pressure.

4) The failure pattern of the soil surrounding the pile produced by the numerical model was similar to those deduced from experimental observations available on literature.

5) The unit shaft resistance around the micropile increases with length and diameter for cohesionless soils and increases with diameter, but decreases with length for cohesive soils. It increases linearly with the tangent of the angle of shear strength, cohesion (independently of slenderness ratio) and coefficient of earth pressure at rest.

6) The unit shaft resistance on clays can be estimated with the same equations for piles type A, B, and D, but in sands it will be underestimated for types B and D micropiles.

7) The coefficient of earth pressure remains almost unchanged after installation.

8) The degree of roughness on the soil/pile interface has a significant effect on the micropile unit shaft resistance.

9) It is of interest to report that the shaft resistance was mobilized before the tip resistance for all pile tested.

10) In case of clay and piles with expanded bulb due to the enlargement of the pile tip the end-bearing resistance delays the shaft resistance.

11) The pressure necessary to expand the shaft on micropiles is a function of length of cavity and soil shear strength.

12) Design procedures for all types of micropiles in sand and in clay are developed and presented in this thesis.

13) In this proposed design procedure new parameters (α and K_2) were introduced and existing ones were modified.

4.2. RECOMMENDATIONS FOR FURTHER RESEARCH

Based on the present study performed in this thesis the following can be proposed:

1) To conduct experimental investigation on prototype micropiles.
2) To study the group efficiency of micropiles.
3) To examine the performance of micropiles subjected to cyclic and seismic loads.
4) To study the performance of micropiles in layered soils.
5) To study the integrity of the structure elements of micropiles in different soil conditions
6) To examine Micropiles/raft interactions.
7) To study micropiles subjected to inclined load.
8) To study the performance of micropiles fully/bonded to the ground.

REFERENCES

Bjerrum, L. (1957). "Norwegian experiences with steel piles in rock". *Geotechnique*, 7 (2), 1957, 73-96.

Brandl, H. (1988). "The interaction between soil and groups of small diameter bored piles." *Proceedings of the 1st International Geotechnical Seminar on Deep Foundations on Bored and Auger Piles*, Ghent/Belgium, June, 3-16.

Bruce, D. A. (1988 and 1989). "Aspects of minipiling practice in the United States." *Ground engineering*, 21 (8), 1988, 20-33 and 22 (1), 1989, 35-39.

Bruce, D. A. (1992). "Structural underpinning by pinpiles." *Proc. 17th Deep Foundations Institute Annual Meeting*, New Orleans, 1992, 49-78.

Bruce, D. A. (1994). "Small-diameter cast-in-place elements for load bearing and in situ earth reinforcement." Chapter 6 in *Ground control and improvement* by P. P. Xanthakos, L. W. Abramson, and D. A. Bruce. John Wiley and Sons, 1994, 87 pp.

Bruce, D. A., and Yeung, C. K. (1984). "Review of minipiling with particular regard to Hong Kong Applications." *Hong Kong Engineering*, June, 12 (6), 1984, 31-54.

Bullivant, R. A., and Bradbury, H. W. (1996). Underpinning: a practical guide. Blackwell Science Ltd, Oxford, England.

Bustamante, M., and Doix, B. (1985). "Une méthode pour le calcul des tirants et des micropieux injectés". *Bulletin de Liaison des Laboratoires des Ponts et Chaussés*, Nov-Dec, 140, 75-92.

Carvalho, D., Mantilla, J. N. R., Albiero, J. H., and Cintra, J. C. A. (1991). "Provas de carga à tração e à compressão em estacas instrumentadas do tipo raiz." *SEFE II – Seminário de Engenharia de Fundações Especiais*, São Paulo, Novembro, 1, 79-87.

CCTG, Fascicule 62, Titre V, (1993). Technical rules for the design and calculation of the foundations of the civil engineering works [Regles techniques de conception et de calcul des foundation des ouvrages de genie civil]. September.

Chen, J. R. (1998). "Case history evaluation of axial behavior of augered-cast-in-place piles and pressure-injected footings." *MS Thesis*, Cornell University, 399 p.

Das, B. M. (1999). "Principles of foundation engineering." *PWS Publishing*, 4th Edition, USA.

Davisson, M. T. (1972). "High capacity piles." *Proc. Lecture Series on Innovations in Foundation Construction*, ASCE, Chicago, 52 p.

Dringenberg, G. E., and Craizer, W. (1990). "Capacidade de carga de micro-estacas injetadas." *IX COBRAMSEF – Congresso Brasileiro de Mecânica dos Solos e Engenharia de Fundações*, Salvador/BA, Novembro, 2(III), 325-332.

FHWA (1997). Drilled and grouted micropiles: state-of-practice review, volume 1: background, classifications, cost. By D. A. Bruce and I. Juran. Report No FHWA-RD-96-016.

FHWA (1997). Drilled and grouted micropiles: state-of-practice review, volume 2: design. By D. A. Bruce and I. Juran. Report No FHWA-RD-96-017.

FHWA (1997). Drilled and grouted micropiles: state-of-practice review, volume 3: construction, QA/QC, and testing. By D. A. Bruce and I. Juran. Report No FHWA-RD-96-018.

FHWA (1997). Drilled and grouted micropiles: state-of-practice review, volume 4: case histories. By D. A. Bruce and I. Juran. Report No FHWA-RD-96-019.

FHWA (1984). Permanent ground anchors, by R. S. Cheney. Report No. FHWA-DP-68-IR.

Fleming, W. G. K., A. J. Weltman, M. F. Randolph, and W. K. Elson. (1985). Piling engineering. First Edition. Surrey University Press. Glasgow. 380 pp. (Second Edition, 1992).

Frank, A. (1971). "Tragfahigkeit von Wurzelpfahlen mit Anwendungsbeispielen", Vortr. Baugrundtag, 1970, Dt. Ges. Erd-u. Grundb., 1971, Essen., 143-164.

Ghaly, A. and Hanna, A.M. (2003). "Response of Anchors to Variations in Displacement-Based Loading." *Canadian Geotechnical Journal*, 40 (3), 694-701

Ghaly, A. and Hanna, A.M. (1994). "Ultimate Pullout Resistance of Single Vertical Anchors." *Canadian Geotechnical Journal*, 31 (5), 1994.

Gouvenot, D. (1975). "Essais de chargement et de flambement de pieux aiguilles." *Annales de l'Institut Technique du Bâtiment et des Travaux Publics,* Comité Français de la Mécanique des Sols et des Fondations, 334, December.

Hanna, A.M. and Nguyen, T.Q. (2003). "Shaft resistance of Single Vertical and Batter Piles in Sand Subjected to Axial Compression Loading." *Journal of Geotechnical and Environmental Engineering,* ASCE, 129 (3), 601-607.

Hanna, A.M., and Nguyen, T.Q. (2002). "An Axisymmetric Model for Ultimate Capacity of a Single Piles in Sand". *Journal of Soil Mechanics and Foundation Engineering*, Japan. 42 (2).

Hassan, K. H. and M. W. O'Neill (1994). Perimeter load transfer in drilled shafts in the eagle ford formation. Geotechnical Special Publication No 38, Design and performance of deep foundations: piles and piers in soil and soft rocks; Edited by P. P. Nelson, T. D. Smith, and E. C. Klukey, ASCE, October, pp. 229-244.

Hirany, A., and Kulhawy, F. H. (1988). "Conduct and interpretation of load tests on drilled shaft foundations:detailed guidelines." *Report EL-5915 (1), EPRI,* Palo Alto, 374p.

Hirany, A., and Kulhawy, F. H. (1989). "Interpretation of load tests on drilled shafts – part 1: axial compression." *Foundation Engineering: Current Principles and Practices (GSP 22),* Ed. FH Kulhawy, ASCE, New York, 1989, 1132-1149.

Ichimura, Y., and Oshita, T. (2000). "Applicability of statnamic load test for micropile". *Proc. 3rd Intl. Workshop on Micropiles,* Ube, Japan, 6p.

Jeon, S., and Kulhawy, F. H. (2001). "Evaluation of axial compression behavior of micropiles." *Proc. of a specialty conf. - Foundation and ground improvement,* Blacksburg VI, ASCE, 460-471.

Jones, D. A., and Turner, M. J. (1980) "Load tests on post-grouted micropiles in London clay." *Ground Engineering*, 13(6), 1980, 47-53.

Koreck, H. W (1978). "Small diameter bored injection piles." *Ground Engineering*, 11(4), 1978, 14-29.

Littlejohn, G. S. (1970). Soil anchors. Ground Engineering Conference. Institution of Civil Engineers, London, pp. 33-44.

Littlejohn, G. S. (1980). Ground anchorage practice. ASCE Conference, Design and Performance of Earth Retaining Structures, Cornell University, Ithaca, NY, June 18-21, pp. 692-733.

Lizzi, F. (1982). Static restoration of monuments. Sagep Publisher. Genova, Italy.

Makarchian, M., and Poulos, H. G. (1994a). "Underpinning by piles; a numerical study." *Proc. 13th ICSMFE*, New Delhi, 4, 1467-1470.

Makarchian, M., and Poulos, H. G. (1996). "Simplified method for design of underpinning piles." *Journal of Geotechnical Engineering*, ASCE, 122 (9), 1996, 745-751.

Makarchian, M., and Poulos, H. G. (1994b). "Numerical study of underpinning by piles for settlement control of strip foundations." *Proc. Vertical and Horizontal deformations of foundations and embankments*, ASCE, Texas-June, 303-313.

Mandel, J. (1936). "Flambement au sein d'un milieu elastique." *Annales des Ponts et Chaussées,* 1936-2ème seminaire, 295-335.

Mascardi, C. A. (1982). "Design criteria and performance of micropiles." *Symposium on Soil and Rock Improvement Techniques Including Geotextiles, Reinforced Earth and Modern Piling Methods,* Bangkok, December. Paper D-3.

Mascardi, C. A. (1970). *Il comportamento die Micropali Sottoposti a Sforzo Assiale.* Momento Flettente e Taglio, Verlag Leeman, Zurich.

Massad, F., Niyama, S., and Rocha, R. (1981). "Vertical load tests on instrumented root-piles." X ICSMFE – International Conf. on Soil Mechanics and Foundation Engineering, Stockholm/Sweden, June, 2, 771-775.

Mayne, P. W. and F. H. Kulhawy (1982). "Ko – OCR relationships in soil." *Journal of the Geotechnical Engineering Division*, ASCE, Volume 108, No GT6, June, pp. 851-872.

Moreno, R. F., and Marco, L. C. (1989). "Interpretação de provas de carga instrumentadas em profundidade." *3º Seminário Técnico de Empresas de Energia de São Paulo*, Eletropaulo, 1-17.

Nilson, A. H., and Winter, G. (1979). Design of Concrete Structures. 9th edition, McGraw-Hill.

Niyama, S., Massad, F., Rocha, R., and Xavier, M. S. (1981). "Análise de provas de carga em micro-estacas injetadas num solo de alteração." *Simpósio Brasileiro de Solos Tropicais em Engenharia*, Rio de Janeiro, Setembro, 3, 683-705.

Ostermayer, M. (1975). Construction Carrying Behavior and Creep Characteristics on ground Anchors, Confereence on Diaphragm Walls and Anchorages, Institute of Civil Engineers, London.

Ostermayer, M. and Sheele, F. (1978). "Research on ground anchors in non-cohesive soils." Revue Francaise de Geotechnique, n. 3, 1978, 92-97.

Brinkgreve, R. B. J. (2001). Plaxis Professional Version 8 Reference Manual, A. A. Balkema Publishers, Netherlands.

Poulos, H. G., and Davis, E. H. (1980). "Pile foundation analysis and design." John Wiley & Sons, Series in Geotechnical Engineering, 397 p.

Randolph, M. F. (1983). "Design of piled raft foundations." *Proc. Int. Symp. on Recent Devel. in Lab. And Field Tests and Analysis of Geotech. Problems,* AIT, Bangkok, Thailand, 525-537.

Randolph, M. F., and Wroth, C. P. (1978). " Analysis of deformation of vertically loaded piles." *Journal of Geotechnical Division,* ASCE, 104(12), 1465-1488.

Rocha, R., Yassuda, A. J., and Massad, E. (1985). "Provas de carga em estaca tipo raiz instrumentada." *SEFE – Seminário de Engenharia de Fundações Especiais*, São Paulo, Setembro, 1(II), 179-193.

Sabini, G., and Sapio, G. (1981). "Behaviour of small diameter bored piles under axial load." *Proc. Of the Int. Conf. On Soil Mech.* and Found. Eng., v2, 823-828.

Salioni, C. (1985). "Capacidade de carga de estacas injetadas." *SEFE – Seminário de Engenharia de Fundações Especiais,* São Paulo, September, 1(2), 13-27.

Singh, S., and Heine, E. I. (1984). "Upgrading existing footings with micro-piles.", P*roc. Intl. Conf. on Case Histories in Geotechnical Eng.,* (3), St. Louis, 1373-1383.

Sodré, D. J. R. (1994). "Análise estatística de métodos de previsão do comportamento de estaca raiz." *Escola de Engenharia de São Carlos*, São Paulo, 175 p.

Thorburn, S., and Hutchison, J. F. (1985). Underpinning. Surrey Univ. Press, London, England.

Tomlinson, M. J. (1957). "Pile design and construction practice." *Dewpoint Publication,* Cement and Concrete Association, London.

Touma, F. T., and Reese, L. C. (1974). "Behaviour of bored piles in sand." *Journal of Soil Mechanics Foundation Division,* ASCE, 100(7), 749-761.

Vesic, A. S. (1972). "Expansion of cavities in infinite soil mass." *Journal of the Soil Mechanics and Foundations Division*, ASCE. March, 1972, 265-290.